AD_____

AWARD NUMBER: DAMD17-02-1-0706

TITLE: TARGET (Translational Approaches for the Reversal, Genetic Evaluation and Treatment) of Lung Cancer

PRINCIPAL INVESTIGATOR: Waun Ki Hong, M.D.
Fadlo R. Khuri, M.D.

CONTRACTING ORGANIZATION: The University of Texas
M.D. Anderson Cancer Center
Houston, Texas 77030

REPORT DATE: September 2005

TYPE OF REPORT: Annual

PREPARED FOR: U.S. Army Medical Research and Materiel Command
Fort Detrick, Maryland 21702-5012

REPORT DOCUMENTATION PAGE

Form Approved
OMB No. 0704-0188

1. REPORT DATE *(DD-MM-YYYY)*	**2. REPORT TYPE**	**3. DATES COVERED** *(From - To)*
01-09-2005	Annual	1 Sep 2004 – 31 Aug 2005

4. TITLE AND SUBTITLE

TARGET (Translational Approaches for the Reversal, Genetic Evaluation and Treatment) of Lung Cancer

5a. CONTRACT NUMBER

5b. GRANT NUMBER
DAMD17-02-1-0706

5c. PROGRAM ELEMENT NUMBER

6. AUTHOR(S)
Waun Ki Hong, M.D. and Fadlo R. Khuri, M.D.

E-Mail: Whong@mdanderson.org

5d. PROJECT NUMBER

5e. TASK NUMBER

5f. WORK UNIT NUMBER

7. PERFORMING ORGANIZATION NAME(S) AND ADDRESS(ES)

The University of Texas
M.D. Anderson Cancer Center
Houston, Texas 77030

8. PERFORMING ORGANIZATION REPORT NUMBER

9. SPONSORING / MONITORING AGENCY NAME(S) AND ADDRESS(ES)
U.S. Army Medical Research and Materiel Command
Fort Detrick, Maryland 21702-5012

10. SPONSOR/MONITOR'S ACRONYM(S)

11. SPONSOR/MONITOR'S REPORT NUMBER(S)

12. DISTRIBUTION / AVAILABILITY STATEMENT
Approved for Public Release; Distribution Unlimited

13. SUPPLEMENTARY NOTES

14. ABSTRACT

TARGET is focused on a series of projects designed to obtain data in the preclinical and clinical settings to help us further understand the epidemiology of lung cancer, the molecular biology, genetics and epigenetics of lung cancer in the context of tobacco-damaged aerodigestive tract tissue, and the anti-cancer activity of several promising new agents, and various treatment and drug delivery approaches in models of lung cancer and other aerodigestive tract tumors.

15. SUBJECT TERMS
lung cancer, genetic markers, molecular epidemiology

16. SECURITY CLASSIFICATION OF:			**17. LIMITATION OF ABSTRACT**	**18. NUMBER OF PAGES**	**19a. NAME OF RESPONSIBLE PERSON**
a. REPORT	**b. ABSTRACT**	**c. THIS PAGE**			**19b. TELEPHONE NUMBER** *(include area code)*
U	U	U	UU	91	USAMRMC

Standard Form 298 (Rev. 8-98)
Prescribed by ANSI Std. Z39.18

TABLE OF CONTENTS

INTRODUCTION

Smoking is a major cause of lung cancer, the most prevalent cancer worldwide and the leading cause of cancer-related mortality in both men and women in the United States. In 2005, lung cancer will cause an estimated 163,510 deaths in the United States, which are more deaths than those predicted for breast, prostate, and colorectal cancers combined (Jemal et al., 2005). The 5-year overall survival rate of patients with lung cancer is extremely poor at less than 16%; this is a mere 3% increase since the 1970s (Jemal et al., 2005).

Conventional treatments of lung cancer (surgery, radiotherapy, and chemotherapy) have reached their limitation in improving overall patient survival and require substantial improvements. A better understanding of the biology of lung cancer is needed to develop new therapeutic modalities for lung cancer.

The TARGET (Translational Approaches for the Reversal, Genetic Evaluation and Treatment of Lung Cancer) program initiated three years ago aims to understand the biology and therapy of lung cancer cell lines, animal models and human subjects. Specifically, the program proposed ten research projects designed to understand the epidemiology, molecular biology, genetics and epigenetics of lung cancer in the context of tobacco-damaged aerodigestive tract tissue, and anti-tumor activities of some promising agents, and to develop improved pulmonary gene delivery approaches and orthotopic murine human lung cancer model to test effects of antiangiogenesis agents.

PROGRESS REPORT

Project 1: Molecular Epidemiology of Lung Cancer

(Principal Investigator: Margaret Spitz, M.D., M.P.H.)

Specific Aim 1.1 To create a specimen and data resource

We will enroll (over two years) a consecutive series of 100 lung cancer cases of any histology, age, gender and ethnicity, undergoing thoracotomy for definitive therapy. These patients will have detailed epidemiologic risk assessments including tobacco exposure, dietary intake and family history. Blood samples, bronchial washings and bronchial biopsies will be obtained on each patient.

Update

We have consented 117 cases since receiving DoD approval in May 2004. 101 of these patients have completed surgical resections to date. These patients are also enrolled in NCI protocol CPN 91-001, which allows for the collection of blood and sputum specimens from lung cancer cases and controls. Table 1 summarizes the collection of specimens. Among the 117 participants, sixty-six (56%) participants are female and fifty-one (44%) are male. 108 (93%) participants are White, five (4%) are Black, and four (3%) participants are Asian.

Table 1 Summary of Specimen Received

Tissue Type	# Rec'd
Tumor	81
Normal	82
Adjacent Bronchus	62
For Culture	41
Blood	90
Bronchial Brushes	99
Sputum	160

Specific Aim 1.2 To determine the genetic susceptibility profile in surrogate tissue

We will perform a panel of genotypic (select polymorphisms in DNA repair genes and 3p21.3 and 10q22 aberrations) and functional (DNA repair capacity, mutagen sensitivity, and COMET) assays of genetic susceptibility on peripheral lymphocyte DNA from the 100 patients identified in Specific Aim 1.

Specific Aim 1.3 To determine the genetic susceptibility profile in target tissue

We will establish bronchial epithelial cell cultures from fresh tumor specimens at thoracotomy of the 100 lung cancer patients from Specific Aim 1 and perform, in parallel, genotypic and phenotypic DNA repair capacity and mutagen challenge assays. We will compare, using FISH analyses, the rate of concordance of DNA deletions at 3p21.3 and 10q22 loci in cells obtained from bronchial washings and peripheral lymphocyte cultures of 50 patients.

Update for Aims 2 and 3

As described in the prior report, we have established a genotypic assay (FISH) and functional assays (DNA repair capacity, mutagen sensitivity, COMET, and telomere length) on peripheral lymphocyte DNA from the patients identified in Specific Aim 1 and commercially available cell cultures.

In the past year, we have further developed dose response curves for both gamma radiation and BDPE (DNA-damaging agent) comet assay experiments and have selected the best dose for each treatment (Figure 1 and 2).

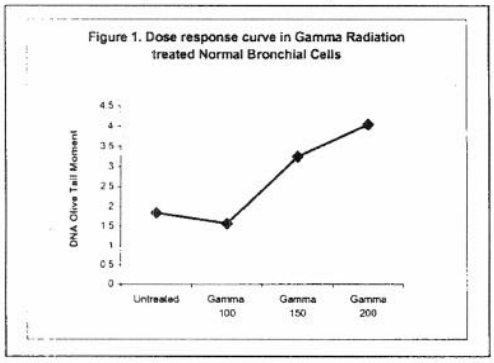

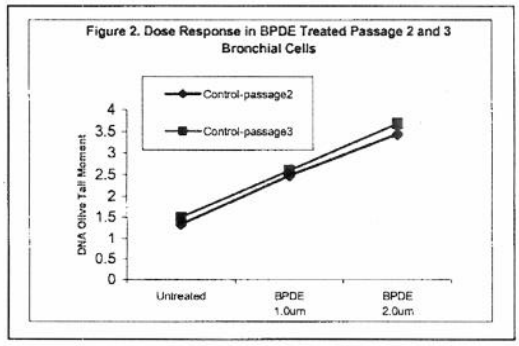

We have also shown the repeatability of the assays over two different time periods (Figures 3-4) and determined effects of cell passage number on the length of the comet tail moment (Figure 2). The results showed no difference of the tail moment length between passage 2 and passage 3 cells. We have chosen the passage 3 cells for the comet assay experiments.

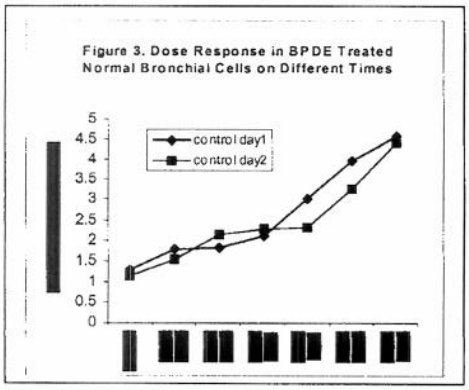

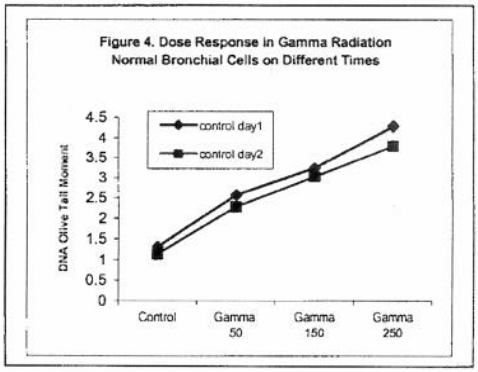

In addition, we have performed FISH analyses for 3p and 10q in the bronchial brushes, touch preparations, and the lymphocytes, and summarized the actual values in Table 2.

Table 2. Summary of FISH data for 3p and 10q deletion

Variables	N	Mean(SD)	Range
cep3/3p-BBNT(%Del)	95	2.35(1.86)	0.0 - 8.0
cep3/3p-BBT(%Del)	96	5.93(4.40)	0.0 - 30.0
cep3/3p-TPT(%Del)	74	17.24(10.26)	3.0 - 53.0
cep3/3p-TPAB(%Del)	37	5.00(3.49)	0.0 - 16.0
cep3/3p-TPNT(%Del)	68	3.78(2.91)	0.0 - 14.0
cep10/10q-BBNT(%Del)	82	1.56(1.43)	0.0 - 6.0
cep10/10q-BBT(%Del)	86	4.30(2.06)	0.0 - 11.0
cep10/10q-TPT(%Del)	66	11.06(6.68)	2.0 - 29.0
cep10/10q-TPAB(%Del)	25	4.96(3.36)	1.0 - 14.0
cep10/10q-TPNT(%Del)	67	2.52(2.15)	0.0 - 9.0
Cep3p-bpde(%Del)	90	2.01(0.59)	0.8 – 4.2
Cep10q-bpde(%Del)	70	1.60(0.58)	0.6 – 3.2

BBNT, bronchial brushings on non-tumor side; BBT, bronchial brushings on tumor side; TPT, touch preparation on tumor side; TPAB, touch preparation on adjacent normal tissue; TPNT, touch preparation on non-tumor side;3p-bpde (del), BPDE-induced 3p deletion; 10q-bpde (del), BPDE-induced 10q deletion.

Specific Aim 1.4 To assess concordance of findings in paired samples

Update

FISH analyses. We have evaluated the correlation between data from bronchial brushes and touch preparations. As summarized in Table 3, there was no correlation overall between pack-years smoked and deletion in 3p and 10q in bronchial brushes from either normal or tumor side. However, there is evidence of statistically significant correlations between 3p and 10q % deletions in bronchial brushes from the tumor side as described in the last report, between 3p % deletion in bronchial brushes from tumor side and 3p deletion in touch preparations from tumor side, and between 3p deletions in touch preparations from tumor, normal, and adjacent side and pack-years smoked.

Table 3. Correlation between data from bronchial brushes and touch preparations

Variable	packyr	Ppackyr	cep3pBBT	Pcep3pBBT	cep3pTPT1	Pcep3pTPT1
	Corr. Coef.	Pvalue	Corr. Coef.	Pvalue	Corr. Coef.	Pvalue
Packyr	1		0.025301605	0.812878131	0.19287334	0.104541775
cep3pBBNT	0.075100429	0.48425895	0.503216661	3.69879E-07	0.233845874	0.056833615
cep3pBBT	0.025301605	0.81287813	1		0.472942033	4.06711E-05
cep3pTPT1	0.19287334	0.10454178	0.472942033	4.06711E-05	1	
cep3pTPAB1	0.212435522	0.2135414	0.020376692	0.906101354	0.273289244	0.10170935
cep3pTPNT1	0.125968481	0.31353069	0.060181466	0.636647542	0.499864638	2.24076E-05
cep10qBBNT	-0.136368489	0.23697165	0.410090647	0.00021223	0.029316824	0.821052373
cep10qBBT	0.023063972	0.83805922	0.371807737	0.000684237	0.253510677	0.039988949
cep10qTPT1	-0.050100654	0.69420667	0.048116108	0.708047929	0.102970117	0.421933413
cep10qTPAB1	0.092132548	0.66852506	0.127250339	0.544414893	0.324393574	0.113636551
cep10qTPNT1	-0.026878208	0.83169144	0.052431482	0.678288628	0.079221777	0.537114146

BBNT, bronchial brushings on non-tumor side; BBT, bronchial brushings on tumor side; TPT, touch preparation on tumor side; TPAB, touch preparation on adjacent normal tissue; TPNT, touch preparation on non-tumor side.

We also received and processed close to 160 sputa and performed FISH and image analysis studies on almost 70 cases. Once we finish the FISH and image analysis, we will evaluate the correlation of the paired samples.

Telomere analysis. We have analyzed the correlation between telomere length in peripheral blood lymphocytes (PBLs) and telomere length in epithelial cells of bronchial brushings. We found a significant correlation between telomere length in PBLs and telomere length in epithelial cells of bronchial brushings on normal side ($p<0.0001$) but not significant on tumor side ($p=0.0838$)(Table 4). This might be due to the telomerase activation on the tumor side. There was also a significant correlation between telomere length in epithelial cells of bronchial brushings on normal side and telomere length in epithelial cells of bronchial brushings on tumor side ($P=0.0001$).

Table 4 Correlation of Telomere Length between PBLs and Lung Epithelial Cells from Bronchial Brushings

Tissue	*N*	*Correlation coefficient*	*P value*
Lymphocytes vs. Brushing normal side	71	0.5074	<0.0001
Lymphocytes vs. Brushing tumor side	73	0.2037	0.0838
Brushing normal vs. Brushing tumor side	69	0.4564	0.0001

We have also examined the correlation between telomere length and 3p aberrations in lymphocytes and target tissues (Table 5). Telomere length in epithelial cells of bronchial brushings on tumor side was significantly inversely associated with 3p aberrations in bronchial brushings from the tumor side ($p=0.0013$) and the normal side ($p=0.0021$), also with 3p aberrations in touch prep from the tumor tissues ($p=0.0064$) and the adjacent normal tissues ($p=0.0083$). Similarly, we found that telomere length in epithelial cells of bronchial brushings on the tumor side was significantly inversely associated with 10q aberrations in bronchial brushings

Table 5 Correlation of Telomere Length with Chromosome 3p Aberrations

Telomere Length	*PBLs*	*BBT*	*BBN*	*TT*	*NT*
LYMPHOCYTES					
N	63	77	75	61	55
Correlation coefficient	0.0793	-0.0771	-0.1608	0.066	0.0447
P-value	0.5365	0.5052	0.1683	0.6135	0.7458
BBN					
N	61	74	73	58	53
Correlation coefficient	0.1494	-0.1171	-0.2185	-0.1082	-0.1525
P-value	0.2504	0.3205	0.0633	0.4188	0.2757
BBT					
N	63	76	74	60	54
Correlation coefficient	0.0301	-0.3633	-0.3516	-0.3483	-0.3558
P-value	0.8146	***0.0013***	***0.0021***	***0.0064***	***0.0083***

BBT, bronchial brushings on tumor side; BBN, bronchial brushings on normal side; TT, tumor tissue; NT, adjacent normal tissue; Correlation coefficients were obtained from Spearman's correlation coefficient test.

from the tumor side (p=0.0261), normal side (p=0.0023), as well as with 3p aberrations in touch prep from the adjacent normal tissues (p=0.0061).

BPDE sensitivity (DNA repair capacity) analysis. We have also analyzed the correlation of BPDE sensitivity with 3p and 10q status. We found that BPDE sensitivity in lymphocytes was significantly positively associated with 3p deletion (p=0.0066) and aberrations (p=0.0024) in lymphocytes, and borderline significantly associated with 10q aberrations (p=0.0570) in lymphocytes (Table 6).

Table 6. Correlation between BPDE sensitivity and 3p and 10q Instability in PBLs

BPDE-sensitivity	*bp3pdel*	*bp10qdel*	*bp3paber*	*bp10qaber*
N	67	67	66	67
Correlation coefficient	0.3289	0.2077	0.3679	0.2337
P-value	***0.0066***	0.0917	***0.0024***	***0.0570***

bp3pdel: BPDE-induced 3p deletion; bp3paber: BPDE-induced 3p aberrations; bp10qdel: BPDE-induced 10q deletion; bp10qaber: BPDE-induced 10q aberrations; Correlation coefficient was obtained from Spearman's correlation coefficient test.

Project 2: Genetic Instability by Smoking Status
(Principal Investigator: Walter Hittelman, Ph.D.)

Specific Aim 2.1 To determine optimal conditions for detecting clonal changes using fluorescent inter-simple sequence repeat PCR (FISSR-PCR), standardize and validate FISSR-PCR for application to bronchial biopsy specimens

In prior Progress Reports, we reported that we had optimized the conditions of FISSR-PCR for DNA fingerprinting and showed that the results were fairly reproducible in premalignant and malignant cell lines. We also showed, using the BEAS2B, 1799, 1198, and 1170I lung cell progression model, that the number of detectable clonal changes increased as cells stepwise progressed from an immortalized to a malignant stage of lung tumor development. We also showed that each of these cell populations contained multiple subclonal populations distinguishable by FISSR-PCR and that the degree of subclonal variation increased as the cell populations moved toward the tumor phenotype. We also showed by sample mixing experiments that this technology was sufficiently sensitive for detecting subclonal variants if they occupied 20% of the total dissected population.

However, we have realized that the use of paraffin-embedded specimens limited our ability to carry out analyses on very small amounts of microdissected material due to limitations in DNA extraction from the paraffin-embedded material, limitations in the size of the PCR products to about 500 base pairs due to formalin-induced DNA cross links, and interference of detergent used in the DNA extraction with the fluorescence signal detection. We therefore decided to

optimize the conditions for FISSR-PCR reactions for use on frozen material. We focused on three initial components of the analysis. First, in collaboration with Dr. Ignacio Wistuba, we compared the laser capture microdissection technique with needle dissection and found that both techniques were suitable. Second, we optimized the DNA extraction methodology from the frozen tissue material, with or without phenol extraction and ethanol precipitation, and examined the effect of column purification of the DNA. Third, we optimized the PCR reaction by examining different PCR systems, including the effect of hot start PCR, different DNA polymerases, different PCR buffer systems, and different PCR temperatures.

Update

In the last year, we finished optimizing the conditions for FISSR-PCR analyses of frozen material, in collaboration with Dr. Ignacio Wistuba, and initiated an analysis of 16 lung cancer cases where we characterized the degree of clonal variation between different regions of the tumor resection specimen, including lung tumor regions (1-12 regions per case; mean 3.1), normal bronchial epithelial regions (1-10 regions per case; mean 4.0), and stromal regions (1-8 regions per case; mean 2.1). We used three primer sets for these studies, including a Fam-$(CA)^8$RG primer, a Fam-$(CA)^8$RY primer, and a FAM-$(AGC)^4$Y primer. All reactions were carried out in triplicate to ensure reproducibility. Only those peaks where all triplicate profiles consistently showed changes at least 50% of peak height were counted as DNA band changes. The utilization of three primer sets permitted analysis of between 224 and 328 different bands. Figure 1 provides an example of a comparison between a bronchial epithelial region (blue, mauve, and turquoise lines) and a stromal standard for the case (red, peach, and yellow lines). As shown in Figure 1, two band changes were evident in the bronchial epithelium compared to the stromal region.

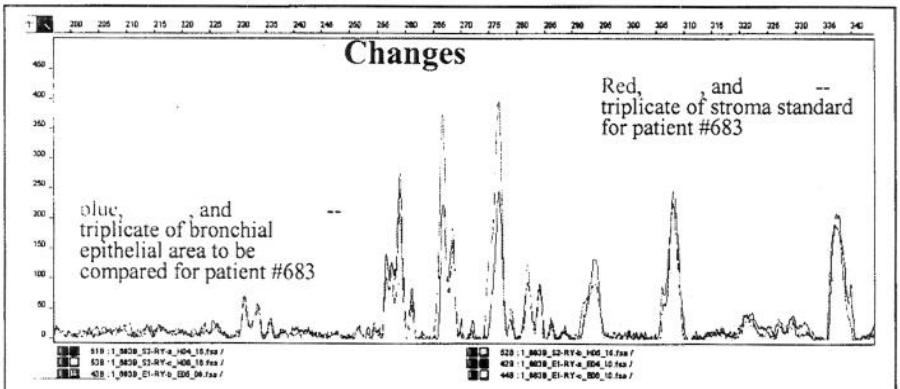

Figure 1. FISSR-PCR analysis example of comparison of a region of normal bronchial epithelium with a stromal region showing evidence for two band changes

The clinical and demographic characteristics of the 16 lung cancer cases whose tumor resections were examined by FISSR-PCR analysis are shown in Table 1. Fifteen of the 16 cases were adenocarcinoma and the remaining case was squamous cell carcinoma. As might be expected for studies based on surgical resection specimens, twelve of the 16 cases were pathological stage I tumors. With regard to smoking status, 9 cases involved former smokers, 5 cases involved current smokers, and two cases involved never smokers.

All regions dissected from the lung cancer specimens showed band alterations based on one standard pattern seen in an associated stromal region. As shown in Figure 2, the tumor regions showed the highest extent of clonal alteration compared to the stromal regions (median 6.03 band changes for 15 tumor region cases analyzed).

Table 1. Patient and Tumor Characteristics

Total patient		16	%
Gender			
	Male	10	62.5
	Female	6	37.5
Age		59.5 (40 – 79)	
Tumor type			
	Adenocarcinoma	15	93.8
	Squamous	1	6.2
Pathological stage			
	I	12	75.0
	III	4	25.0
Metastasis		None	
Smoking status			
	Never	2	12.5
	Former	9	56.25
	Current	5	31.25

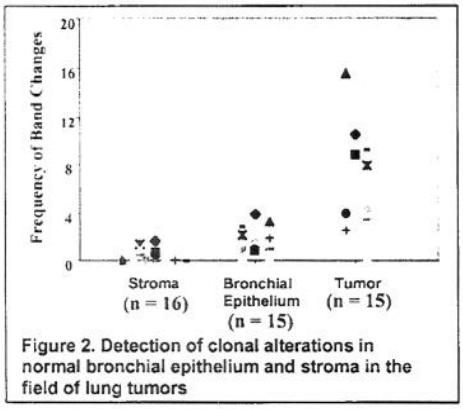

Figure 2. Detection of clonal alterations in normal bronchial epithelium and stroma in the field of lung tumors

Nevertheless, the degree of clonal change varied between tumor cases. Of importance, significant levels of clonal change were also apparent in regions dissected from normal-appearing bronchial epithelium in the lung cancer specimens, albeit at lower levels than that observed in the tumor regions (median, 1.89 band changes). Again, the degree of clonal change in normal appearing bronchial epithelium differed between cancer cases. Of interest, and somewhat surprisingly, small levels of clonal alterations were also detected in the stromal regions in some lung cancer cases (median, 0.43). While the levels of clonal alteration in the stroma were generally small compared to that found in the bronchial epithelium and in the tumor regions, it was still detectable in some cases at fairly high levels. An example of the changes observed in one lung tumor specimen is illustrated in Figure 3 and Table 2. In this case, as shown in Figure 3, 16 separate tumor regions and 3 normal regions were microdissected and subjected to FISSR-PCR analysis. The frequency of band changes in this case for the tumor regions was 14.6 while that in the normal regions was 1.6. Of interest, not all tumor regions showed identical band changes. While each region might have shown some common changes, there were also differences in specific band changes from region to region, suggesting both clonal evolution and subclonal variation within the lung tumor specimen. Also of interest, some of the normal regions contained identical individual band changes also found in the tumor, suggesting a possible precursor to product relationship. On the other hand, other normal regions showed no common changes with the tumor specimen suggesting a different premalignant pathway from that associated with the specific multistep tumorigenesis pattern in the tumor.

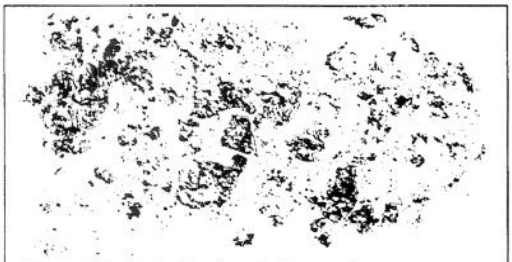

Figure 3. Regions microdissected from on lung cancer case

Tumor areas #7, #14, #15, and #16 share common DNA band changes (blue) and evidence for subclonal evolution (pink to cyan to green).

Area #14: 175G, 418G, 423G, 445L, 456G, 505L, 554L, 724L, 736G

Area #16: 175G, 418G, 423G, 445L, 456G, 505L, 724L, 736G

Area #15: 418G, 423G, 445L, 456G, 505L, 724L, 736G

Area #7: 423G, 445L, 456G, 505L, 724L

Seen in different non-tumor areas: 274L, or 385L, or 505L, or 554L, or 724L, suggests early precursor regions that evolves independently in tumor and non-tumor regions

Table 2. Examples of band changes observed in different tumor and normal regions of the case shown in Figure 3.

The data shown in Figure 2 suggested that there might be some relationship between the degree of clonal alteration in the tumor regions with that in the bronchial epithelial regions in the tumor specimen. When compared on a case-by-case basis, however, the relationship was not strictly monotonic (Figure 4). Similarly, while lung tumor specimens from former smokers

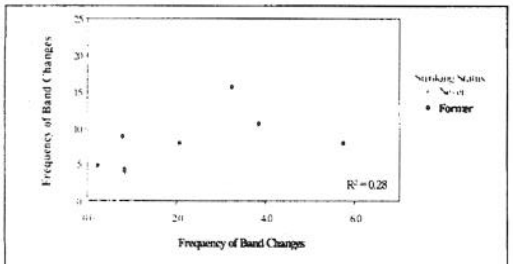

Figure 4. Correlation of the degree of clonal alterations apparent in the tumor regions compared to the bronchial epithelium.

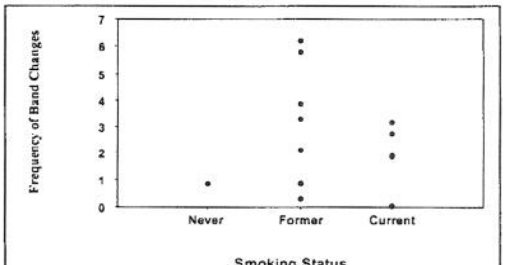

Figure 5. Relationship between smoking status and the frequency of clonal alterations detected in the tumor regions.

showed a slightly higher median frequency of clonal changes compared to current smokers, there was a high degree of overlap in clonal alteration frequencies between the two groups (Figure 5).

Taken together, these studies suggest that FISSR-PCR together with microdissection is sufficiently sensitive to quantify clonal and subclonal changes in lung tissues, including tumor, normal bronchial epithelium, and even stromal regions. These data validated our prior studies and that of others using LOH analysis that lung tumorigenesis represents a field process where tobacco exposure can create genetic changes throughout the exposed lung tissue leading to the presence of multifocal clonal outgrowths. The levels of clonal alteration in the bronchial epithelium tend to be less than that in the adjacent tumors. Nevertheless, there was weak concordance between the levels of clonal alteration in the tumor and in the normal bronchial epithelium, providing support for a strength component to the field effect. This finding is important in the setting of estimating risk of individuals without cancer since it suggests that random biopsies can still provide quantitative information for the tissue field as a whole. The studies in former smokers further support our prior in situ hybridization data suggesting that, despite smoking cessation, clonal outgrowths remain in the exposed tissue and contribute to the development of malignancy. Studies are currently ongoing in other projects to better understand the mechanisms that drive clonal outgrowth and continued genomic instability in lung tissues of former smokers.

The data were summarized in the Proc. AACR, 2004 (Lu and Hittelman).

Specific Aim 2.2 **To determine whether smoking status influences changes in clonal frequency and whether chemopreventive intervention has differential impact on clonal outgrowths in current and former smokers**

Update

Now we have developed the FISSR-PCR technique and are ready to examine and compare the degree of clonal alterations in the bronchial epithelium of current and former smokers who are at increased risk for lung cancer in association with their history of tobacco smoke exposure.

Our original research plan proposed the use of paraffin-embedded bronchial biopsies of subjects who participated in one of our chemoprevention clinical trials for current or former smokers where we had already characterized their degree of clonal alterations by FISH. However, as described above, we found that the FISSR-PCR assay is much more robust when frozen tissue is utilized. We therefore have identified a series of frozen biopsies from a group of individuals who were previously studied on these trials and chose two groups for further study based on the presence of high or low clonal alterations detected by FISH on paraffin embedded specimens.

To determine whether chemopreventive intervention has differential impact on clonal outgrowths in current and former smokers, we have started to analyze some cases. We have carried out the PCR reactions for more than 15 cases that had participated in the 4-HPR (chemopreventive agent) clinical trial that involved current smokers. As of this report, the FISSR-PCR data of three cases is available. In one case where two epithelial and two stromal regions were microdissected and analyzed by FISSR-PCR using two separate primers, compared to one of the stromal regions, one epithelial region showed 8 band changes while another epithelial region showed one change. Interestingly, the two stromal regions differed by one band. When six paraffin-embedded biopsies of this same case had been analyzed by chromosome in situ

hybridization previously, the chromosome indices had ranged from 1.44 to 1.54 (considered high) and the degree of chromosome polysomy had ranged from 4 – 5.8% (also considered high). Another specimen that showed basal cell hyperplasia showed 4 band changes in two separate epithelial regions and 1-2 band changes in two separate stromal regions. This case had previously shown chromosome indices of 1.28 – 1.35 and polysomes of 1.2-3.1% in six biopsy sites. A third case showed a low level of clonal alteration in one microdissected region. Thus, the early results from our ongoing analysis suggest that we can utilize FISSR-PCR to detect clonal alterations in the bronchial epithelium of individuals without lung cancer who are at increased lung cancer risk associated with their smoking history. In parallel, we will carry out FISH analyses on adjacent sections of these same biopsies to determine whether the two technologies yield parallel or distinct information.

The results were published in the Proc. AACR, 2004 (Lu et al.).

Project 3: Epithelial Biomarkers of Lung Cancer: Evaluation of Airway Secretions to Study Lung Carcinogenesis

(Project Leader: Ja Seok Koo, Ph.D.)

Specific Aim 3.1 To identify proteins whose secretion or release is different in squamous metaplastic tracheobronchial epithelial cells as compared to normal mucous epithelial cells

Primary normal human tracheobronchial epithelial (NHTBE) cells maintained in retinoic acid (RA)-sufficent media generate a fully-differentiated mucociliary bronchial epithelium, in contrast the cells become squamous metaplasia in RA-deficient media. This Aim seeks to identify proteins whose secretion or release is different in squamous metaplastic epithelial cells as compared to normal mucous epithelial cells. The identified squamous metaplasia-secreted/released proteins may be potential biomarkers to detect premalignant lesions in the early stage of lung carcinogenesis.

Update

Using the optimized conditions for 2D PAGE analysis we developed in the last years, we have found at least 174 unique spots in the ASF of squamous metaplastic NHTBE cells (Figure 1).

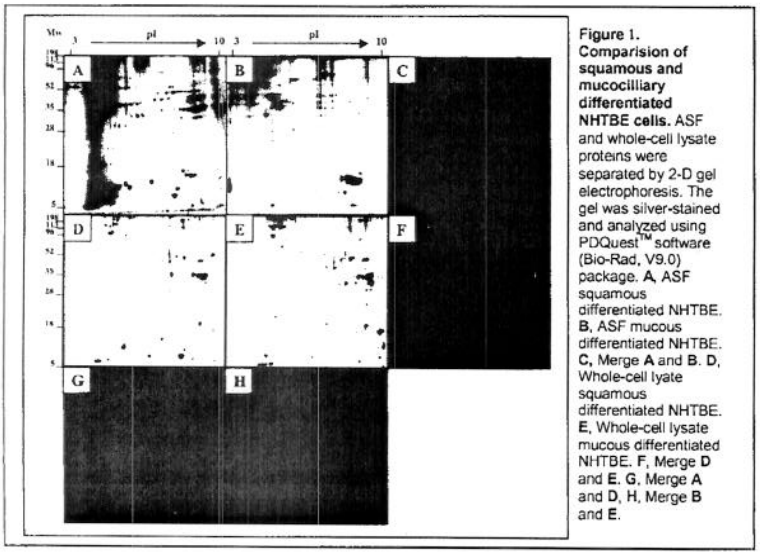

Figure 1. Comparision of squamous and mucocilliary differentiated NHTBE cells. ASF and whole-cell lysate proteins were separated by 2-D gel electrophoresis. The gel was silver-stained and analyzed using PDQuest™ software (Bio-Rad, V9.0) package. **A**, ASF squamous differentiated NHTBE. **B**, ASF mucous differentiated NHTBE. **C**, Merge **A** and **B**. **D**, Whole-cell lyate squamous differentiated NHTBE. **E**, Whole-cell lysate mucous differentiated NHTBE. **F**, Merge **D** and **E**. **G**, Merge **A** and **D**, **H**, Merge **B** and **E**.

Further analyzing the 174 spots using liquid chromatography-tandem mass spectrometry, we identified 23 unique proteins (Figure 2 and Table 1). Among them, squamous cell carcinoma antigen 1 (SCCA1), SCCA2, Annexin I, Annexin II, S100A8, and S100A9 were further confirmed for their unique expression and secretion in the ASF from the squamous metaplasia (Figure 3). A manuscript is in preparation. Specific Aim 1 has been completed.

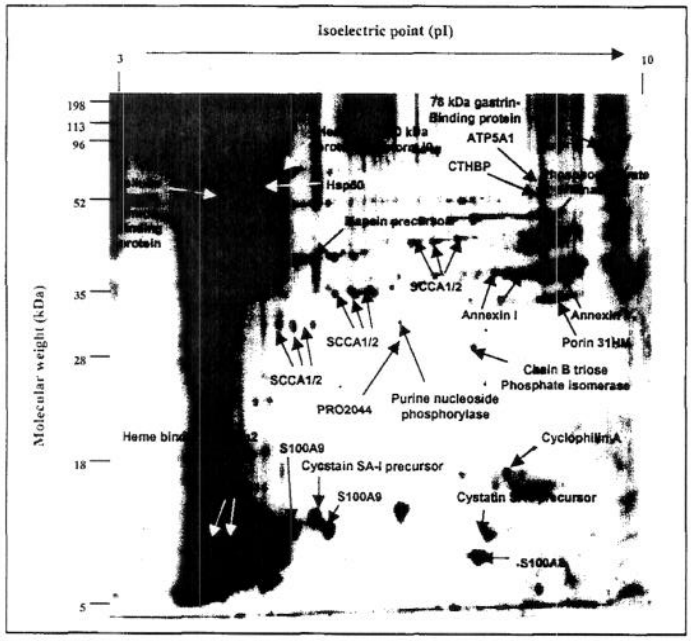

Figure 2. Typical 2-D PAGE picture of ASF squamous metaplasia NHTBE cells. Five hundred μg of proteins in ASF squamous NHTBE were separated by 2-D gel electrophoresis and silver-stained. More than 174 spots were differentially expressed in ASF squamous NHTBE cell. Arrow indicate differentially expressed spots identified by LC-MS/MS. The corresponding identifications are listed in Table 1.

Table 1. . List of uniquely expressed proteins in ASF squamous metaplasia NHTBE cell culture

Spot ID	Protein name	Accession number	Mr.(kDa)	pI
1	S100A8	NP_002955	10.9	6.7
2	Cystatin SA-I precursor	A28001	15.2	5.9
3	S100A9	NP_002956	13.2	5.6
4	S100A14	NP_055723	11.6	5.4
5	Chain A, Cyclophilin A Complexed With Cyclosporin A	3CYSA	17.9	8.1
6	Annexin I	NP_000691	37.3	8.1
7	Annexin II	NP_004030	36.6	8.5
8	Squamous cell carcinoma antigen 1 (SCCA1)	P29508	42.1	5.3
9	Squamous cell carcinoma antigen 2 (SCCA2)	P48594	42.1	7.0
10	Maspin precursor (Protease inhibitor 5)	P36952	42	5.2
11	Phosphoglycerate kinase 1	P00558	45.0	8.5
12	78 kDa gastrin-binding protein	P40939	78.0	9.0
13	60 kDa heat shock protein (Hsp60)	P10809	60.0	4.5
14	Heat shock 70kDa protein 8 isoform 1	NP_006588	69.7	8.0
15	Cytosolic thyroid hormone-binding protein (CTHBP)	P14618	57.3	8.5
16	Cellular thyroid hormone binding protein (p55)	P07237	55.0	4.0
17	ATP5A1 protein	AAH39135	60.9	8.5
18	Purine nucleoside phosphorylase	P00491	31.2	5.6
19	Porin 31HM	AAB20246	32.8	8.8
20	PRO2044	AAF22034	29.0	6.0
21	Chain B triose phosphate isomerase	1HTIB	26.7	6.5
22	Heme binding protein 2	NP_956492	20.5	4.0

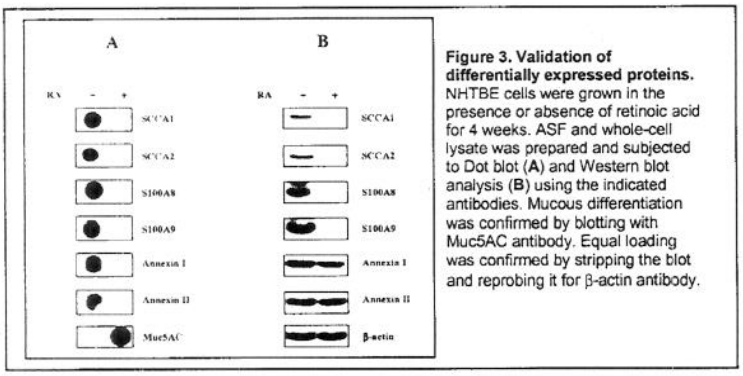

Figure 3. Validation of differentially expressed proteins. NHTBE cells were grown in the presence or absence of retinoic acid for 4 weeks. ASF and whole-cell lysate was prepared and subjected to Dot blot (**A**) and Western blot analysis (**B**) using the indicated antibodies. Mucous differentiation was confirmed by blotting with Muc5AC antibody. Equal loading was confirmed by stripping the blot and reprobing it for β-actin antibody.

Specific Aim 3.2 To identify and characterize abnormal proteins secreted by lung squamous cell carcinomas

Update

First, we tested whether the proteins identified from Specific Aim 1, which were abnormally overexpressed in non-tumorigenic squamous metaplasia compared to NHTBE cells, maintained their high levels in tumorigenic carcinoma cells. We found that expression of SCCA1 and 2 was progressively increased in transformed/tumorigenic lung carcinogenesis model cell lines (Figures 4-5) and only detected in squamous cell carcinomas, not in adenocarcinomas (Figure 6).

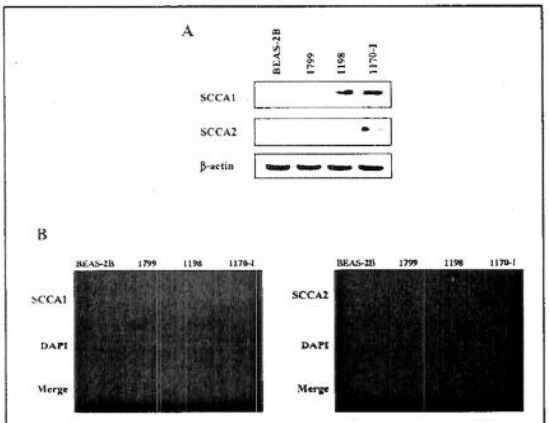

Figure 4. Expression pattern of SCCA1 and SCCA2 in lung carcinogenesis model cell lines. A, Immortalized human brochial epithelial (HBE, BEAS-2B and 1799) cells, transformed HBE cells (1198), and malignant HBE cells (1170-I) were analyzed. Equal amount of whole-cell lysate was subjected to Western blot analysis against SCCA1 and SCCA2 antibodies. ***B,*** Cells grown on coverslips were analyzed by fluorescence immunofluorescence analysis using same antibodies, followed by secondary antibody of Alexa Fluor-488 goat anti-mouse IgG. Nuclei were stained with DAPI (blue) and then merged with a fluorescent micrograph of SCCA and DAPI staining.

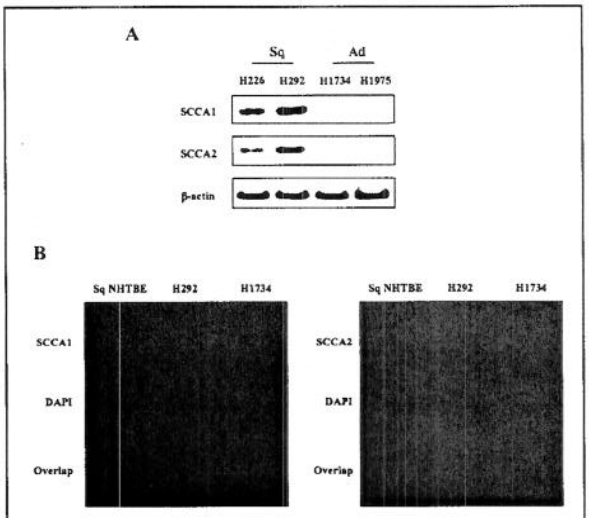

Figure 5. Expression pattern of SCCA1 and SCCA2 in NSCLC cells. A, NSCLC cell lines (squamous carcinoma cell line, NCI-H226 and NCI-H292; adenocarcinoma cell line, NCI-H1734 and NCI-H1975) grown and then whole-cell lysate was subjected to Western blot analysis against SCCA1 and SCCA2 antibodies. ***B,*** Cells grown on coverslips were analyzed by fluorescence immunochemistry analysis using the same antibodies.

As an alternative approach proposed in the grant, we also used an Affymetrix oligonucleotide chip technique to globally examine molecular changes in non-small cell lung carcinoma (NSCLC) cells. Comparing the gene expression profile of the NCI-H292 NSCLC cell line with that of NHTBE cells grown in a three-dimensional organotypic culture system that permits maintenance of the normal pseudostratified mucociliary phenotype characteristic of bronchial epithelium *in vivo*, we found that 1,683 genes showed a >1.5-fold change in expression in the H292 cell line relative to the NHTBE cells. Specifically, 418 genes were downregulated and 1,265 were upregulated in the H292 cells. The expression data for selected genes were validated in several different NSCLC cell lines using quantitative real-time PCR and Western blot analysis. Further analysis of the differentially expressed genes revealed that WNT responses, apoptosis, cell cycle regulation and cell proliferation were significantly altered in the H292 cells. Functional analysis using fluorescence-activated cell sorting confirmed concurrent changes in the activity of these pathways in the H292 line. These findings showed that NSCLC cells displayed the deregulation of the WNT, apoptosis, proliferation and cell cycle pathways as has been found in many other cancer types.

Data were published in *Mol Genet Genomics* (Ju et al., 2005). Specific Aim 2 has been completed.

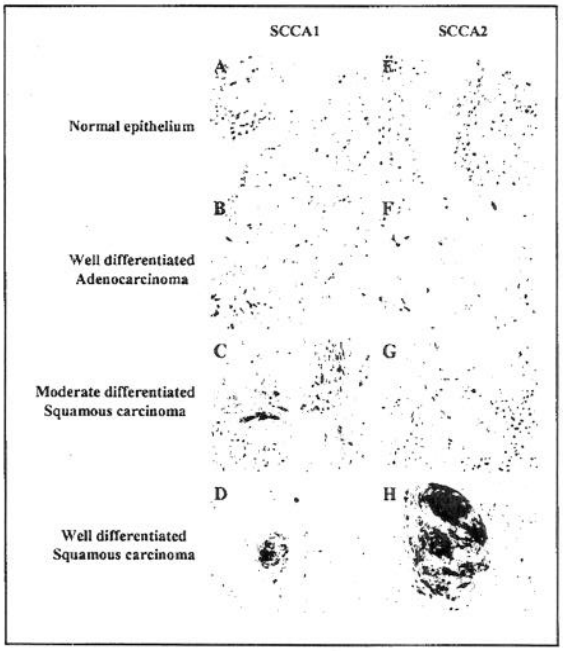

Figure 6. Immunohistochemical staining of SCCA1 and SCCA2. Normal epithelium tissue sections (***A***, ***E***), well-differentiated adenocarcinoma tissue sections (***B***, ***F***), moderate differentiated squamous carcinoma tissue (***C***, ***G***), and well-differentiated squamous carcinoma tissue sections (***D***, ***H***) were stained using anti-SCCA1 (Right panels) and anti-SCCA2 antibodies (Left panels).

Specific Aim 3.3 To evaluate the efficacy of differentially secreted proteins as novel biomarkers using readily-accessible clinical specimens

We proposed to examine whether the candidate biomarkers identified in Specific Aims 1 and 2 can serve as useful biomarkers for early detection of lung cancer using easily-accessible sputum and bronchial washing samples.

Update

Originally, we planned to obtain 50 subjects for this study after receiving approval for collection and laboratory analysis of sputum and bronchial washings. But since we have also involved a NIH Lung P01 program (PI- Waun Ki Hong) where we are responsible for collecting and using the same samples but for different purposes, we decided to use these samples for this aim as well, which saved time and effort in obtaining IRB approval.

We first examined SCCA 1 and SCCA2. 125 bronchial washing specimens were analyzed for SCCA1 and SCCA2 expression by immunoblotting. Processed bronchial washings containing total 50 μg of protein were subjected for dot-blotting using antibodies against SCCA1 and SCCA2. Currently, we are evaluating whether expression of SCCA1and SCCA2 is correlated

with histological phenotypes of the bronchial epithelia of the subjects. This study will be completed in the coming year.

Specific Aim 3.4 **To establish primary bronchial epithelial cells in culture and evaluate the expression of candidate biomarkers in bronchial epithelia of lung cancer patients.**

We proposed to investigate the expression and regulation of the biomarkers in bronchial epithelial cells in cultures and to address whether the molecular alterations are persistent during the development and differentiation of bronchial epithelium of the lung cancer patients. The source for epithelial cells is from bronchial biopsy tissues collected from 100 newly diagnosed, and previously untreated lung cancer patients who are undergoing surgery at M. D. Anderson Cancer Center.

Update

To date, we have obtained 44 bronchial tissue specimens from surgically removed lung sections of 44 different patients. Bronchial epithelial cells were successfully isolated from 36 tissue specimens and stored in liquid nitrogen for further studies proposed in Specific Aim 3.4.

To determine whether the epithelial cells have the capability to regenerate bronchial epithelia, bronchial epithelial cells isolated from 6 different patients were cultured by organotypic air-liquid interface culture method. The cultures successfully reconstructed pseudostratified bronchial epithelium. We are currently testing the expression of the putative biomarkers identified from Specific Aims 3.1 and 3.2 in the organotypically cultured primary bronchial epithelial cells from the lung cancer patients.

Project 4: Prognostic Role of Promoter Hypermethylation of Death-Associated Protein (DAP) Kinase and p16 in Early-Stage Non-Small Cell Lung Cancer

(Project leader: Charles Lu, M.D.)

Specific Aim 4.1 **To examine the relationship between hypermethylation of the death-associated protein (DAP) kinase gene promoter and disease-free, disease-specific, and overall survival in completely resected, early-stage NSCLC.**

Specific Aim 4.2 **To examine the relationship between hypermethylation of the p16 gene promoter and disease-free, disease-specific, and overall survival in completely resected, early-stage NSCLC.**

Specific Aim 4.3 **To examine the relationship between hypermethylation of the p16 promoter and history of tobacco smoke exposure in early-stage NSCLC.**

Specific Aim 4.4 **To determine the independent prognostic significance of the molecular biomarkers after adjusting for relevant clinicopathologic variables**

The specific goal of this research proposal is to determine the prognostic importance of promoter hypermethylation of selected candidate genes in patients with early-stage, resected NSCLC who have been followed as part of a clinical research database. This study will create a high-quality database that includes clinical information in addition to surgical pathology data. Subjects in this study are identified from a clinical research database of patients who have undergone surgical resection by faculty members of the Department of Thoracic and

Cardiovascular Surgery, The University of Texas M. D. Anderson Cancer Center. This database was established in 1997, and includes all patients who undergo thoracic surgical resection at M. D. Anderson Cancer Center. Detailed demographic, clinical, and pathologic data are recorded using standardized data collection forms. Follow-up clinical information is also collected at each clinic visit. Patients with completely resected NSCLC with pathologic stages I or II who do not receive post-operative adjuvant therapy (either chemotherapy or chest radiotherapy) are eligible for this protocol. The proposed sample size is 300 subjects.

A query of the Department of Thoracic Surgery clinical research database yielded an initial list of 559 patients who underwent surgery between January 1, 1997 and December 31, 2001. To date, the medical records of these 559 patients have been screened, and 362 (64.7%) eligible subjects have been identified. Our collaborator in the Department of Pathology (Dr. Ignacio Wistuba) has reviewed these screened patients to confirm tumor histology and to determine if sufficient surgical tissue samples (paraffin blocks) exist to perform the required hypermethylation assays. 285 paraffin blocks have been retrieved. 282 subjects have had DAP kinase and p16 promoter hypermethylation assays performed on their tumor specimens in the laboratory of Dr. Li Mao. Subjects with available tumor tissue and hypermethylation assays completed have been entered into the study database.

Update

In the past year, we further conducted a thorough review of the clinical data for these subjects (gender, age, tumor histology, preoperative clinical variables, performance status, weight loss, smoking status), and obtained updated follow-up information (date of disease recurrence, date of death/last follow-up, development of second primary tumors) from our institution's medical informatics Department, the Social Security Death Index, and direct telephone inquiries. Patient characteristics are summarized in Table 1.

Characteristic	Number (%)
Total number	282
Gender	
Male	128 (45.4)
Female	154 (54.6)
Race	
White	255 (90.4)
Black	13 (4.6)
Other	14 (5.0)
Smoking Status	
Current	113 (40.0)
Former	103 (36.5)
Never	66 (23.4)
Stage	
IA	135 (47.8)
IB	92 (32.6)
IIA	11 (3.9)
IIB	44 (15.6)
Histology	
Adenocarcinoma	171 (60.6)
Adenosquamous carcinoma	6 (2.1)
Bronchioloalveolar Carcinoma (BAC)	8 (2.8)
Squamous Cell Carcinoma	82 (29.1)
Large Cell Carcinoma	10 (3.5)
Other	5 (1.8)
Grade	
Well differentiated	43 (15.2)
Moderately differentiated	120 (42.6)
Poorly differentiated	112 (39.7)
N/A	7 (2.5)
ECOG Performance Status	
0	178 (63.1)
1	103 (36.5)
2	1 (0.4)
Weight Loss >/=5%	19 (6.7)
Outcome Events	
Deaths	107 (37.9)
Recurrent NSCLC	60 (21.3)
Second Primary Tumors	23 (8.2)

Table 1. Summary of Patient Characteristics Who Have Hypermethylation Data of DAP Kinase and p16 Kinase

We are now in the process of conducting correlation analysis between the status of hypermethylation of DAP kinase and p16 and patient survival and tobacco smoke exposure. Manuscript preparation will begin shortly thereafter.

This project has produced a valuable clinical-pathological database.

Project 5: An Epigenetic Approach to Lung Cancer Therapy
(Principal Investigator: Reuben Lotan, Ph.D.)

The objective of Project 5 is to examine the potential of using agents such as histone deacetylase inhibitor SAHA and demethylating agent 5-aza-2-deoxycytidine (5-aza-CdR) that modulate epigenetic events of deacetylation and demethylation and their combination for chemoprevention and therapy of lung and head and neck cancers.

In the past year we have made progress in all Specific Aims.

Specific Aim 5.1 **To evaluate ability of SAHA and 5-aza-CdR used as single agents and in combination to inhibit *in vitro* growth and induce apoptosis in various lung cancer cell lines**

Previously we reported that premalignant lung bronchial epithelial cells and premalignant oral cavity epithelial cells were very sensitive to SAHA and 5-aza-CdR when used as single agents while normal cells were less affected by SAHA.

Update
In the past year, we conducted extensive sequential and combination treatments of premalignant and malignant lung epithelial cells with 5-aza-2-deoxycytidine followed by a combination of the same agent with SAHA. The sequential treatment resulted in more than additive growth inhibitory effects and in some dose ranges the results even appeared to be synergistic. Dr. Jack Lee, who leads the Biostatistics Core, is evaluating the data now.

Specific Aims 5.2 and 5.4 **To study mechanism of action of SAHA, 5-aza-CdR and their combinations on cell growth inhibition and apoptosis induction**

Update

For the last three years, we have made substantial progress in this Aim. We submitted a manuscript describing our findings on the mechanism of apoptosis induction by SAHA to the journal Molecular Cancer Therapeutics (Lotan et al., 2005). It has been reviewed favorably but the reviewers asked for several additional experiments. Therefore, we performed the experiments required to get the paper published and are preparing to resubmit the revised manuscript. The new experiments have led to the following results: 1) we used a new antibody that recognizes both intact and cleaved poly(ADP)ribose polymerase (PARP) and the new data confirmed that SAHA-induced apoptosis involved cleavage of the caspase-3 substrate PARP; 2) to determine whether inhibition of Fas signaling and specific caspases increases tumor cell survival, we used a clonogenic survival assay. We found that blocking activation of specific caspases and Fas signaling using small interfering RNA (SiRNA) increased tumor cell survival in the presence of SAHA; 3) the same SiRNAs also showed that both caspases 8 and 9 mediated apoptosis after SAHA treatment; 4) we also tested the possibility that SAHA activated

death receptors DR4 and DR5, which bind the ligand TRAIL. Only minor increase in DR4 and no change in DR5 were noted after SAHA treatment.

Specific Aim 5.3 **To determine the ability of SAHA, 5-aza-CdR and their combinations to inhibit the growth of non-small cell lung cancer cells implanted subcutaneously in athymic nude mice**

Update

We performed the *in vivo* experiments as described below. Sixty eight female 4-week-old athymic *nu/nu* nude mice (Harlen, Inc. Indianapolis, IN) were injected s.c. bilaterally with 1×10^6 cells of non-small cell lung cancer cell line H157ASRARbeta in 0.1 ml of PBS. The mice were maintained without any treatment until tumors reached a volume of ~100 mm^3. For administration to mice, SAHA was dissolved and diluted in a vehicle of DMSO. Each group of mice received 25, 50, or 100 mg/kg SAHA daily as a single agent or combined with a fixed 5-aza-CdR dose of 1 mg/kg by i.p. injection. The mice were weighed three times during the experimental period to assess toxicity of the treatments, and the tumors were measured every three days using calipers. Tumor volume was calculated from the two-dimensional caliper measurements using the following formula: Tumor volume = length x $(width)^2 \times \pi/6$

The treatment period was planned for 21 days when the vehicle-treated group of mice was expected to develop tumors with about 1 cm diameter. However, the groups that received 1mg/kg 5-aza-CdR only and combination with SAHA (25, 50 and 100 mg/kg) started dying of toxicity on Day 10 of the treatment. Therefore, we decided to sacrifice all animals to end this experiment on Day 12 of treatment. This did not compromise the experiment insofar as the vehicle-treated group (DMSO) of mice developed tumors with 1 cm diameter by Day 12. On the final day of the study, all mice were sacrificed by carbon dioxide inhalation and the body and tumor were weighed. The subcutaneous tumor was removed and divided into two pieces; one was snap frozen in liquid nitrogen and one was fixed in 10% formalin and embedded in paraffin. SAHA alone did not cause weight loss or mortality at any of the doses used. However, 5-aza-CdR was toxic and caused about 50% of mortality by Day 12. The results indicated that SAHA caused a dose dependent decrease in tumor growth and 5-aza-CdR was also somewhat effective at 1 mg/Kg. Furthermore, combinations of SAHA and AZA at each SAHA dose were more effective than either agent alone.

We will repeat the experiments with lower 5-aza-CdR concentrations and lower tumor cell initial injection to allow for a longer treatment period and will use the tumors for Specific Aim 5.4 to elucidate the *in vivo* anti-tumor effects.

Specific Aim 5.4 **To investigate mechanisms of *in* vivo anti-tumor activity of SAHA, 5-aza-CdR, and their combinations**

Once we observe some anti-tumor activity of SAHA, 5-aza-CdR, or their combinations in athymic nude mice, we can proceed with Specific Aim 5.4.

Specific Aim 5.5 **To analyze differential gene expression between untreated and treated NSCLC cells with SAHA, 5-aza-CdR and their combinations using Affymetrix oligonucleotide microarrays and characterize genes that may mediate apoptosis induction.**

Update

We completed the analysis of genes that are regulated by SAHA , 5-aza-dC, or the combination using an Affymetrix oligonucleotide micro array U133A. The Bioinformatics group of the

Affymetrix Core processed the results of the analysis and found that using a cutoff of 2.5 fold change, 25 genes were upregulated and 33 downregulated by 5-aza-dC; 59 genes upregulated and 9 downregulated by SAHA.

In the coming year, we plan to first confirm some of these genes by quantitative -PCR and then analyze them by using pathway software to determine functions of selected genes as mediators of cell growth inhibition or apoptosis. For further functional studies, we will overexpress these genes in cell lines that do not express them or silence them with interfering RNA in cells that express the genes constitutively.

Project 6: The Role of the Farnesyl Transferase Inhibitor SCH66336 in Treatment of Carcinoma of the Aerodigestive Tract

(Project leader: Fadlo Khuri, M.D.)

Specific Aim 6.1 To evaluate effects of SCH66336 on Ras downstream signaling and apoptosis and angiogenesis in lung and head and neck squamous cell carcinoma cells

Update

Previously, we reported that SCH66336 inhibited cell growth and decreased p-Raf and Akt, but did not modulate Erk1/2 activities in the head and neck cancer cell lines. In the current study, we further examined effects of SCH66336 on Akt and Raf/ERK signaling pathways in a panel of non-small cell lung cancer (NSCLC) cells and found that SCH66336 did not decrease the levels of p-Akt, Akt, Raf-1, p-ERK1/ERK2, and ERK1/ERK2. In at least two of the cell lines, SCH66336 actually increased p-Akt and p-GSK3β (a well-known substrate of Akt) levels in a dose- and time-dependent manner (Figure 1). We also examined the effects of another farnesyl transferase inhibitor (FTI), R115777, on these signaling pathways. Interestingly, we found that R115777 did not decrease the levels of p-Akt, Akt, Raf-1, p-ERK1/ERK2, and ERK1/ERK2 either. Like CH66336, R115777 increased p-Akt and p-GSK3β levels in some NSCLC cell lines (Figure 2).

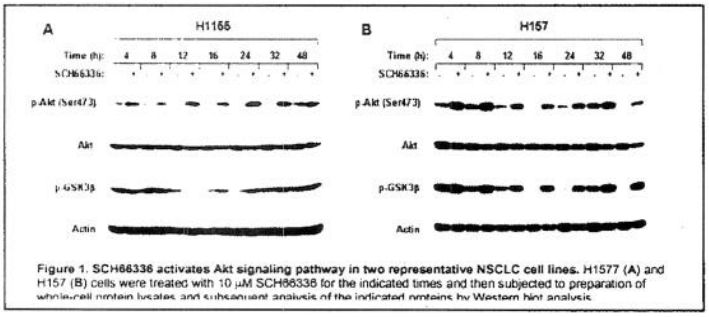

Figure 1. SCH66336 activates Akt signaling pathway in two representative NSCLC cell lines. H1577 (A) and H157 (B) cells were treated with 10 μM SCH66336 for the indicated times and then subjected to preparation of whole-cell protein lysates and subsequent analysis of the indicated proteins by Western blot analysis.

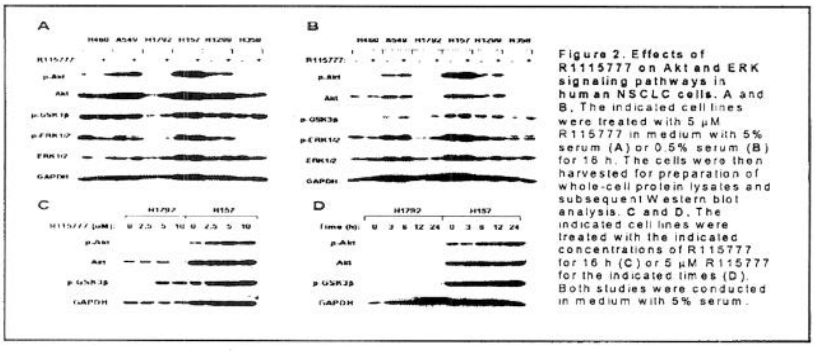

Figure 2. Effects of R1115777 on Akt and ERK signaling pathways in human NSCLC cells. A and B, The indicated cell lines were treated with 5 μM R115777 in medium with 5% serum (A) or 0.5% serum (B) for 16 h. The cells were then harvested for preparation of whole-cell protein lysates and subsequent Western blot analysis. C and D, The indicated cell lines were treated with the indicated concentrations of R115777 for 16 h (C) or 5 μM R115777 for the indicated times (D). Both studies were conducted in medium with 5% serum.

These results suggest that inhibition of protein farnesylation in some NSCLC cell lines activates Akt survival signaling pathway. We are currently investigating whether FTI-induced Akt activation leads to cell resistance to FTIs.

Specific Aim 6.2 **To evaluate effects of SCH66336 on protein expression in lung and head and neck cancer cell lines and determine roles of affected proteins as biomarkers of response to treatment with SCH66336**

As proposed in our grant, we planned to use two-dimensional gel electrophoresis (2-DE) and mass spectrometry strategy to identify proteins whose expression is affected by Farnesyl transferase inhibitors (FTIs), focusing on apoptosis-associated proteins. Since several laboratories in different institutes have started to use the same strategy to identify FTI – affected targets, we decided to adopt a different approach.

Currently, there are two major apoptotic pathways, death receptor-mediated pathways and mitochondrial-mediated pathways (Green et al., 2000). Death receptor 5 (DR5) has attracted much attention because its ligand TRAIL preferentially induces apoptosis in transformed or malignant cells, demonstrating potential as a tumor-selective apoptosis-inducing cytokine for cancer treatment (Wang et al., 2003; Almasan et al., 2003). We also know that certain therapeutic agents induce the expression of DR5 and trigger apoptosis (Fulda et al., 2004; Debatin et al., 2004). Thus, we decided to directly examine the effects of SCH66336 on the death receptor-mediated pathways.

Update

We found that SCH66336 activated caspase-8 and its downstream caspases, whereas the caspase-8 specific inhibitor Z-IETD-FMK or small interfering RNA (siRNA) abrogated SCH66336-induced apoptosis. Moreover, SCH66336 increased the expression of DR5 and its cell surface distribution in NSCLC cells as well as other types of cancer cell lines. The combination of SCH66336 with its ligand TRAIL further enhanced induction of apoptosis. Overexpression of a dominant-negative FADD mutant or silencing of DR5 expression using a siRNA attenuated SCH66336-induced apoptosis. These results indicate a critical role of DR5-mediated extrinsic apoptotic pathway in SCH66336-induced apoptosis. Moreover, the potencies of FTIs on DR5 induction are associated with their abilities to inhibit protein farnesylation and to induce apoptosis. Collectively, we conclude that FTIs, particularly SCH66336, induce DR5 expression leading to a caspase-8-mediated apoptosis and enhancement of TRAIL-induced apoptosis. These effects may be related to their farnesylation inhibitory activity. Detailed work can be reviewed in the Journal *Cancer Research* (Sun et al., 2005).

In parallel, we also found that R115777 upregulated DR5 expression and enhanced TRAIL-induced apoptosis in human NSCLC cells. Silencing of DR5 expression abrogated R115777-induced enhancement of TRAIL-induced apoptosis, suggesting that R115777 enhances TRAIL-induced apoptosis through DR5 upregulation. An additional experiment showed that R115777 also increased DR5 mRNA levels, suggesting that R115777 increases DR5 expression at the transcriptional level. Collectively, we have identified DR5 as a protein that is regulated by FTIs and plays an important role in mediating FTI-induced apoptosis.

Because the protein c-FLIP is well known to inhibit the death receptor-mediated apoptosis, we examined the effects of FTIs on c-FLIP. We found that FTIs increased the levels of c-FLIP in some NSCLC cell lines, particularly those having Akt activation upon FTI treatment, but decreased c-FLIP levels in other NSCLC cell lines. It seems that cells exhibiting increased c-

FLIP upon FTI treatment were less sensitive to FTI-induced apoptosis than those with decreased c-FLIP on FTI treatment. The impact of c-FLIP modulation in FTI-induced apoptosis of NSCLC cells is under investigation.

Taken together, we have so far identified two proteins, DR5 and c-FLIP, which are modulated by FTIs in FTI-induced apoptosis.

Specific Aim 6.3 **To evaluate the efficacy of SCH66336 as an inhibitor of growth and an inducer of apoptosis in an orthotopic model of head and neck squamous cell carcinoma**

Update
SCH66336 did not work effectively as a single agent in the clinic, thus we will focus our study on the efficacy of the combination of a FTI with other agents such as PI3K inhibitors or Akt inhibitors in animal models. We hypothesize that blockage of Akt activation induced by an FTI will enhance FTI's anticancer efficacy.

Specific Aim 6.4 **To investigate mechanisms of farnesyl transferase inhibitor - induced apoptosis in combination with retinoids such as 4-HPR or taxanes such as docetaxel and paclitaxel in non-small cell lung cancer and squamous head and neck cancer cell lines**

As described in the last report, in collaboration with Dr. Giannakakou's group at the Winship Cancer Institute, we found that SCH66336 increased microtubule stabilization and acetylation, and suppressed microtubule dynamics. The treatment of the combination of low doses of SCH66336 with paclitaxel markedly enhanced tubulin acetylation (a marker of microtubule stability) as compared with either drug alone. Further, we identified that this synergistic effect required functional histone deacetylase 6 (HDAC6) (a only known tubulin deacetylase), but not a catalytic-mutant HDAC6.

Detailed description of this work can be reviewed in the Journal *Cancer Research* (Marcus et al., 2005).

Project 7: Mechanisms and Therapeutic Applications of the Tumor Suppressor Gene *FUS1* in Lung Cancer
(Project Leaders: Lin Ji and Rajagopal Ramesh)

Specific Aim 7.1 **To determine the global molecular changes and cellular responses to FUS1-mediated tumor-suppressor activities in human NSCLC cells by high throughput gene and protein expression profiling.**

We will use gene microarrays and ProteinChip arrays and an inducible-FUS1 expression system to determine the gene and protein expression patterns mediated by induction of FUS1 in NSCLC cells at either a therapeutic or physiological level. The specific targets of FUS1 protein will be identified by comparison of the gene and protein expression profiles, and proteins of interest will be isolated.

As reported previously, we have established FUS1-stable transfectants of NSCLC cell lines, which allow us to detect gene and protein expression changes mediated by FUS1 expression

under physiological conditions. We have developed a novel two- dimensional liquid chromatography (2D-LC) method for the fractionation and separation of crude protein lysates and for protein profiling and identification using a ProteinChip Array-based surface enhanced laser deposition/ionization time of flight mass spectrometry (SELDI-TOF-MS). We have successfully applied this technology to perform a proteomic analysis for evaluating modulations of protein expression in FUS1-expressing tumor cells, compared with non-expressing controls. From protein expression profiles, we have been able to detect more than 50 protein peaks that represent the differentially expressed protein species in response to the activation of FUS1 protein in lung cancer cells.

Update

In the last year, we have also performed gene expression profiling on RNA samples prepared from the same inducible FUS1-expression NSCLC cells as used for protein profiling described above. Instead of using Affymetrix HG-U133A GeneChips, we used more advanced Illumina Sentrix BeadChips (Illumina Inc., San Diego) for whole-genome expression profiling of multiple samples on a single chip. The Illumina BeadChip holds six whole-genome human samples on one chip, interrogating approximately 48,000 transcripts in each sample from the estimated 30,000 genes in the human genome. We have identified approximately 210 genes whose expression was modulated by the activation of FUS1 in the FUS1-deficient NSCLC cells. We are now in a process to systematically analyze these FUS1-targeted cellular proteins and genes based on the protein and gene expression profiles by using an integrated bioinformatics tools and biological pathway finding software to elucidate the FUS1-activated biological pathways as we planned in this study.

Specific Aim 7.2 **To elucidate the molecular mechanism of FUS1 in lung cancer pathogenesis by determining the expression and subcellular localization of the FUS1 protein in human normal lung tissue and tumor samples at various stages of lung cancer development.**

We have previously demonstrated the loss of expression or a defect of myristoylation of the Fus1 protein in human primary lung cancer and cancer cell lines and showed that myristoylation is required for Fus1-mediated tumor-suppressing activity. The restoration of the wild-type FUS1 in 3p21.3-deficient non-small cell lung carcinoma (NSCLC) cells significantly suppressed tumor cell growth by induction of apoptosis and alteration of cell cycle kinetics *in vitro* and *in vivo*. We also found that FUS1 protein directly interacts with the apoptotic protease-activating factor 1 (Apaf-1) and functions as a key mediator in the Apaf-1-mediated apoptosis signaling pathway by recruiting and directing cytoplasmic Apaf1 to mitochondria and ER membrane and activating it in situ.

Update

In the last year, we further identified that Apaf-1 protein expression is universally detected in various lung cancer cell lines, most of which lack FUS1 expression. Activation of wt-FUS1 protein in FUS1-defficient cancer cells recruits cytoplasmic Apaf-1 proteins to the critical mitochondria and perinuclear membranes for apoptosome assembly and apoptosis induction. The apaf-1 protein appeared to be inactive in the FUS1-defficient tumor cells as demonstrated by the lack of the ATPase activity that is essential for the formation of the Apaf1-apoptosome and the activation of caspase-9. Induced or enforced expression of the endogenous or the exogenous FUS1 proteins activates Apaf-1 by induction of its ATPase activity in situ through FUS1-Apaf1 protein interaction, triggers release of Cytochrome C, activates caspases 9 and 2, and induces apoptosis. These findings are summarized in Figure 1 .

As proposed, we further refined the FUS1 protein expression in stage 1 NSCLC by using tissue microarrays (Figure 2). We found that about 45% of these lung tumors showed a complete loss of FUS1 expression, 52% exhibited a marginal low level expression, and only 2 of 83 tumors showed a normal level of FUS1 expression. These results suggest a role of FUS1 as a potential tumor suppressor and a role in lung cancer development due to the inactivation of FUS1 in primary lung cancer possibly by a mechanism of haploinsufficiency in human chromesome 3p21.3 region.

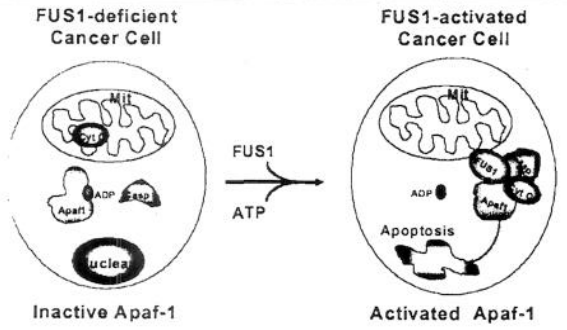

Figure 1. FUS1-mediated activation of Apaf1-mediated apoptotic pathway in human lung cancer. Loss of FUS1 protein expression and/or deficiency of posttranslational myristoyl modification of FUS1 proteins were found in a majority (>70%) of human primary lung tumor and tumor-derived cell lines. Apaf1 were universally detected in almost all lung cancer cell lines tested but were spatially and temporally inactive due to lack of the essential ATPase activity. Reactivation of FUS1 in FUS1 deficient tumor cells, recruits Apaf1 to a crucial mitochondrial or ER and peri-nuclear membrane subcellulocations, triggers cyto C release, and activate Apaf1 in situ through a direct protein-protein interaction, and, therefore, facilitates Apaf1-mediated apoptosome assembly and activation of caspase cascades and apoptosis.

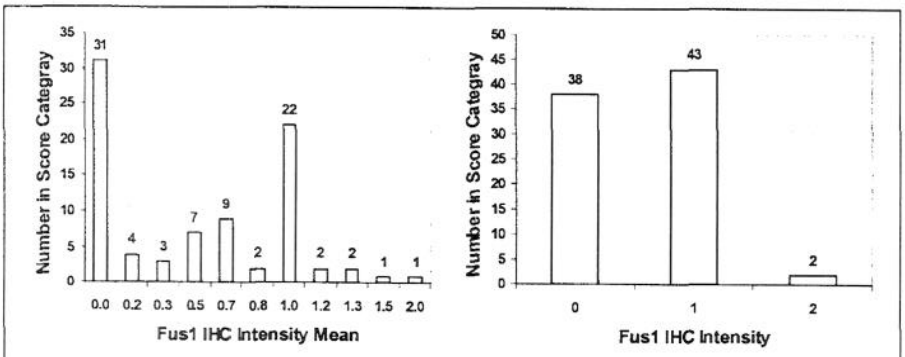

Figure 2. FUS1 IHC Staining from the Tissue Microarray in Stage I NSCL Patients (n = 83). The scale is 0-2 with 2 being the most intense staining. It is interesting that about half the patients show no staining. For comparison we need to know the level of expression in normal tissues. This is the first large series for FUS1 IHC.

Specific Aim 7.3 **To quantitatively evaluate interactions of the *FUS1* gene with other 3p21.3 TSGs for their tumor-suppressing activities *in vitro* and *in vivo***

We propose to study the additive, synergistic, or antagonistic effects of the interactions of the FUS1 gene with other 3p21.3 tumor suppressor genes.

Update

As reported previously, we noticed that the tumor suppression function of FUS1 and several other potential 3p21.3 TSGs were directly or indirectly dependent of p53 activity. In this study, we evaluated the combined effects of FUS1 and p53 on tumor cell growth and apoptosis induction in NSCLC cells co-transfected with FUS1- and p53-nanoparticles and explored molecular mechanisms of their mutual actions *in vitro*. We found that co-expression of wt-p53

with the wt-FUS1, but not the dysfunctional myristoylation-deficient mutant (mt-FUS1), synergistically inhibited cell proliferation and induced apoptosis in various human NSCLC cells (Figure 3). We found that the observed synergistic tumor suppression by FUS1 and p53 concurred with the FUS1-mediated down regulation of MDM2 expression and the resultant accumulation and stabilization of p53 protein as well as up-regulation of Apaf-1 expression and activation of caspase cascade in Apaf-1-associated apoptotic pathway in human NSCLC cells. Our results therefore revealed a novel molecular mechanism involving FUS1-mediated tumor suppression function and its interaction with other cellular components in the pathways regulating p53 and Apaf-1 activities.

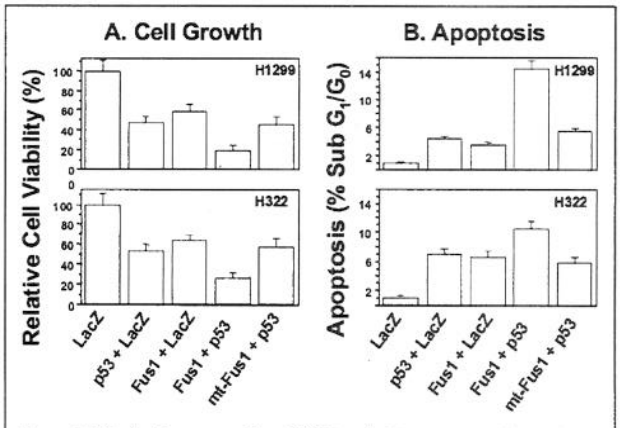

Figure 3. Effects of co-expression of FUS1 and p53 on tumor cell growth and apoptosis in NSCLC H1299 and H322 cells. H1299 (FUS1 and p53-nun) and H322 (FUS1-nun and p53-mutant) cells were co-transfected with FUS1- and p53 plasmid DNAs for 48 h. Cell viability was determined by a XTT asay and apoptosis by TUNEL-staining with FACS, respectively. **mt-FUS1**, dysfunctional mutant of wt-FUS1.

Another aspect we investigated but beyond the scope of the proposed work is to determine interaction effects of FUS1 with chemotherapy or radiotherapy on anti-tumor activity of lung cancer. We evaluated the anti-tumor effects of over-expressed FUS1, or FUS1 plus p53, with DNA-damaging agents cisplatin (CDDP) and γ-radiation on human NSCLC cells and explored molecular mechanisms of their mutual actions *in vitro*. We found that enforced expression of FUS1, or FUS1 plus p53, enhanced the sensitivities of NSCLC cells to these DNA-damaging agents. We also found that coexpression of p53 with wild type FUS1 (wt-FUS1), but not its dysfunctional myristoylation-deficient mutant (mut-FUS1), significantly enhanced sensitivities of NSCLC cells to treatment with CDDP or radiation. Moreover, we found that the observed enhancement of chemosensitivity and radiosensitivity by FUS1, or FUS1 plus p53, is associated with FUS1-mediated down-regulation of Mdm2 expression and the resultant accumulation of p53 as well as the up-regulation of Apaf-1 expression in NSCLC cells.

Specific Aim 7.4 **To determine the dose-limiting toxicity and biodistribution of the FUS1-lipoplex in a murine model and in a non-human primate model and to evaluate the therapeutic effect of the FUS1-lipoplex in local, solid tumors and experimental metastatic lung tumors.**

Results from these preclinical studies in this Aim have been summarized and reported previously. These studies were used for a successful filing of a Phase I clinical trial for FDA approval. Currently, the systemic treatment of DOTAP:cholesterol:FUS1 DNA complexes is in a Phase I trial for late stage lung cancer patients.

Specific Aim 7.4 has been accomplished.

Project 8: Therapeutic Targeting of bcl-xl Expression in Non-Small Cell Lung Carcinoma
(Principal Investigator: W Roy Smythe, M.D.)

The project was completed and reported in 2004.

Project 9: Use of Perfluorocarbons to Enhance Pulmonary Gene Transfer
(Principal Investigator: Ara Vaporciyan, M.D.)

In the past year, our laboratory encountered a number of delays. Some personal issues resulted in loss of manpower for two months. In addition, an adequate amount of the adenoviral vector and the β-gal substrate were not available for the experiments. A new supply of adenoviral vector and adequate source of the β-gal thus had to be prepared.

Specific Aim 9.1 **To determine the ability of PFC to diminish the immune response, both innate and subsequent cellular and humoral responses, to intratracheal administration of adenoviral vector**

As described in the last report, we found that intratracheal administration of adenovirus allows transfection in the lung parenchyma only and the transfection efficiency was significantly increased when followed by intratracheal administration of PFC. However, the second pulmonary transfection after repeated administration of adenovirus and then PFC was not successful. This year, we repeated those experiments, but the results confirmed our previous findings. Since we could not carry out Specific Aim 9.1 to define the immune response by PFC, we thus decided to discontinue the study. The budget for this Aim has been reallocated to other TARGET projects.

Specific Aim 9.2 **To determine the ability of PFC to enhance repeated gene transfer through reduction and mechanistical disruption of the humoral response**

Based on our preliminary *in vitro* data, PFC applied directly to lung cancer cell lines in culture can increase the transfection ability of both adenovirus and liposomal vectors. The well-characterized cell lines A549 and H460, when exposed to PFC for 30 minutes prior to transfection with adenoviral vector, had an increased expression of the vector by 90% and 41% respectively. The results using a liposomal vector showed an equally enhanced expression.

However, as mentioned above, when we intratracheally administered adenovirus followed by PFC to animals, they had a greatly diminished expression of the vector although the first injection generated a favorable expression. We found that the animal lung contained a significant amount of PFC even 21 days after the first injection. We speculated that the residual PFC in the lung might cause the poor transfection. Thus, this year, we attempted to adopt another approach, hoping to prevent the accumulation of PFC within the alveolar compartment of the lung.

We exposed animals to PFC via an intravenous injection followed by intratracheal administration of adenoviral vector. Animals were initially injected intravenously with a 5ml/kg dose of PFC. However, the majority of the animals receiving this dose were unable to survive. Death ensued within 10 to 20 minutes of injection. Assays for lipopolysaccaride (LPS) revealed no detectable levels of PLS in the PFC source thus indicating that a contaminated supply of PFC was not a cause of the animals' death. Repeated experiments using this dose resulted in the same outcome. Autopsy of the animals revealed a pale lung tissue. When this tissue was homogenized and the homogenate was allowed to settle, a definite layer of PFC could be seen. It was apparent that the PFC was unable to travel through the pulmonary capillary bed and was trapped in the lung limiting pulmonary blood flowing and resulting in animal death. A reduced dose of 1 ml/kg of PFC was therefore utilized. These animals survived overnight but uniformly

succumbed 12 hours after the injection. Autopsy of these animals identified a similar problem as seen in the higher dosed animals.

There are fluorocarbon compounds of PFC specifically designed for intravenous injection. Use of these fluorocarbon PFCs may prevent death and allow enhanced transfection via the method described above. Attempts were made to contact a company that would provide the source for the intravenous formulation of PFC. Alliance Pharmaceuticals is an American corporation that did produce two forms of these fluorocarbon PFCs. The first agent was designed for liquid ventilation (named Liquivent) and the second was designed for intravenous injection as a blood replacement (named Oxygent). We had initially attempted to obtain Liquivent when we began our studies with PFC but Alliance Pharmaceuticals was unable to provide any Liquivent due to ongoing clinical trials exploring its role in liquid ventilation. They now no longer produce this product. We again attempted to contact Alliance Pharmaceuticals to obtain the intravenous PFC product, Oxygent, however the company has entered into an agreement with a Chinese pharmaceutical company to produce and test this agent for blood conservation during surgery. As a result, they are unable to provide any of the material to our laboratory.

Therefore, in the coming year, we will switch back to test the intratracheal administration of PFC with intravenous injection of a liposomal vector since, as we demonstrated previously, the animals could not tolerate intratracheal injection of liposomal vector.

Specific Aim 9.3 **To determine the ability of PFC to allow continued penetration of the pulmonary parenchyma in the setting of an animal model of severe emphysema**

Specific Aim 9.4 **To determine the ability of PFC-mediated gene transfer to effectively transducer a model of multifocal lung cancer**

If we succeed in Specific Aim 9.2, we can proceed with Specific Aims 9.3 and 9.4.

Project 10: Development of Novel Murine Models of Lung Cancer and Evaluation of Antiangiogenic Agents

(Principal Investigators: Roy Herbst, M.D., Ph.D. and Michael O'Reilly, M.D.)

The primary goal of this project is to provide a rational basis for use of antiangiogenic agents with conventional and emerging modalities in the treatment of lung cancer.

Specific Aim 10.1 **To develop and validate orthotopic and metastatic murine lung cancer models for testing the efficacy of anti-angiogenic agents alone and in combination with cytotoxic agents**

As reported last year, we have developed and validated murine models of orthotopic and metastatic human lung cancer for testing the efficacy of antiangiogenic agents alone and in combination with cytotoxic chemotherapy. Experimental murine models of primary human non-small cell and small cell lung cancer are now in place to study the biology and therapy of human lung cancer. Our publications in Clinical Cancer Research (Onn et al., 2003) and AACR abstract (Isobe at al, 2004) describe the details of the study.

This Specific Aim has been accomplished.

Specific Aim 10.2 **To evaluate effects of anti-angiogenic agents alone and in combination with chemotherapeutic agents in orthotopic and metastatic murine models of human lung cancer**

Update
We reported last year that using our primary and metastatic lung cancer models we completed studies of antiangiogenic therapy alone and in combination with chemotherapeutic agents.

An oral angiogenesis inhibitor ZD6474 that targets VEGFR2 and EGFR resulted in the near complete suppression of malignant growth of established lung tumors and prevented pleural effusion formation and inhibited chest wall invasion in our orthotopic lung model. In contrast, systemic weekly therapy with Taxol had little or no effect on lung cancer progression. A manuscript describing the findings was submitted to *Journal of Clinical Investigation* (Wu et al., 2005). These studies have also provided preliminary data for an R01 grant application we are currently working on (we withdrew the PO1 grant application submitted last year).

In addition, ZD6474 was effective against lung adenocarcinoma in our brain and bone metastatic models. The activity of ZD6474 was enhanced by combined therapy with Taxotere or Taxol in the brain metastatic models (lung adenocarcinoma), but Taxol antagonized ZD6474 activity in the bone metastatic model, suggesting that organ microenvironment influences response to combined antiangiogenic and cytotoxic therapies. These data were presented at the annual meeting of AACR (Wu et al, AACR, 2004).

We have initiated a new clinical trial with antiangiogenic therapy combined with chemotherapy.

This Specific Aim has been accomplished.

Specific Aim 10.3 **To optimize combinations and sequences of anti-angiogenic therapy with chemotherapy for treatment of lung cancer**

Update
We are currently studying ZD6474 in combination with Taxol and a new multitargeted anti VEGF agent ZD2171, alone and in different sequences with chemotherapy.

Specific Aim 10.4 **To develop surrogate markers of response to therapy using immunohistochemical and gene expression analysis of tumor tissues**

Previously, we reported that endothelial cell apoptosis preceded tumor cell apoptosis after ZD6474 treatment in the orthotopic human lung adenocarcinoma murine model, suggesting that the effect on the vasculature may be a useful surrogate for tumor response to ZD6474.

Update
We are soon to initiate a clinical trial that will study ZD6474 in untreated NSCLC patients. The mandatory tumor biopsies from this trial will be used to evaluate endothelial cell apoptosis and inhibition of VEGFR and EGFR receptor phosphorylation, which could be used as surrogate endpoints of ZD6474 effect.

Core B: Biostatistics & Data Management Core
(Core Director, J. Jack Lee, Ph.D.; Core Co-Director, B. Nebiyou Bekele, Ph.D.)

Core Goals:

- To provide the statistical design, sample size and power calculations for each project.
- To facilitate prospective data collection and quality control of data for animal experiments and basic science studies associated with the TARGET program.
- To provide all statistical data analysis including descriptive statistical analysis, hypothesis testing, estimation, modeling of prospectively generated data.
- To generate statistical reports for all projects.
- To collaborate and assist all project investigators in the publication of scientific results.

From the inception of the TARGET program, the Biostatistics and Data Management Core has worked actively with the project leaders in their research efforts, especially in the areas of biostatistical advice and consulting, the initial design of studies, and analysis of experimental results.

In the last year, the Core, in collaboration with Dr. Ruth Katz (Investigator on Project 1), analyzed various data sets relating to the relationship between deletions of the 3p and 10q genes and overall survival for patients with NSCLC. The results were published in *Cancer* (Barkan et al., 2005). Three more articles are in preparation.

We has also assisted Dr. Charlie Lu's project (Project 4). In collaboration with Dr. Lu, we have analyzed six molecular factors including DAP kinase potentially prognostic for overall survival of resectable Stage I NSCLC patients. The data were published in *Journal of Clinical Oncology* (Lu et al., 2004). Currently, we are in the process of analyzing the correlation between hypermethylation of DAP kinase and patient survival.

In addition, Dr. Jack Lee, in collaboration with Dr. Reuben Lotan (Principal Investigator of Project 5), is evaluating the data of growth inhibitory and apoptosis effects of histone deacetylase inhibitor SAHA and demethylating agent, 5-aza-2-deoxycytidine, on lung cancer cell lines generated in Specific Aim 5.1.

KEY RESEARCH ACCOMPLISHMENTS:

Project 1: Molecular Epidemiology of Lung Cancer

- Found statistically significant correlations between 1) 3p deletion in touch preparations from tumor, normal, and adjacent sides and pack-years smoking; 2) 3p deletion in bronchial brushes and in touch preparations both from tumor side; 3) telomere length in peripheral blood lymphocytes and in epithelial cells of bronchial brushings on normal side ($p<0.0001$), but not significant on tumor side ($p=0.0838$); 4) telomere length in epithelial cells of bronchial brushings on normal side and in epithelial cells of bronchial brushings on tumor side ($P=0.0001$).
- Found significantly inverse association of 1) telomere length in epithelial cells of bronchial brushings on tumor side with 3p aberrations in bronchial brushings from the tumor side ($p=0.0013$) and the normal side ($p=0.0021$), also with 3p aberrations in touch prep from the tumor tissues ($p=0.0064$) and the adjacent normal tissues ($p=0.0083$); 2) telomere length in epithelial cells of bronchial brushings on the tumor side with 10q aberrations in bronchial brushings from the tumor side ($p=0.0261$), normal side ($p=0.0023$), as well as with 3p aberrations in touch prep from the adjacent normal tissues ($p=0.0061$).
- Found 1) significantly positive association of DNA-damaging agent BPDE sensitivity in lymphocytes with 3p deletion ($p=0.0066$) and aberrations ($p=0.0024$) in lymphocytes; 2) borderline significant association with 10q aberrations ($p=0.0570$) in lymphocytes.

Project 2: Genetic Instability by Smoking Status

- FISSR-PCR together with microdissection is sufficiently sensitive to quantify clonal and subclonal changes in lung tissues, including tumor, normal bronchial epithelium, and even stromal regions.
- FISSR-PCR data provide validation of prior studies utilizing premature chromosome condensation, in situ hybridization, and LOH analysis that lung tumorigenesis represents a field process where tobacco exposure can create genetic changes throughout the exposed lung tissue leading to the presence of multifocal clonal outgrowths.
- The levels of clonal alteration found in the bronchial epithelium tend to be less than that found in the adjacent tumors.
- Weak concordance between the levels of clonal alteration in the tumor and in the normal bronchial epithelium was observed. This finding is important in the setting of estimating risk of individuals without cancer since it suggests that random biopsies can still provide quantitative information for the tissue field as a whole.

Project 3: Epithelial Biomarkers of Lung Cancer: Evaluation of Airway Secretions to Study Lung Carcinogenesis

- Identified 23 unique proteins in the apical surface fluid from the squamous metaplasia, including squamous cell carcinoma antigens (SCCA), annexin I and II, S100A9, and S100A8.
- Expression of SCCA1 and 2 was progressively increased in transformed/tumorigenic cell lines and only detected in well-differentiated squamous cell carcinoma, not in adenocarcinoma cells.
- Confirmed that the WNT, apoptosis, and cell cycle pathways were concurrently deregulated in NSCLC cells as compared to organotypically cultured normal bronchial epithelial cells.

- Successfully generated bronchial epithelium recapitulating *in vivo* bronchial epithelium using primary bronchial epithelial cells isolated from surgically resected lung tissue specimens.

Project 4: Prognostic Role of Promoter Hypermethylation of Death-Associated Protein (DAP) Kinase and p16 in Early-Stage Non-Small Cell Lung Cancer

- Completed biomarker assays and updated clinical follow-up data.
- Created a valuable database that will enable the conduct of future exciting molecular prognostic studies.

Project 5: An Epigenetic Approach to Lung Cancer Therapy

- Established the mechanism by which SAHA induces apoptosis as the increased expression of Fas (death receptor) and activation of the Fas ligand/Fas mediated apoptosis pathway.
- Discovered subsets of genes that are either up or down regulated by SAHA alone, 5-aza alone, or by their combination.
- Discovered that SAHA and 5-aza-CdR each alone has anti-tumor activity but their combination is more effective than each agent alone.

Project 6: The Role of the Farnesyl Transferase Inhibitor SCH66336 in Treatment of Carcinoma of the Aerodigestive Tract

- FTIs (SCH66336 and R115777) induce growth arrest and apoptosis independent of Akt and Raf/ERK signaling pathways in human NSCLC cells.
- SCH66336 and R115777 activate Akt surviving pathways in some FTI-resistant NSCLC cell lines.
- FTIs increase DR5 expression and enhance TRAIL-induced apoptosis. Induction of DR5 expression contributes to SCH66336-induced apoptosis.
- FTIs modulate the expression of FLIP either by decreasing its expression or by increasing its levels, depending on cell lines.
- *DR5* and *FLIP* were identified to be FTI-regulated genes.
- The functional HDAC6 is required for the synergistic effect of SCH66336 with taxanes.

Project 7: Mechanisms and Therapeutic Applications of the Tumor Suppressor Gene *FUS1* in Lung Cancer

- Identified many cellular targets in FUS1-mediated tumor suppressor activities in lung cancer cells by a high throughput gene and protein expression profiling using technologies of gene microarrays and ProteinChip arrays.
- Demonstrated that Fus1 functions as a key mediator in Apaf1-mediated mitochondrial apoptosis pathway by recruiting and directing cytoplasmic Apaf1 protein to a critical cellular location and activating it in situ through a direct protein-protein interaction, and, therefore, facilitating Apaf1-mediated apoptosome assembly and activation of the caspase cascades and apoptosis.
- Co-expression of FUS1 and p53 could synergistically inhibit lung cancer cell growth and the wt-Fus1 may play a critical role in modulating the sensitivity of tumor cells to the chemotherapeutic agents, especially DNA damaging agents such as Cisplatin, and to ionizing radiation.
- The systemic treatment of DOTAP:cholesterol:FUS1 DNA complexes is in a Phase I trial for late stage lung cancer patients.

Project 9: Use of Perfluorocarbons to Enhance Pulmonary Gene Transfer

- Intravenous administration of regular PFC caused animal death, thus not suitable for the study of ability of PFC to enhance repeated gene transfer of adenovirus vector.

Project 10: Development of Novel Murine Models of Lung Cancer and Evaluation of Antiangiogenic Agents

- Developed and validated murine models of orthotopic and metastatic human lung cancer
- Evaluated effects of antiangiogenic therapy alone and in combination with chemotherapeutic agents using the orthotopic and metastatic lung cancer models.

Core B: Biostatistics & Data Management Core

- Provided statistical supports for projects 1, 4, and 5, leading to two publications in the journals of *Cancer* and *Journal of Clinical Oncology*.

REPORTABLE OUTCOMES

Manuscripts:

1. Barkan GA, Caraway NP, Jiang F, Zaidi TM, Fernandez R,Vaporciyan A, Morice R, Zhou X, Bekele BN, Katz R. Comparison of molecular abnormalities in bronchial brushings and tumor touch preparations. Cancer 105: 35-43, 2005.
2. Ju Z, Kapoor M, Newton K, Cheon K, Ramaswamy A, Lotan R, Strong LC, Koo JS. Global detection of molecular changes reveals concurrent alteration of several biological pathways in non-small cell lung cancer cells. Mol Genet Genomics Jul 28;1-14, 2005.
3. Lin Ji, John D. Minna, Jack A. Roth. 3p21.3 Tumor Suppressor Cluster: Prospects for Translational Applications. Future Oncology 1: 79-92, 2005.
4. Lu C, Soria JC, Tang X, Xu XC, Wang L, Mao L, Lotan R, Kemp B, Bekele BN, Feng L, Hong WK, Khuri FR . "Prognostic Factors in Resected Stage I Non-Small Cell Lung Cancer (NSCLC): A Multivariate Analysis of Six Molecular Markers". J Clin Oncol 22: 4575-83, 2004.
5. Marcus Zhou J, O'Brate A, Hamel E, Wong J, Nivens M, El-Naggar A, Yao TP. Khuri FR, Glannakakou P. The synergistic combination of the farnesyl transferase inhibitor lonafarnib and paclitaxel enhances tubulin acetylation and requires a functional tubulin deacetylase. Cancer Res 65: 3883-3893, 2005.

Abstracts and Presentations:

1. Etzel CJ, Zhang Q, Schabath M, Dong Q, Wu XF, Wei QY, Spitz MR. Building a comprehensive quantitative risk assessment model for lung cancer. Proc. AACR 46: #4051 2005.
2. Guanglin Wu, Futoshi Uno, Ralph Arlinghuas, Vikas Kundra, John D. Minna, Jack A. Roth, Lin Ji. Inactivation of c-Abl and c-Kit activities and inhibition of SCLC cell growth by a combination treatment with FUS1-nanoparticle and Gleevec in vitro and in vivo. Proc. AACR 46: #5021, 2005.

3. Guanglin Wu, Wuguo Deng, Vikas Kundra, Bingliang Fang, Jack A. Roth, Lin Ji. A novel synthetic hTERT-Mini-CMV chimera promoter-driven tumor-selective and high-efficiency expression of transgene for systemic cancer gene therapy. Proc. AACR 46: #3358, 2005.

4. Hiroyuki Kawashima, Charles Lu, Jonathan Kurie, Sunil Chada, John D. Minna, Jack A. Roth, Lin Ji, Synergistic inhibition of EGFR tyrosine kinase and tumor cell growth in non-small cell lung cancer (NSCLC) by combination treatment with FUS1-nanoparticles and Gefitinib. Proc. ASCO: #7081, 2005.

5. Hiroyuki Kawashima, Futoshi Uno, Jonathan Kurie, John D. Minna, Jack A. Roth, Lin Ji. Synergistic inhibition of EGFR tyrosine kinase activity and NSCLC cell growth by combination treatment with FUS1-nanoparticle and gefitinib. Proc. AACR 46: #2707, 2005.

6. Lu T, Wistuba II, Hittelman WN. Detection of clonal and subclonal outgrowths in the upper aerodigestive tract of current and former smokers with lung cancer. Proc. AACR 46: #2230, 2005.

7. Isobe T, Onn A, Wu WJ, Shintani T, Itasaka S, Shibuya K, Hong WK, O`Reilly MS, Herbst RS. Biology and therapy of human small cell lung cancer (SCLC) in novel orthotopic nude mouse models. AACR 45, 2004.

8. Kentaro Ueda, Hiroyuki Kawashima, Wuguo Deng, John D. Minna, Jack A. Roth, Lin Ji. Inactivation of the potential 3p21.3 tumor suppressor NPRL2 significantly correlates with the cisplatin-induced resistance in human NSCLC Cells. Proc. AACR 46: #1494, 2005.

9. Lu T, Hittelman WN. Quantitative fluorescence inter-simple sequence repeat PCR (FISSR-PCR) for subclonal analysis of bronchial cell populations. Proc. AACR 45, 2004.

10. Spitz MR, Wei QY, Wu XF, Integrative Molecular Epidemiology: From Risk Assessment to Outcome Prediction. Symposium on Fundamental Research on Cancer, Houston, TX, October 2005.

11. Wu WJ, Isobe T, Itasaka S, Shintani T, Langley RR, Onn A, Hansen JC, O`Reilly MS, Herbst RS. ZD6474, a small molecule targeting VEGF and EGF receptor signaling, inhibits lung angiogenesis and metastasis and improves survival in an orthotopic model of non-small cell lung cancer. AACR 45, 2004.

12. Wuguo Deng, Futoshi Uno, John D Minna, Jack A. Roth, Lin Ji. Synergistic tumor suppression by coexpression of FUS1 and p53 concurrences with FUS1-mediated down regulation of MDM2, accumulation of p53, and activation of Apaf1-dependent apoptotic pathway in human NSCLC cells. Proc. AACR 46: #3516, 2005.

Research Opportunity

- Initiated a new Phase II clinical trial with antiangiogenic therapy combined with chemotherapy for non-small cell lung cancer patient based on the findings of Project 10.

Grant Application

- R01 grant application (2005): Vascular targeted therapy of non-small cell lung cancer (PI: Roy Herbst, M.D.)

CONCLUSIONS

In the third year of the grant period, most of the projects are nearly completed in terms of their specific aims and should be finished with the one-year unfunded extension in 2006. Over the year, 5 manuscripts have been published and several others submitted to peer-reviewed journals including *Nature*, *Journal of Clinical Investigation*, and *Cancer Research*. We are applying for a new R01 grant and a new phase II clinical trial will be initiated. We can report the following conclusions.

Project 1 identified some statistically significant correlations among genetic markers including 3p deletion and aberration, 10q aberration, telomere length, and DNA repair sensitivity within target tissue (normal side vs tumor side) and surrogate tissue. The concordance of these markers in paired surrogate and target tissues is not yet established.

Project 2 optimized the FISSR-PCR technique which was sensitive enough to quantify clonal and subclonal changes in lung tissues and validated prior studies using different techniques such as FISH. Effects of smoking status and chemopreventive intervention on clonal outgrowth haven't been finalized by using FISSR-PCR.

Project 3 found some secreted proteins (SCCA1 and SCCA2) from squamous metaplastic bronchial epithelia, but their efficacy as novel biomarkers to detect early carcinogenesis of squamous cell carcinomas in the lung is under study and will be completed in 2006.

Project 4 completed collection of hypermethylation data of DAP kinase and p16 and relevant patient data and is now in the process of conducting correlation analysis between the status of hypermethylation of DAP kinase and p16 and patient survival and tobacco smoke exposure to determine prognostic role in early-stage non-small cell lung cancer.

Project 5 found the anti-tumor activity of histone deacetylase inhibitor SAHA and demethylating agent 5-aza-CdR *in vitro* and SAHA-induced apoptosis was via activation of Fas-mediated apoptosis pathway. Their anti-tumor activities *in vivo* are under study and will be completed in 2006.

Project 6 demonstrated that farnesyl transferase inhibitor SCH66336 induced apoptosis by increasing DR5 expression and TRAIL-induced apoptosis, independent of downregulating Akt and Raf/ERK pathways. The synergistic effect of SCH66336 with taxanes required the functional HDAC6.

Project 7 revealed a novel molecular mechanism involving FUS1-mediated tumor suppression function and its interaction with other cellular components in the pathways regulating p53 and Apaf-1 activities. The findings imply that a treatment targeting multiple pathways by combining functionally synergistic tumor suppressors such as FUS1 and p53 with chemotherapy or radiotherapy may be an effective therapeutic strategy for NSCLC and other cancers.

Project 9 has not generated positive results based on the proposed studies and a final attempt is ongoing. Conclusions will be drawn in 2006.

Project 10 concludes that the orthotopic murine model of lung cancer is a valuable tool to test the antiangiogenic agents and their combination with cytotoxic agents. The model provides a rational basis for development of anti-angiogenic therapy with conventional and emerging modalities in the treatment of lung cancer.

Biostatistics & Data Management Core is providing ongoing statistical support for Projects 1, 4, and 5.

References:

- Almasan A, Ashkenazi A. Apo2L/TRAIL:apoptosis signaling, biology, and potential for cancer therapy. Cytokine Growth Factor Rev 14: 337-348, 2003.
- Debatin KM, Krammer PH. Death receptors in chemotherapy and cancer. Oncogene 23:2950-2966, 2004.
- Fulda S, Debatin KM. Exploiting death receptor signaling pathways for tumor therapy. Biochim Biophys Acta 1705:27-41, 2004.
- Jemal A, Murray T, Samuels A, Ghafoor A, Ward E and Thun MJ. Cancer statistics, 2005. CA Cancer J Clin 53:5-26, 2005.
- Onn A, Isobe T, Itasaka S, Wu W, O'Reilly MS, Hong WK, Fidler IJ, Herbst RS. Development of an orthotopic model to study the biology and therapy of primary human lung cancer in nude mice. Clin Cancer Res 9:5532-5539, 2003.
- Green DR. Apoptotic pathways: paper wraps stone blunts scissors. Cell 102: 1-4, 2000.
- Wang S, El-Deiry WS. TRAIL and apoptosis induction by TNF-family death receptors. Oncogene 22:8628-8633, 2003.

APPENDIX
Published Manuscripts, Abstracts, Presentations

CANCER
CYTOPATHOLOGY

Comparison of Molecular Abnormalities in Bronchial Brushings and Tumor Touch Preparations

Potential Use of Fluorescence In Situ Hybridization to Identify Predictive Markers in Early-Stage Lung Carcinomas

Güliz A. Barkan, M.D.[1]
Nancy P. Caraway, M.D.[1]
Feng Jiang, M.D.[1]
Tanweer M. Zaidi, M.D.[1]
Ricardo Fernandez, B.S.[1]
Ara Vaporcyin, M.D.[2]
Rodolfo Morice, M.D.[3]
Xian Zhou, M.S., B.S.[4]
Benjamin Nebiyou Bekele, Ph.D.[4]
Ruth L. Katz, M.D.[1]

[1] Department of Pathology, The University of Texas M. D. Anderson Cancer Center, Houston, Texas.

[2] Department of Thoracic and Cardiovascular Surgery, The University of Texas M. D. Anderson Cancer Center, Houston, Texas.

[3] Department of Pulmonary Medicine, The University of Texas M. D. Anderson Cancer Center, Houston, Texas.

[4] Department of Biostatistics and Applied Mathematics, The University of Texas M. D. Anderson Cancer Center, Houston, Texas.

Presented at the 92nd Annual Meeting of the United States and Canadian Academy of Pathology, Washington, D.C., March 22–28, 2003.

Supported by Grant P50CA70907 (The University of Texas at Southwestern Medical Center and M. D. Anderson Cancer Center Specialized Programs of Research Excellence in Lung Cancer), Grant DAMD17-02-1-0706 (Translational Approaches for the Reversal, Genetic Evaluation, and Treatment of Lung Cancer), and Grant REP-NO1-CN-85083-57 (Workstatement 55: Identification of Predictive Image Analysis Features in Archival Histological Sections Which Predict Recurrence of Lung Cancer or Metastatic Disease) from the National Cancer Institute, and by funding from the Division of Pathology and Laboratory Medicine, The University of Texas M. D. Anderson Cancer Center, for research projects by fellows.

The authors thank Aazam B. Alizabeh and Abha Khanna for their technical assistance, Holly Turner-Jones and Raquel Vilts for their administrative assistance, and Vysis, Inc. (Downers Grove, IL) for providing a portion of the LAVysion probes used in the current study.

BACKGROUND. Preneoplastic lung lesions and early-stage lung carcinomas are associated with molecular abnormalities. The authors performed a pilot study to evaluate the use of DNA fluorescence in situ hybridization (FISH) probes to ascertain whether these biomarkers can predict nonsmall cell lung carcinoma (NSCLC).

METHODS. Fourteen bronchial brushings ipsilateral to the tumor (BB/Ts), tumor touch imprints, and touch imprints of the bronchus adjacent to the tumor obtained from 15 patients with early-stage NSCLC were analyzed. The LAVysion multicolor probe set consisting of probes to 5p15, 6, 7p12, and 8q2 and the in-house probes 3p22.1 and 10q22 was used. Using the LAVysion multicolor probe set, 25 epithelial cells were counted and considered positive if > 5 cells were abnormal. Using 3p22.1 and 10q22, ≥ 100 nuclei per slide were scored. The results were tabulated as the percentage of cells with deletions compared with the centromeric probes 3 and 10. Greater than 2% of the deletions were positive for 3p22.1 and 10q22. Bronchial washings from patients without lung tumors were used as controls.

RESULTS. The BB/Ts were negative for malignant cells by cytologic evaluation and the LAVysion probe set; however, the combined in-house probes for 3p22.1 and 10q22 tested on BB/Ts predicted cancer in 100% of cancer patients. FISH positivity in the lung cancers was 100% for 3p22.1 deletions, 79% for 10q22 deletions, and 57% for LAVysion probes. When compared with the bronchial epithelium, tumor cells showed a 3.7-fold excess of 3p22.1 deletions, a 2-fold excess of 10q22 deletions, and a 12.6-fold excess of abnormal cells.

CONCLUSIONS. The current study indicated that detection of molecular abnormalities in bronchial epithelial cells via FISH was very useful in identifying patients at high risk for developing lung carcinoma. The molecular abnormalities identified in the BB/Ts were detected at elevated levels in the tumor specimens. ***Cancer (Cancer Cytopathol)* 2005;105:35–43.** © *2004 American Cancer Society.*

KEYWORDS: lung, nonsmall cell, cancer, fluorescence in situ hybridization, early detection, bronchial brushing.

Address for reprints: Ruth L. Katz, M.D., Department of Pathology, Unit 53, The University of Texas M. D. Anderson Cancer Center, 1515 Holcombe Boulevard, Houston, TX 77030; Fax: (713) 792-2067; E-mail: rkatz@mail.mdanderson.org

Received May 24, 2004; revision received October 8, 2004; accepted October 14, 2004.

DOI 10.1002/cncr.20800
Published online 16 December 2004 in Wiley InterScience (www.interscience.wiley.com).

Lung carcinoma is the leading cause of cancer deaths and accounts for 28% of all deaths in the United States annually. Furthermore, the American Cancer Society estimated that there would be 169,500 new cases of lung carcinoma in 2001.[1] The mortality rate of lung carcinoma is almost 90%, and the 5-year survival rate in patients with advanced-stage lung carcinoma is 2.5%.[2,3] The high mortality rate is due, in part, to the lack of an effective diagnostic modality for early detection. Although chest X-rays and sputum cytology have long been used as screening modalities, these tests do not detect a sufficient number of lung carcinomas at an early enough stage to improve survival.[4] For this reason, lung carcinoma screening is not a routine practice in the general public or even among those at increased risk for lung carcinoma, such as smokers. Thus, new methods are needed to detect early-stage lung carcinoma and its precursors in patients at high risk.

In recent years, several chromosomal and molecular abnormalities have been identified in non-small cell lung carcinomas (NSCLC), even at early stages, although early-stage carcinomas have been found to have fewer molecular alterations than advanced-stage carcinomas. Lung carcinoma development has been proposed to reflect a field cancer process in which the whole lung is exposed to a carcinogenic insult, such as tobacco smoke, increasing the risk of multistep tumor development in the respiratory tract epithelium.[5] We hypothesized that a pattern of genetic abnormalities involving chromosomal regions 3p, 5q, 7p, 8q, and 10q in bronchial epithelial cells obtained from bronchial brushings from the tumor side (BB/Ts) is an early indicator of lung carcinoma. In the current study, we sought to determine whether a field effect exists in cytologically normal epithelium of the bronchial tree in the presence of established lung carcinoma with the use of DNA fluorescence in situ hybridization (FISH) probes. This information may be useful in identifying patients at high risk for developing lung carcinoma via endoscopic brush cytology.

MATERIALS AND METHODS

Patient and Control Population

Fifteen patients with NSCLC were entered into our prospective study. All of them had a lung mass that was operable. In addition, none of them had undergone chemotherapy or irradiation. Fifteen control subjects were selected from a group of individuals who were at high risk for developing lung carcinoma due to their smoking history but did not have a detectable lesion on a chest X-ray. Written informed consent for participation was obtained through an institutional review board protocol. All of the patients' and control subjects' charts were reviewed for a significant medical history and smoking history. The patients' histologic lung sections were also reviewed.

Specimens

The patients underwent bronchoscopy just before surgical excision. Bronchial brushings were taken from the main stem bronchus on the tumor-bearing side. After the excision, touch imprints from the resected lung tumors (TP/Ts) and from macroscopically unremarkable bronchi adjacent to the tumors (TP/ABs) were made. Also, bronchial washings (BWs) taken from the control subjects were used as controls.

Specimen Preparation

BB/Ts were obtained from only 14 of the 15 patients. The BB/Ts were received in saline. Cytospins were prepared for cytology and FISH analysis. The cytology slides were fixed in Carnoy solution and stained with Papanicolaou stain, whereas the air-dried slides were stained with Diff-Quik (Baxter Scientific, Deerfield, IL). The cytologic features of all of the specimens (BB/Ts, TP/Ts, and TP/ABs) were assessed. Both the cytospins and touch imprints were fixed for FISH in methanol and acetic acid at a ratio of 3:1 before labeling. Cytospins were also prepared for the control subjects and stained with Papanicolaou stain. As in the study cases, FISH was performed for three probe sets.

DNA Probe Sets

Three probe sets were used. One was the commercially available multicolor probe set LAVysion (Vysis, Downers Grove, IL). This set included four probes: a centromeric probe to chromosome 6 generated from a repetitive probe sequence and three unique sequence probes to 5p15 (LSI 5p15), 7p12 (LSI EGFR), and 8q24 (LSI MYC). The probes were labeled with Spectrum Aqua, Spectrum Green, Spectrum Red, and Spectrum Gold, respectively. The second probe set included centromeric 3 (CEP3; Vysis) and the locus-specific probe 3p22.1, which was developed in-house. The third probe set consisted of centromeric 10 (CEP10; Vysis) and the locus-specific probe 10q22, which was also developed in-house. These probes were mixed with blocking DNA, enriched in repetitive sequences, and hybridized to the specimens.

DNA for 3p22.1 and 10q22 was labeled by using a nick translation kit (Roche Diagnostics Corporation, Indianapolis, IN). DNA and the labeling enzyme were placed in a 15 °C water bath for 1 hour. Next, the probe was transferred to ice. A gel was run to determine the length of the DNA fragments, which had to be 500–2000 base pairs. The probe was then placed in a 65 °C water

TABLE 1
Univariate Analysis of Distribution of Covariates by Cancer Status

Cancer	No.	Mean	SD	Minimum	Median	Maximum	*P* value
Age							0.004
No	15	56.9	11.1	42	57	83	
Yes	15	69.8	7.5	57	71	84	
Pack-years							0.33
No	15	37.6	25.0	0	30	87	
Yes	15	48.8	33.2	0	50	120	
3p:CEP3-BB/T							< 0.0001
No	15	1.2	0.9	0	1	2	
Yes	15	7.2	3.3	3	7	14	
3P:CEP3-TP/T							< 0.001
No	15	1.2	0.9	0	1	2	
Yes	15	23.9	13.2	9	22	53	
3P:CEP3-TP/AB							< 0.001
No	15	1.2	0.9	0	1	2	
Yes	13	7	3.8	2	6	16	
10q:CEP10-BB/T							0.0002
No	14	0.8	0.8	0	1	2	
Yes	15	4	2.1	2	4	9	
10q:CEP10-TP/T							< 0.001
No	14	0.8	0.8	0	1	2	
Yes	15	13.7	7.0	5	10	27	
10q:CEP10-TP/AB							< 0.001
No	14	0.8	0.8	0	1	2	
Yes	13	6	3.3	3	5	14	
LAVy-BB/T							0.25
No	15	0.3	0.5	0	0	1	
Yes	14	1.1	1.7	0	0	5	
LAVy-TP/T							< 0.001
No	15	0.3	0.5	0	0	1	
Yes	14	8.6	8.1	0	6	23	
LAVy-TP/AB							0.28
No	15	0.3	0.5	0	0	1	
Yes	12	0.8	1.2	0	0	3	

BB/T: bronchial brushing on tumor side; LAVy: LAVysion; 3p:CEP3: ratio of 3p deletions to CEP3; 10q:CEP10: ratio of 10q deletions to CEP10; TP/T: touch preparation of tumor; TP/AB: touch preparation of adjacent bronchus; SD: standard deviation.

bath for 15 minutes and stored in a 20 °C freezer. The detailed methodology for this in-house probe preparation was described previously by Jiang and Katz.[6]

Fluorescence In Situ Hybridization Procedure

Slides were immersed in 2 × standard sodium citrate (SSC) for 3 minutes at 77 °C and then in a protease solution (50 mL of 1 × phosphate-buffered saline [PBS], pH < 2.0, and 25 mg of protease). Protease digestion was then performed (5–6 minutes for cytospins and 7–8 minutes for touch preparations). Slides were then washed in 1 × PBS for 5 minutes and subsequently fixed in a 1% formaldehyde solution for 5 minutes. Afterward, the slides were again washed with 1 × PBS for 5 minutes and dehydrated in sequential 70%, 85%, and 100% ethanol solutions. After a brief period of drying, the probe mixture was applied to the target areas on each slide, covered with a coverslip, and sealed with rubber cement. The slides were then kept in a hybrid machine (Vysis) for ≥ 20 hours at 37 °C. After the rubber cement and coverslips were removed, the slides were washed in a 50% formamide solution (pH 7.45) in 3 separate jars for 10 minutes each at 45 °C. Next, the slides were washed in 2 × SSC for 10 minutes at 45 °C and then in 2 × SSC/0.1% ethoxylated octyl phenol (NP-40) for 10 minutes. The slides were then dried. Slides were counterstained with 4′ 6-Diamidine-2-phenylindole dihydrochloride (DAPI; 10 μL per slide), coverslipped, and viewed under a fluorescent microscope (Leica DWRXA or Leica DMLB; Leica Microsystems, Inc., Buffalo, NY) with the appropriate filters for the probes.

Using the LAVysion multicolor probe, 25 nonoverlapping cells with distinct signals were counted per

sample, and the chromosomal abnormalities were scored. A cell was abnormal if it had aneusomy of two or more chromosomes. If more than five cells were abnormal, the sample was positive as per the recommendation of the probe manufacturer based on studies performed with another multicolor probe (UroVysion; Vysis). For 3p22.1 and 10q22, the hybridized slides were counted with the use of appropriate filter sets for visualizing Spectrum Green or Spectrum Orange as well as DAPI counterstain. In addition, ≥ 100 nuclei from each slide were scored with a triple filter. The nuclei of individual cells that did not overlap were chosen for analysis. Slides were analyzed only if 80% of the cells were interpretable in the field of view and the brightness of the signals was ≥ 2+ on a scale of 0–3+. Each cell was scored individually for the number of green (3p22.1 or 10q22) and orange signals (CEP3 or CEP10, respectively) that were used as internal controls. Cells with fewer green signals than orange signals were positive, reflecting deletion. The ratio of green to orange signals was interpreted as the percentage of deleted cells. To avoid misinterpretation due to insufficient hybridization, cells were counted only if at least one bright orange and one bright green signal were present. Split signals were counted as one if the space between them was less than the diameter of a single signal. A control specimen was used for each batch. Based on a leave-one-out analysis, > 2% of the deletions were positive for 3p22.1 and 10q22.

Data Analysis

Univariate data were summarized using standard descriptive statistics in Table 1. The purpose of our study was to assess the predictive ability of various genetic deletions with respect to cancer status. Instead of concentrating exclusively on the significance of *P* values, we focused on the prediction rate of each marker. When prediction is the primary goal of analysis, the gold standard in assessment of the predictor is a test and validation set. Usually, such a set is used when the sample size is adequately large. Our sample was small, so we implemented a leave-one-out validation scheme to assess the predictive ability of the genetic markers using univariate logistic regression. With this scheme, we modeled the relation between the response variable and predictor for all but one data point. Once a model was fit, the response was then predicted for the data point that was left out. This process was repeated for all data points. The sensitivity and specificity values were then calculated based on the leave-one-out validation results and are presented in Tables 2–4. With small samples, this procedure is more robust in modeling overfitting and results in more realistic predictions when compared with native methods.[7] In addition, associations between categorical variables were assessed via crosstabulation and the Fisher exact test.[8] All of the computations were carried out with the use of the SAS software program (SAS Institute Inc., Cary, NC) on a Dell personal computer (Dell, Round Rock, TX) equipped with the Windows NT operating system (Microsoft, Redmond, WA) via standard procedures.[9]

TABLE 2
Leave-One-Out Table for 3p:CEP3-BB/T Using a Deletion Rate of > 2% to Predict Cancer Status

	Cancer (%)	
Predicted cancer	Yes	No
Yes	15 (100.0)	0 (0.0)
No	0 (0.0)	15 (100.0)

3p:CEP3: ratio of 3p deletions to CEP3; BB/T: bronchial brushing on tumor side.

TABLE 3
Leave-One-Out Table for 10q:CEP10-BB/T Using a Deletion Rate of > 2% to Predict Cancer Status

	Cancer (%)	
Predicted cancer	Yes	No
Yes	15 (100.0%)	3 (21.4%)
No	0 (0.0%)	11 (78.6%)

10q:CEP10: ratio of 10q deletions to CEP10; BB/T: bronchial brushing on tumor side.

TABLE 4
Leave-One-Out Table for Combined 3p:CEP3-BB/T and 10q:CEP10-BB/T Using a Deletion Rate of > 2% to Predict Cancer Status

	Cancer (%)	
Predicted cancer	Yes	No
Yes	15 (100.0)	0 (0)
No	0 (0.0)	14 (100.0)

3p:CEP3: ratio of 3p deletions to CEP3; 10q:CEP10: ratio of 10q deletions to CEP10; BB/T: bronchial brushing on tumor side.

RESULTS

Patients

The study included 12 men and 3 women with a mean age of 69.8 years (range, 57–84 years). One of the patients was a nonsmoker, and all of the others had a smoking history ranging from 9.5 to 120.0 pack-years. The control specimens were from 15 patients who did not have a history of lung carcinoma. The control

FIGURE 1. Tumor touch imprints showing an adenocarcinoma. (Papanicolaou stain, original magnification × 200.)

FIGURE 2. Bronchial brush specimen showing unremarkable bronchial epithelium on cytospin preparations. (Papanicolaou stain, original magnification × 600.)

subjects were 8 men and 7 women with a mean age of 56.9 years (range, 42–83 years). Fourteen of the control subjects had a smoking history ranging from 15 to 75 pack-years.

Cytology/Histology

Histologic examination of the excised tumor specimens showed that there were six adenocarcinomas (Fig. 1), seven squamous cell carcinomas, and two NSCLCs with sarcomatoid change. Touch imprint preparations were made from all of the tumors.

On cytologic evaluation, the BB/Ts were negative for malignant cells (Fig. 2). However, basal cell hyperplasia, squamous metaplasia, goblet cell metaplasia, and rare dysplastic cells were detected in four, five, three, and three specimens, respectively. TP/ABs, which were available from 12 patients, showed carcinoma in 1 specimen, dysplasia in 1 specimen, and bronchial hyperplasia/reactive bronchial epithelium in three specimens. Cytologic evaluation of the BWs demonstrated basal cell hyperplasia in five patients and squamous metaplasia in four patients.

FIGURE 3. Interphase fluorescence in situ hybridization (FISH) analysis on bronchial brushings showing a normal diploid population comprising two aqua, two green, two red, and two gold signals using a multicolor FISH analysis probe set (aqua, 6 centromeric; green, 7p12; red, 5p15; and gold, 8q24). (FISH, original magnification × 600.)

Fluorescence In Situ Hybridization Analysis

LAVysion multicolor FISH analysis showed that all 14 BB/Ts were negative for malignant cells (Fig. 3). However, five BB/Ts showed single chromosomal abnormalities, predominantly polysomy of 7p12. Also, 11 of the 14 specimens showed deletions of both 3p22.1 (Fig. 4) and 10q22 (Fig. 5). In the carcinomas, the incidence values of positivity were 57% (8 of 14) for the LAVysion probe set (Fig. 6), 100% (14 of 14) for 3p22.1 deletions (Fig. 7), and 79% (11 of 14) for 10q22 deletions (Fig. 8). LAVysion multicolor FISH analysis failed to demonstrate abnormal cells in TP/ABs, although 8 of 12 (67%) and 11 of 12 (92%) of these touch imprints were positive for 3p22.1 and 10q22, respectively. When compared with the adjacent bronchial epithelium, tumor cells showed a 3.7-fold excess of 3p deletions, a 2-fold excess of 10q deletions, and a 12.6-fold excess of abnormal cells by the LAVysion test. Table 1 shows the distribution of the age, pack-years of smoking, and FISH results of the patients and control subjects according to cancer status. The sensitivity and specificity values of the LAVysion multicolor probe set in detecting molecular abnormalities in the BB/Ts were 40% and 73%, respectively. The sensitivity and specificity

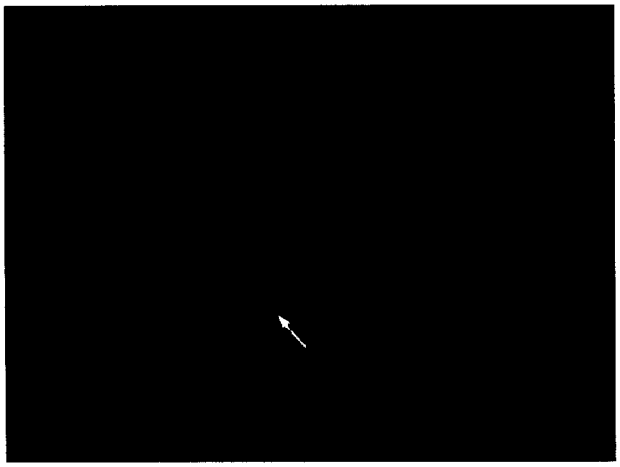

FIGURE 4. Interphase fluorescence in situ hybridization (FISH) analysis on a bronchial brush specimen from the tumor side showing a nucleus with a deletion (arrows) of 3p22.1 (one green signal, 3p22.1, relative to two red signals, CEP3). (FISH, original magnification × 600.)

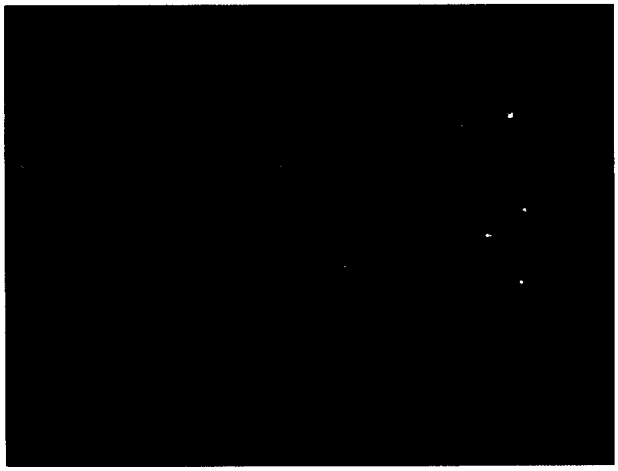

FIGURE 6. Interphase fluorescence in situ hybridization (FISH) analysis on tumor touch imprints showing enlarged aberrant nuclei with polysomies of CEP 7p12, 5p15, and 8q24 indicated by extra red, green, gold, and aqua signals using the multicolor FISH probe set. (FISH, original magnification × 600.)

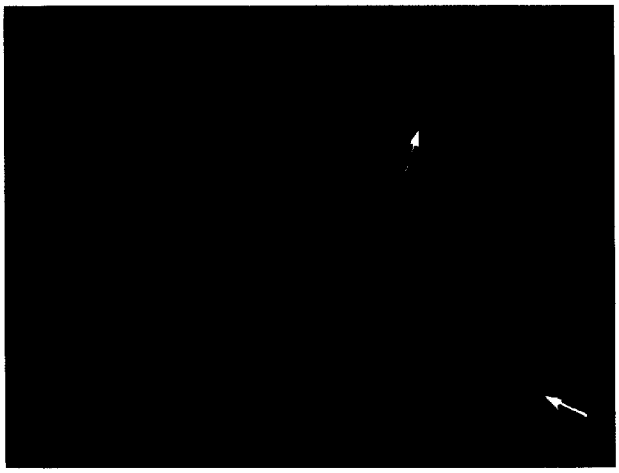

FIGURE 5. Interphase fluorescence in situ hybridization (FISH) analysis on bronchial brush specimens from the tumor side showing deletions (arrows) of the 10q22 locus-specific probe (loss of green signals, 10q22, relative to red signals, CEP10). (FISH, original magnification × 600.)

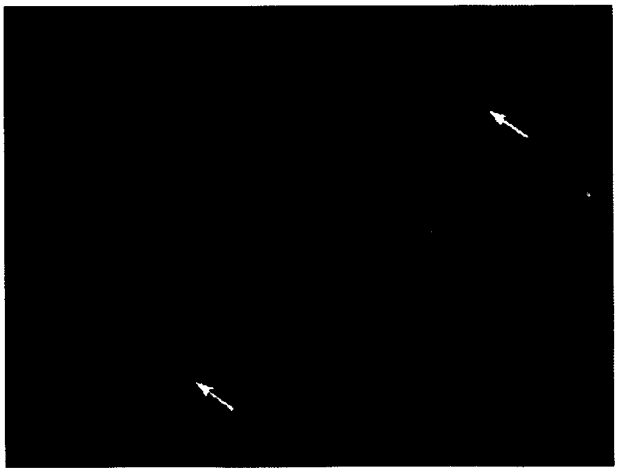

FIGURE 7. Interphase fluorescence in situ hybridization (FISH) analysis on tumor touch imprints showing deletions (arrow) of the 3p22.1 locus-specific probe (loss of green signals, 3p22.1, relative to red signals, CEP3). (FISH, original magnification × 600.)

values of 3p deletions > 2% in the BB/T to predict tumor were both 100% (Table 2). The sensitivity and specificity values of 10q deletions from BB/T were 100% and 78.6%, respectively (Table 3). The leave-one-out method showed that a 2% cutoff for both 3p and 10q deletions resulted in 100% sensitivity and specificity for the presence of cancer (Table 4). There was not a significant difference in the molecular abnormalities observed in the BB/Ts, TP/ABs, and TP/Ts of the patients with squamous cell carcinoma and those with adenocarcinoma (Table 5). Finally, the effect of smoking could not be determined with the current data, as there was not a sufficient number of patients or control subjects who were nonsmokers.

DISCUSSION

Currently, there are no efficient or accurate screening methods for early detection of lung carcinomas.[4] The lack of standard screening procedures often leads to diagnosis of these tumors at an advanced stage, which is associated with a poor prognosis and a high mortality rate. The standard of practice in the evaluation of patients for a possible lung carcinoma is a chest

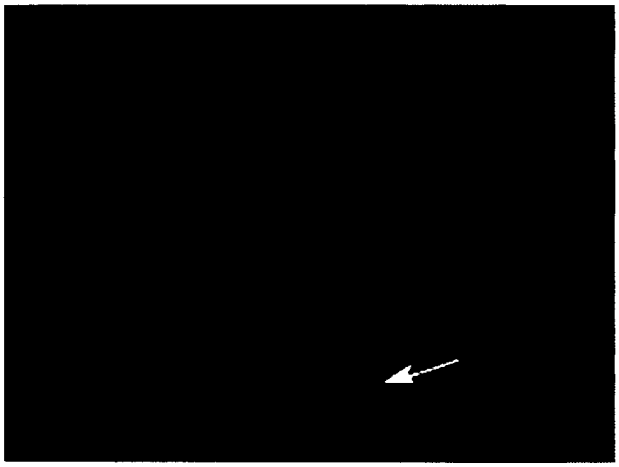

FIGURE 8. Interphase fluorescence in situ hybridization (FISH) analysis on tumor touch imprints showing tumor nuclei with deletions (arrow) of the 10q22 locus-specific probe (loss of green signals, 10q22, relative to the red signals, CEP10). (FISH, original magnification × 600.)

X-ray and pulmonary function tests followed by a computed tomography scan. Sputum cytology is usually not submitted due to its low sensitivity in detecting neoplastic cells. In patients with a suspected central mass, bronchoscopy is performed and bronchial washes, bronchial brushes, and transbronchial biopsy specimens are obtained. If the mass is peripheral, then the first approach is usually via a percutaneous fine-needle aspiration biopsy. In the current study, we focused on bronchial brush specimens from the side of the suspected tumor as a less invasive method to diagnose the presence of early lung carcinoma. We demonstrated that although most BB/Ts do not contain frankly malignant cells according to cytologic analysis, the majority of them displayed obvious molecular abnormalities of 3p22.1 and 10q22 according to FISH.

In recent years, multiple chromosomal and molecular alterations have been demonstrated in early-stage lung carcinomas[10–15] using comparative genomic hybridization,[16–19] microsatellite instability analysis,[19,20] and FISH.[21–25] Of these techniques, FISH has been used successfully for the targeted analysis of numeric chromosomal abnormalities in interphase nuclei in various types of solid tumors.[26–29] Interphase FISH is a relatively easy technique that can detect rare events such as a deletion or addition of a specific gene in a single cell nucleus derived from normal-appearing or cancer cells.

3p is presumed to be the site of multiple tumor suppressor genes, including FHIT (3p14) and RASSF1A (3p21.3). Recent molecular studies showed deletions in the 3p region in morphologically normal areas of bronchial epithelium in patients with lung carcinoma.[30] Deletions in this region are believed to be early and frequent events in lung carcinoma tumorigenesis.[4,30]

The 10q22 probe used in our study encompasses the gene encoding the surfactant-associated protein (SP-A). SP-A is a hydrophilic protein that facilitates the surface-tension-lowering properties of surfactant phospholipids in alveoli, regulates surfactant phospholipid synthesis, and counteracts the inhibitory effects of plasma proteins released during lung injury.[31] We postulate that low levels of SP-A, such as those resulting from genetic deletions, may increase host susceptibility to infections and the effects of carcinogenic agents. Loss of 10q22 also has been identified in NSCLC, especially squamous cell carcinoma.[32,33] In a large retrospective study of patients with Stage I cancer, we demonstrated that deletion of 10q22 in bronchial tissue adjacent to NSCLC is strongly associated with early recurrence of lung carcinoma (unpublished data).

The LAVysion four-color probe set comprises a cocktail of 5p, 7p, 8q, and centromeric 6 nucleic acid probes and has been designed to enhance the detection of malignant cells of NSCLC in sputum samples. Gene amplification in the 5p region is one of the most consistent alterations in NSCLCs and is strongly associated with tumor development, progression, and metastasis. The epidermal growth factor receptor (EGFR) gene, which is located on chromosome 7p, is overexpressed in BWs from smokers as well as in NSCLCs.[34] Although EGFR overexpression by immunohistochemistry is increased in patients at high risk for developing lung carcinoma, especially smokers,[35] EGFR as an independent prognostic factor appears to be controversial.[36] *C myc* is a nuclear phosphoprotein that participates in cell growth and tumor development by activating transcription of growth-stimulating genes. *C-myc* is located on chromosome 8q and is amplified in both small cell and non-small cell lung carcinomas.

In a retrospective study of BWs from 46 patients with histologically proven lung carcinoma, Sokolova et al.[22] found that the sensitivity for the detection of carcinoma cells was 82% for FISH with the LAVysion multicolor probe. In comparison, others found the sensitivity of cytology to be 54%.[23] In a similar multicolor FISH study by Romeo et al.[14] comparing tumor touch imprints of nonsmall cell carcinomas and sputa, the authors noted high frequencies of abnormal cells in all 20 imprints. However, none of the cytologically normal sputa demonstrated any abnormalities in FISH with the multicolor probe.

TABLE 5
Examination of Differences in Molecular Abnormalities by Site Versus Histology

Histology	No.	Mean	SD	Minimum	Median	Maximum	*P* value
3p:CEP3-BB/T							0.70
Adenocarcinoma	6	7.67	3.14	3.14	3	7.5	
Squamous Ca	8	7.13	3.89	3.68	3	6	
3p:CEP3-TP/AB							0.94
Adenocarcinoma	5	6.80	3.27	3.27	2	8	
Squamous Ca	7	7.71	4.55	4.27	3	6	
3p:CEP3-TP/T							0.95
Adenocarcinoma	6	22.67	5.47	5.47	13	23.5	
Squamous Ca	8	26.63	15.94	16.90	9	22	
10q:CEP10-BB/T							0.56
Adenocarcinoma	6	4.17	2.04	2.04	2	4	
Squamous Ca	8	3.88	2.65	2.47	2	3	
10q:CEP10-TP/AB							0.35
Adenocarcinoma	5	6.40	1.67	1.67	5	6	
Squamous Ca	7	6.14	4.59	4.22	3	4	
10q:CEP10-TP/T							0.85
Adenocarcinoma	6	15.17	7.99	7.99	8	12	
Squamous Ca	8	13.25	7.06	6.67	5	10	
LAVy-BB/T							0.14
Adenocarcinoma	5	2.40	2.30	2.30	0	3	
Squamous Ca	8	0.25	0.49	0.46	0	0	
LAVy-TP/T							1.00
Adenocarcinoma	5	8.80	8.87	8.87	0	6	
Squamous Ca	8	8.75	8.83	8.68	0	5.5	
LAVy-TP/AB							0.54
Adenocarcinoma	5	0.60	1.34	1.34	0	0	
Squamous Ca	6	1.00	1.26	0	.5	3	

BB/T: bronchial brushing on tumor side; LAVy: LAVysion; 3p:CEP3: ratio of 3p deletions to CEP3; 10q:CEP10: ratio of 10q deletions to CEP10; TP/T: touch preparation of tumor; TP/AB: touch preparation of adjacent bronchus; Ca: carcinoma; SD: standard deviation.

In the current study, evaluation of molecular abnormalities in bronchial epithelial cells via FISH was very useful in identifying patients who were at high risk for developing lung carcinoma. Deletions of 3p22.1 and 10q22 were detected at least two to four times more often in BB/Ts than abnormal cells by LAVysion probe set, which were detected only infrequently in BB/Ts when compared with TP/Ts. These results may reflect the finding that the tumor suppressor genes on 3p22.1 and 10q22 are deleted earlier in the genetic instability events involved in carcinogenesis than the oncogenes located on 5p15, 7p12, and 8q24. Therefore, 3p22.1 and 10q22 appear to be far more sensitive markers than the multicolor probe set in detecting a field effect in early-stage lung carcinomas. It is noteworthy that there was no significant difference in the molecular abnormalities of 3p22.1 and 10q22 for the different histologies of NSCLC regardless of anatomic site, suggesting that these abnormalities occur in the tumor stem cells before histologic differentiation takes place.

Our findings are compelling and may lead to the use of FISH as a valuable adjunct to cytology of bronchial brush specimens in high-risk patients with radiographically detected lung lesions, the majority of which are benign. A larger prospective trial must be performed to validate the current study in establishing the use of FISH analysis of bronchoscopy specimens and eventually sputa, as an adjunct to cytology in the early detection of lung carcinoma.

REFERENCES

1. American Cancer Society. Cancer facts and figures. Atlanta: American Cancer Society, 2002.
2. Mulshine JL, Linnoila RI, Jensen SM, et al. National targets for the early detection of lung cancer. *J Natl Cancer Inst Monogr.* 1992;13:183–190.
3. American Lung Association. Best practices and program services: trends in lung cancer morbidity and mortality. New York: American Lung Association, 2001.
4. Fossella FV, Komaki R, Putman JB, editors. Lung cancer. New York: Springer-Verlag, 2003.
5. Braakhuis BJ, Tabor MP, Kummer JA, Leemans CR, Brakenhoff RH. A genetic explanation of Slaughter's concept of field cancerization: evidence and clinical implications. *Cancer Res.* 2003;63:1727–1730.

6. Jiang F, Katz RL. Use of interphase fluorescence in situ hybridization as a powerful diagnostic tool in cytology. *Diagn Mol Pathol.* 2002;11:47–57.
7. Efron B, Tibshirani RJ. An introduction to the bootstrap. New York: Chapman & Hall, 1993.
8. Snedecor GW, Cochran WG. Statistical methods. 7th ed. Ames: Iowa State University Press, 1980.
9. SAS Institute. SAS/STAT user's guide. Version 8. Cary, NC: SAS Institute, Inc., 1999.
10. Michelland S, Gazzeri S, Brambilla E, Robert-Nicoud M. Comparison of chromosomal imbalances in neuroendocrine and non-small-cell lung carcinomas. *Cancer Genet Cytogenet.* 1999;114:22–30.
11. Feder M, Siegfried JM, Balshem A, et al. Clinical relevance of chromosome abnormalities in non-small cell lung cancer. *Cancer Genet Cytogenet.* 1998;102:25–31.
12. Taguchi T, Zhou JY, Feder M, Litwin S, Klein-Szanto AJ, Testa JR. Detection of aneuploidy in interphase nuclei from non-small cell lung carcinomas by fluorescence in situ hybridization using chromosome-specific repetitive DNA probes. *Cancer Genet Cytogenet.* 1996;89:120–125.
13. Kubokura H, Tenjin T, Akiyama H, et al. Relations of the c-myc gene and chromosome 8 in non-small cell lung cancer: analysis by fluorescence in situ hybridization. *Ann Thorac Cardiovasc Surg.* 2001;7:197–203.
14. Romeo MS, Sokolova IA, Morrison LE, et al. Chromosomal abnormalities in non-small cell lung carcinomas and in bronchial epithelia of high-risk smokers detected by multitarget interphase fluorescence in situ hybridization. *J Mol Diagn.* 2003;5:103–112.
15. Testa JR, Siegfield JM. Chromosomal abnormalities in human non-small cell cancer. *Cancer Res.* 1992;52(9 Suppl.): 2702s–2706s.
16. Ried T, Petersen I, Holtgreve-Grez H, et al. Mapping of multiple DNA gains and losses in primary small cell lung carcinomas by comparative genomic hybridization. *Cancer Res.* 1994;54:1801–1806.
17. Taubald A, Liehr T, Ries J, Girod S, Hassfurter E, Gebhart E. CGH detected DNA sequence copy number amplifications can be confirmed by interphase-FISH: new possibilities for prognostic approaches in oral squamous carcinomas. *Int J Mol Med.* 1998;2:555–560.
18. Taguchi T, Cheng GZ, Bell DW, et al. Combined chromosome microdissection and comparative genomic hybridization detect multiple sites of amplification DNA in a human lung carcinoma cell line. *Genes Chromosomes Cancer.* 1997; 20:208–212.
19. Gazdar AF, Minna JD. Molecular detection of early lung cancer. *J Natl Cancer Inst.* 1999;91:299–301.
20. Lilloglou T, Mahoney P, Xinaranos G, et al. Cancer-specific genomic instability in bronchial lavage: a molecular tool for lung cancer detection. *Cancer Res.* 2001;61:1309–1313.
21. Sanchez-Cespedes M, Ahrent SA, Piantadosi S, et al. Chromosomal alteration in lung adenocarcinoma from smokers and nonsmokers. *Cancer Res.* 2001;61:1309–1313.
22. Sokolova IA, Bubendorf L, O'Hare A, et al. A fluorescence in situ hybridization-based assay for improved detection of lung cancer cells in bronchial washing specimens. *Cancer.* 2002;96:306–315.
23. McCarthy PM, Jelsing NC. An advocacy perspective on screening and early diagnosis of lung cancer. *Cancer.* 2000; 89:2510–2514.
24. Tockman MS. Advances in sputum analysis for screening and early detection of lung cancer. *Cancer Control.* 2000;7: 19–24.
25. Schenk T, Ackermann J, Brunner C, et al. Detection of chromosomal aneuploidy by interphase in situ hybridization in bronchoscopically gained cells from lung cancer patients. *Chest.* 1997;111:1691–1696.
26. Stamouli MI, Ferti AD, Panani AD, et al. Application of multiplex fluorescence in situ hybridization in the cytogenetic analysis of primary gastric carcinoma. *Cancer Genet Cytogenet.* 2002;135:23–27.
27. Fuller CE, Perry A. Fluorescence in situ hybridization (FISH) in diagnostic and investigative neuropathology. *Brain Pathol.* 2002;12:67–86.
28. Dalquen P, Kleiber B, Grilli B, Herzog M, Bubendorf L, Oberholzer M. DNA image cytometry and fluorescence in situ hybridization for noninvasive detection of urothelial tumors in voided urine. *Cancer.* 2002;96:374–379.
29. Engel H, Friedrich J, Kleespies C, et al. Detection of chromosomal aberrations in tumor cells and tumor infiltrating lymphocytes by molecular cytogenetics in patients with gynecological cancer. *Cancer Genet Cytogenet.* 1998;106:159–165.
30. Zabarovsky ER, Lerman MI, Minna JD. Tumor suppressor genes on chromosome 3p involved in the pathogenesis of lung and other cancers. *Oncogene.* 2002;21:6915–6935.
31. Khubchandani KR, Snyder JM. Surfactant protein a (SP-A): the alveolus and beyond. *FASEB J.* 2001;15:59–69.
32. Petersen S, Aninat-Meyer M, Schluns K, Gellert K, Dietel M, Petersen I. Chromosomal alterations in the clonal evolution to the metastatic stage of squamous cell carcinomas of the lung. *Br J Cancer.* 2000;82:65–73.
33. Petersen S, Wolf G, Bockmuhl U, Gellert K, Dietel M, Petersen I. Allelic loss on chromosome 10q in human lung cancer: association with tumor progression and metastatic phenotype. *Br J Cancer.* 1998;77:270–276.
34. Piyathilake CJ, Frost AR, Manne U, et al. Differential expression of growth factors in squamous cell carcinoma and precancerous lesions of the lung. *Clin Cancer Res.* 2002;8: 734–744.
35. Barsky SH, Roth MD, Kleerup EC, Simmons M, Tashkin DP. Histopathologic and molecular alterations in bronchial epithelium in habitual smokers of marijuana, cocaine, and/or tobacco. *J Natl Cancer Inst.* 1998;90:1198–1205.
36. Brabender J, Danenberg KD, Metzger R, et al. Epidermal growth factor receptor and HER2-neu mRNA expression in non-small cell lung cancer is correlated with survival. *Clin Cancer Res.* 2001;7:1850–1855.

Mol Gen Genomics (2005)
DOI 10.1007/s00438-005-0014-7

ORIGINAL PAPER

Z. Ju · M. Kapoor · K. Newton · K. Cheon
A. Ramaswamy · R. Lotan · L. C. Strong · J. S. Koo

Global detection of molecular changes reveals concurrent alteration of several biological pathways in nonsmall cell lung cancer cells

Received: 23 September 2004 / Accepted: 6 May 2005

Abstract To identify the molecular changes that occur in non-small cell lung carcinoma (NSCLC), we compared the gene expression profile of the NCI-H292 (H292) NSCLC cell line with that of normal human tracheobronchial epithelial (NHTBE) cells. The NHTBE cells were grown in a three-dimensional organotypic culture system that permits maintenance of the normal pseudostratified mucociliary phenotype characteristic of bronchial epithelium in vivo. Microarray analysis using the Affymetrix oligonucleotide chip U95Av2 revealed that 1,683 genes showed a >1.5-fold change in expression in the H292 cell line relative to the NHTBE cells. Specifically, 418 genes were downregulated and 1,265 were upregulated in the H292 cells. The expression data for selected genes were validated in several different NSCLC cell lines using quantitative real-time PCR and Western analysis. Further analysis of the differentially expressed genes indicated that WNT responses, apoptosis, cell cycle regulation and cell proliferation were significantly altered in the H292 cells. Functional analysis using fluorescence-activated cell sorting confirmed concurrent changes in the activity of these pathways in the H292 line. These findings show that (1) NSCLC cells display deregulation of the WNT, apoptosis, proliferation and cell cycle pathways, as has been found in many other types of cancer cells, and (2) that organotypically cultured NHTBE cells can be used as a reference to identify genes and pathways that are differentially expressed in tumor cells derived from bronchogenic epithelium.

Keywords Microarray analysis · Gene expression profile · Biological pathways · Normal human tracheobronchial epithelium (NHTBE) · Nonsmall cell lung cancer (NSCLC)

Communicated by G. Georgiev

Z. Ju · M. Kapoor · A. Ramaswamy
Section of Cancer Genetics and Microarray Core Facility,
The University of Texas M. D. Anderson Cancer Center,
Houston, TX, 77030, USA

L. C. Strong
Department of Molecular Genetics, The University of Texas M. D. Anderson Cancer Center, Houston, TX, 77030, USA

K. Newton · K. Cheon · R. Lotan · J. S. Koo (✉)
Department of Thoracic/Head and Neck Medical Oncology,
The University of Texas M. D. Anderson Cancer Center,
Houston, TX, 77030, USA
E-mail: jskoo@mdanderson.org
Fax: +1-713-7945997

Z. Ju
Molecular Biosciences Research Group, Department of Chemistry and Biochemistry, Texas State University, San Marcos,
TX, 78666, USA

Introduction

Lung cancer remains a leading cause of cancer death, with an overall 10-year survival rate as low as 8–10% (Fry et al. 1999). It was estimated that more than 170,000 new cases of lung cancer would appear in the United States in 2003 and that about 150,000 individuals would die of the disease (Jemal et al. 2003). Lung cancer occurs in two major subtypes—nonsmall cell lung carcinoma (NSCLC) and small cell lung carcinoma. NSCLC accounts for approximately 80% of all cases, and is further classified as adenocarcinoma, squamous cell carcinoma or large cell carcinoma, based on cell morphology. It is widely accepted that the progenitor cell of adenocarcinoma and squamous cell carcinoma is the epithelial cell of the lung. Squamous cell carcinoma originates mainly from genetically altered surface epithelial cells in the conducting airways, while adenocarcinoma arises from alveolar type II epithelial cells in the lung itself. A better understanding of the etiology and pathogenesis of epithelial cancers should facilitate the identification of novel and better targets for the treatment and prevention of NSCLC.

The recent development of cDNA and oligonucleotide microarray analysis enables us to comprehensively analyze gene expression profiles in NSCLC cells and classify lung cancers at the molecular level (for recent reviews, see Petty et al. 2004; Whitsett et al. 2004 and

references therein). However, the use of epithelial tissue from sites adjacent to tumors as the normal control in such studies has drawn criticism (Braakhuis et al. 2004), as this tissue often includes histologically normal but genetically abnormal cells (Braakhuis et al. 2003). In the present study we have used primary organotypically cultured normal human tracheobronchial epithelial (NHTBE) cells as our control. We previously demonstrated that primary TBE cells adopt the mucociliary epithelial organization found in vivo when grown and maintained in a retinoid-sufficient bronchial epithelial growth medium (BEGM) using a three-dimensional organotypic air–liquid interface (ALI) culture method. We have already demonstrated the utility of this system for studying the physiology of airway epithelium (Koo et al. 1999a, b). Given that lung cancers originate from epithelial cells and that NSCLC cell lines represent mixed histotypes, we chose the human mucoepidermoid pulmonary carcinoma line NCI-H292 (H292) as the counterpart of normal bronchial epithelial cells to identify differentially expressed genes. The H292 cells retain epithelial morphology in culture, and are defined as a mucin-producing NSCLC cell line because they stain positive for mucicarmine (mucous differentiation). They also stain positively for keratin and vimentin, which are indicative of squamous differentiation. The cells have been widely used as surrogate epithelial cells for studying the regulation of *MUC5AC*, a marker for mucin gene expression in the mucous goblet cell of the bronchial surface epithelium (Takeyama et al. 1999; Koo et al. 2002; Lemjabbar and Basbaum 2002).

We used RNAs isolated from fully differentiated NHTBE cells and from the H292 NSCLC cell line to identify expressed genes by oligonucleotide microarray analysis on Affymetrix chips. The results revealed that 1,683 genes were differentially expressed (i.e., showed a >1.5-fold change in transcription level). Analysis of the differentially expressed genes revealed concurrent alterations in several biological pathways, including WNT and apoptosis pathways, cell cycle regulation and cell proliferation, in the H292 cell line. The differential expression of selected genes was further verified by real-time PCR and Western analysis in several other NSCLC cell lines. The NHTBE cells promise to be a useful control for the study of lung epithelial carcinogenesis. This study describes alterations in biological networks associated with NSCLC carcinogenesis, and provides a valuable resource for the identification and characterization of diagnostic markers and targets for lung cancer prevention and therapeutics.

Materials and methods

Three-dimensional organotypic ALI culture of NHTBE cells

Passage 1 NHTBE cells (Clonetics, San Diego, CA, USA) were subcultured once and then stored in liquid nitrogen. The stored cells were used for further cultures as described previously (Koo et al. 1999a, b). Briefly, 1×10^5 passage-2 NHTBE cells were seeded onto 24-mm permeable membranes (Transwell-Clear culture inserts; Corning, Acton, MA, USA) in a 1:1 mixture of BEGM (Clonetics) and Dulbecco's Modified Eagle's Medium (DMEM) supplemented with insulin (5 μg/ml), hydrocortisone (0.072 μg/ml), epidermal growth factor (0.5 ng/ml), T_3 (10^{-8} M), transferrin (10 μg/ml), epinephrine (0.6 μg/ml), bovine pituitary extract (0.8%), BSA (0.5 mg/ml), gentamicin (50 μg/ml) and retinoic acid (5×10^{-8} M). The cultures were kept submerged for the first 7 days, and the medium was removed from the apical compartment to provide the air–liquid interface (ALI) on day 7 or 8 when the cultures were confluent. Culture was continued under these conditions for a further 21 days (changing the medium daily) to generate fully differentiated mucociliary bronchial epithelial cells.

Culture of NSCLC cell lines

The NSCLC cell lines NCI-H226 (H226), H292, NCI-H520 (H520), NCI-H1563 (H1536), NCI-H1703 (H1703), NCI-H1734 (H1734), NCI-H1975 (H1975), NCI-H2228 (H2228), NCI-H2170 (H2170), and A549 were purchased from the American Type Culture Collection (Manassas, VA, USA). All of the cell lines were maintained in RPMI 1640 medium (Gibco BRL, Life Technologies, Grand Island, NY, USA) supplemented with 10% fetal bovine serum (Hyclone, Logan, Utah), penicillin (100 U/ml), and streptomycin (100 mg/ml) on treated, nonpyrogenic, polystyrene tissue culture dishes at 37°C and a pH of 7.0–7.2 in a humidified atmosphere (95% air/5% CO_2). Total RNA for microarray analysis and real-time PCR, and whole-cell lysates for Western analysis, were prepared from the cultured cells 3 days after the monolayers had become confluent.

Histology

For histological analysis, NHTBE and H292 cells were grown on porous membrane inserts (Transwell-Clear plates) in their optimal media (BEGM:DMEM mixture and RPMI with 10% FBS, respectively; see above) for 28 and 10 days, respectively. The detailed method was described previously (Gray et al. 1996; Koo et al. 1999b). The cultures were fixed in 10% neutral buffered formalin, embedded in paraffin, sectioned, and stained with hematoxylin-eosin (HE). The sections were then examined under the microscope and photographed.

RNA and oligonucleotide microarray preparation

Total RNA was extracted from cells using the RNeasy Kit (Qiagen, Valencia, CA, USA) according to the manufacturer's protocol. The Affymetrix (Santa Clara,

CA, USA) GeneChip U95Av2 was employed for microarray hybridizations. This GeneChip carries 12,626 human genes. Each gene is represented by 11–20 different 25mers referred to as perfect match (PM) oligonucleotides, and each PM oligonucleotide is paired with a mismatch (MM) oligonucleotide having a 1-base mismatch at the thirteenth base. Each of the 11–20 PM–MM pairs representing a gene is termed a 'probe set'. Thus, the U95Av2 chip contains 12,626 probe sets. The oligonucleotides are directly synthesized on a silicon chip using a combination of photolithography and combinatorial chemistry.

For microarray hybridization, we followed the protocol described in the Affymetrix manual to synthesize double-stranded cDNA from mRNA and then used this cDNA to synthesize complementary RNA (cRNA). The cRNA was labeled and used for hybridization with the GenChips. Briefly, 5 μg of total RNA was converted into first-strand cDNA by reverse transcription (RT) in a 20-μl reaction containing 200 U of SuperScript II (Invitrogen, Carlsbad, CA, USA) and 100 pmol of T7-$(dT)_{24}$ primer [5′-GGCCAGTGAATTGTAATACGACTCACTATAGGGAGGCGG-$(dT)_{24}$-3′ (GeneSet, San Diego, CA, USA). The reaction was incubated at 42°C for 1 h. The second strand of the cDNA was synthesized at 16°C for 2 h in the presence of DNA polymerase I (40 U), DNA ligase (10 U), RNase H (2 U), and 1x second strand buffer (Invitrogen). The double-stranded cDNA was then blunt-ended using 20 U of T4 DNA polymerase, purified by extraction with phenol/chloroform, and transcribed into cRNA in the presence of biotin-labeled ribonucleotides using the BioArray HighYield RNA Transcript Labeling Kit (Affymetrix) as described by the manufacturer. This biotin-labeled cRNA was purified using the Qiagen RNeasy Kit, quantified, and fragmented by incubation at 94°C for 35 min in the presence of 1 (fragmentation buffer [40 mM TRIS-acetate (pH 8.0), 100 mM potassium acetate, and 30 mM magnesium acetate]. The fragmented cRNA was then used for hybridization to the U95Av2 chip at 42°C for 16 h. The chips were washed and stained using Affymetrix GeneChip Fluidic, and scanned and visualized using a GeneArray Scanner (Hewlett-Pacrkard, Palo Alto, CA, USA).

To maintain experimental consistency, approximately equal numbers of cells were collected at similar stages, and the same group of researchers performed the RNA isolation and microarray hybridization in a repeat experiment.

Data collection and bioinformatic analysis

The microarray hybridization data were collected using the Affymetrix Microarray Suite 5.0 software (MAS 5.0). After collection, the data were exported to the Affymetrix MicroDB for further analysis using the Affymetrix Data Mining Tool 3.0 (DMT). The signal-intensity data extracted with the DMT were statistically analyzed using S-plus 2000 software (Mathsoft, Cambridge, MA, USA) to obtain correlation coefficients and scatter plots for evaluation of the reproducibility and quality of the array analysis. The qualified data sets were then analyzed using DNA-Chip Analyzer software (dChip) (Li and Wong 2001). Briefly, the array data sets were first normalized using a default baseline array; the PM–MM model was then employed to calculate the expression values. To identify the differentially expressed genes using dChip, we set 100 as the average signal-intensity difference to avoid the effects of unreliable low intensity, and used the lower confidence bound of fold change (LBFC; 90%) as the conservative relative change (1.5×). The differentially expressed genes were then subjected to clustering, categorical, and pathway analysis using dChip and public databases such as PubMed (http://www.ncbi.nlm.nih.gov/entrez/query.fcgi?db=PubMed), EASEonline (http://david.niaid.nih.gov/david/upload1.asp) and the Kyoto Encyclopedia of Genes and Genomes (KEGG, http://www.genome.ad.jp/kegg/). Details of the genes (and gene products) specifically considered in this present work are listed in the Tables.

Quantitative real-time PCR (qRT-PCR)

We used qRT-PCR to validate 15 of the differentially expressed genes identified via microarray analysis. The primer pairs used are listed in Table 1. PCR was performed in 25-μl volumes in an iCycler (Bio-Rad, Hercules, CA, USA) using SYBR Green PCR Core Reagents (Applied Biosystems). The reaction contained 0.2-mM primers (Invitrogen), 3-mM $MgCl_2$, and 3 μl of the RT mix. The housekeeping gene glyceraldehyde-3-phosphate dehydrogenase (GAPDH) was chosen as the reference. Each sample was duplicated in each run, and the experiment was repeated four times. The reactions for tested genes and GAPDH were set up in separate wells of the same 96-well plate, and a prerun using a well factor solution (Bio-Rad) to subtract the background was carried out, followed by an initial denaturation step at 95°C for 10 min. PCR was performed for 40 cycles of denaturation at 95°C for 20 s, and elongation at 60°C for 60 s. Because GAPDH was consistently expressed at a moderate level in the microarray experiment, each PCR result was normalized against the value for GAPDH.

Western analysis

Western analysis used to confirm that differential gene expression was reflected at the translation level. Antibodies raised against beta-catenin (E-5, 1:500), CDK1 (B-6, 1:1000), CCNB1 (GNS-1, 1:1000), GAS6 (D-18, 1:1000), AKT (C-20, 1:1000), API (IAP-1, 1:1000), and BCL2 (C-2, 1:1000) were purchased from Santa Cruz Biotechnology (Santa Cruz, CA, USA). An anti-β-actin

Table 1 Primer pairs used for qRT-PCR

Target gene	Sequence (5′–3′)
AATF	TCAGCCTGTCCCAGAGAGTT and CGAAGGAGCTGGTGGTAAAA (AATF)
AKT	CACACCACCTGACCAAGATG and CTGGCCGAGTAGGAGAACTG-3′
API5	ACAGGCCGACCTAGAACAGA and AGGGAGAACCTGCTCACAGA
AXL	GACGGGTCTGTGTCCAATCT and ACGAGAAGGCAGGAGTTGAA
BCLX	GGAGCTGGTGGTTGACTTTC and CTCCGATTCAGTCCCTTCTG
CDK1	CTTTTCCATGGGGATTCAGA and AGGCTTCCTGGTTTCCATTT
CYCS	TGGGGAAATTGCTTCACTGT and CTTCAACCCTTGCCTTTAAGA
GAS6	GGACCTCGTGCAGCCTATAA and CCTGGATGGTGGTGTCTTCT
IGFBP4	GACCATCGTCCTTCCTCTCA and GTCTGGACCTCGTGACCATT
KRT6E	CATTGGAGGTGGCTTCAGTT and GAGGAGGAGGTGGTGGTGTA
LOH11CR2A	AACCCAAGCCTGATGTCAAC and ACTTGCTGGAGTCTCCCTGA
MYC	GGCAAAAGGTCAGAGTCTGG and GTGCATTTTCGGTTGTTGC
SFRP1	GCTCCAGTTTGCATTTGGAT and ACCTGAGCCTCCTGCATCTA
TF	CCTGATCCATGGGCTAAGAA and CCTCCACAGGTTTCCTGGTA
TP53	TTTGGGTCTTTGAACCCTTG and CCACAACAAAACACCAGTGC

antibody (AC-15, 1:5,000) was purchased from Sigma (St. Louis, MO, USA) and used as an internal control. Whole-cell extracts were obtained by lysing cells with 1 ml of lysis buffer [(20% glycerol, 4% SDS, and 0.3% dichlorodiphenyltrichloroethane in 20 mM TRIS–HCl, (pH 6.8)] per well. The cell lysate was quantified, and a total of 30 µl of the lysate was electrophoresed on SDS-polyacrylamide gels (10%) and transferred to nitrocellulose membranes. Membranes were blocked, incubated with primary antibodies, and subsequently incubated with diluted (1:2,000) horseradish peroxidase-conjugated goat antirabbit IgG or goat antimouse IgG (Bio-Rad). Labeled bands were detected using the SuperSignal West Pico Chemiluminescent Substrate (Pierce, Rockford, Ill.) and exposed to Hyper MP autoradiography film (Amersham, Little Chalfont, Bucks., UK) or Kodak Scientific Image Film (Eastman Kodak, Rochester, NY, USA). β-Actin was used as an internal control.

Fluorescence-activated cell sorting (FACS)

FACS was used to monitor the cell cycle, apoptosis, cell proliferation, and the mitochondrial membrane potential. For cell cycle analysis, cells were seeded in 2 ml of medium at a density of 1×10^5 cells/well in 6-well plates. After the cells had reached confluence, the attached cells were flushed twice with 1× phosphate-buffered saline (PBS), trypsinized, washed, and resuspended in 1xPBS.

For cell cycle analysis, a 2-ml aliquot of cell suspension (approximately 10^6 cells) was added to 5 ml of 95% ethanol under gentle vortexing, and then fixed for at least 30 min at room temperature. The fixed cells were then pelleted by centrifugation, resuspended in 1 ml of (50 µg/ml) propidium iodide (PI; Sigma) and 100 µl of 1 mg/ml RNase (Roche, Indianapolis, Ind.), and incubated at 37°C for 30 min before being loaded onto a FACScan (BD Biosciences, Franklin Lakes, NJ, USA).

For apoptosis analysis, the cell pellet ($\sim10^6$ cells) obtained after trypsinization and washing was resuspended and stained using the Annexin-V-FLUOS staining kit (Roche) as described in the manufacturer's instructions. Cells that had not been stained with annexin were used as the controls.

For cell proliferation analysis, cells were seeded into 6-well culture plates at a density of 1×10^5 cells/well. After the cells reached the exponential growth stage, bromodeoxyuridine (BrdU) was added directly to the medium at a final concentration of 10 µM. The cells were incubated at 37°C for 60 min and stained using the Anti-BrdU-FITC Kit (BD Biosciences) following the manufacturer's instructions. Cells that had not been exposed to anti-BrdU-FITC were used as controls. The absorbance of the FITC at 488 nm was measured using a FACScan (BD Biosciences).

For mitochondrial membrane potential analysis, the mitochondrial membrane potential was normalized and measured using two-color staining with MitoTracker Green (MTGreen) and CMXRosamine (CMXRos) dyes (Molecular Probes, Eugene, OR, USA). Confluent cells were harvested and resuspended at a concentration of 10^6 cells/ml in prewarmed cell culture medium. A 1-ml aliquot was removed to a 15-ml Falcon tube and incubated in a 37°C water bath for at least 5 min. Next, 1 µl each of the dye stock solutions (200 µM MTGreen and 200 µM CMXRos) was added to the cell suspension and mixed well. The cell suspension was incubated at 37°C for 60 min in the dark. The cells were then washed three times using 1 ml of 1xPBS, and the cell pellet was resuspended in 500 µl of medium. Immediately after staining, flow cytometry was performed with a FACScan (BD Biosciences) using an excitation wavelength of 488 nm. We measured the emissions with a 530-nm bandpass filter for MTGreen and a 630-nm long-pass filter for CMXRos.

Statistical analysis

The qRT-PCR and FACS data were subjected to statistical analysis. The qRT-PCR experiment was repeated two to four times with duplicates of each sample. In each qRT-PCR, a GAPDH standard curve was generated using the log-starting quantity of a serial dilution of the RT mix. The serial dilution factor was $1/2^n$ ($n=5$); each

dilution was measured in duplicate. Data acquisition and standard curve generation were performed using an iCycler 3.0 (Bio-Rad). Transcript levels were calculated from the slope of the standard curve using the formula $x\{y-b\}/a$, where x is the $\log_{10}$ value of the transcript-starting amount, y is the C_t value, a is the slope, and b is the y interception. The relative change was obtained using the ratio of inverse $\log_{10}$ values of x between the tumor and normal cells. Standard errors (SE) were obtained for the fold change based on the repeated QRT-PCR experiments using statistical functions in the Excel software program (Microsoft, Redmond, WA, USA).

The FACS analysis was repeated at least three times. FACS data were collected using a FACScan (BD Biosciences) and analyzed using the WinMDI software (version 2.8) (http://facs.scripps.edu/software.html) and Excel statistical functions.

Results

Histological analysis of NHTBE and H292 cells grown in ALI culture

Primary or early passage NHTBE cells were cultured under organotypic ALI conditions in defined serum-free medium supplemented with growth factors and hormones as described previously (Koo et al. 1999a, b). The morphological pattern of differentiation mimicked that of pseudostratified mucociliary bronchial epithelium in vivo, as shown in Fig. 1. Basal cells attached to the basement membrane and a significant number of ciliated cells were clearly visible in the polarized columnar epithelium that formed in the culture system. Under these conditions, the ability of these cells to differentiate into mucous and ciliated cells was maintained. The use of ALI cultures for the study of bronchial epithelial cell biology was demonstrated previously (Gray et al. 1996; Kolodziejski et al. 2002; Koo et al. 1999b; Singer et al. 2004). In sharp contrast, H292 NSCLC cell lines cultured under similar conditions generated multiple layers of cells that did not display any obvious basal-apical polarity.

Fig. 1 **a, b** Histological analysis of NHTBE and H292 cells grown in ALI culture. **a** NHTBE cells were grown under ALI conditions in the presence of retinoic acid (5×10^{-8} M) for 28 days, then fixed in 10% neutral buffered formalin, embedded in paraffin, sectioned, and stained with hematoxylin and eosin. For the detection of mucous goblet cells, the section was also stained with Alcian Blue–Periodic Acid Schiff's (*arrows*). **b** Histological section of H292 cells grown in RPMI1640 supplemented with 10% fetal bovine serum for 10 days in ALI culture were prepared and stained with hematoxylin and eosin as described above for NHTBE cells

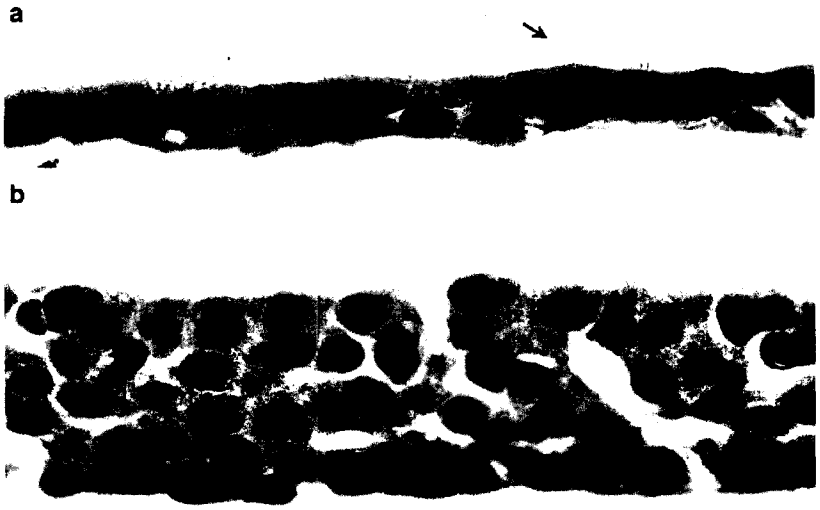

Oligonucleotide microarray analysis

To elucidate the molecular events involved in lung epithelial carcinogenesis, we examined global gene expression in NHTBE cells and the H292 cell line using the Affymetrix oligonucleotide chip U95Av2 as described in Materials and methods. The experiment was performed in duplicate. To check the quality of the experiment, we generated scatter plots and calculated correlation coefficients between replicates. We found a strong correlation between replicates within the same samples. The correlation coefficient was 0.97 for NHTBE replicates (Fig. 2a) and 0.99 for H292 replicates (Fig. 2b), and the linear relationship in the x–y plane was close to diagonal (Fig. 2a, b), indicating that the replicates within the samples were highly reproducible and consistent. In contrast, the relationship between replicates of different samples (Fig. 2c–f) was marked by a high degree of scatter and was not linear. Accordingly, the correlation coefficients (0.79, 0.79, 0.85, and 0.85, respectively) were much lower than those for within-sample comparisons, indicating that the nature of the samples had a greater effect on data variation than handing error. Therefore, we concluded that these microarray hybridizations were

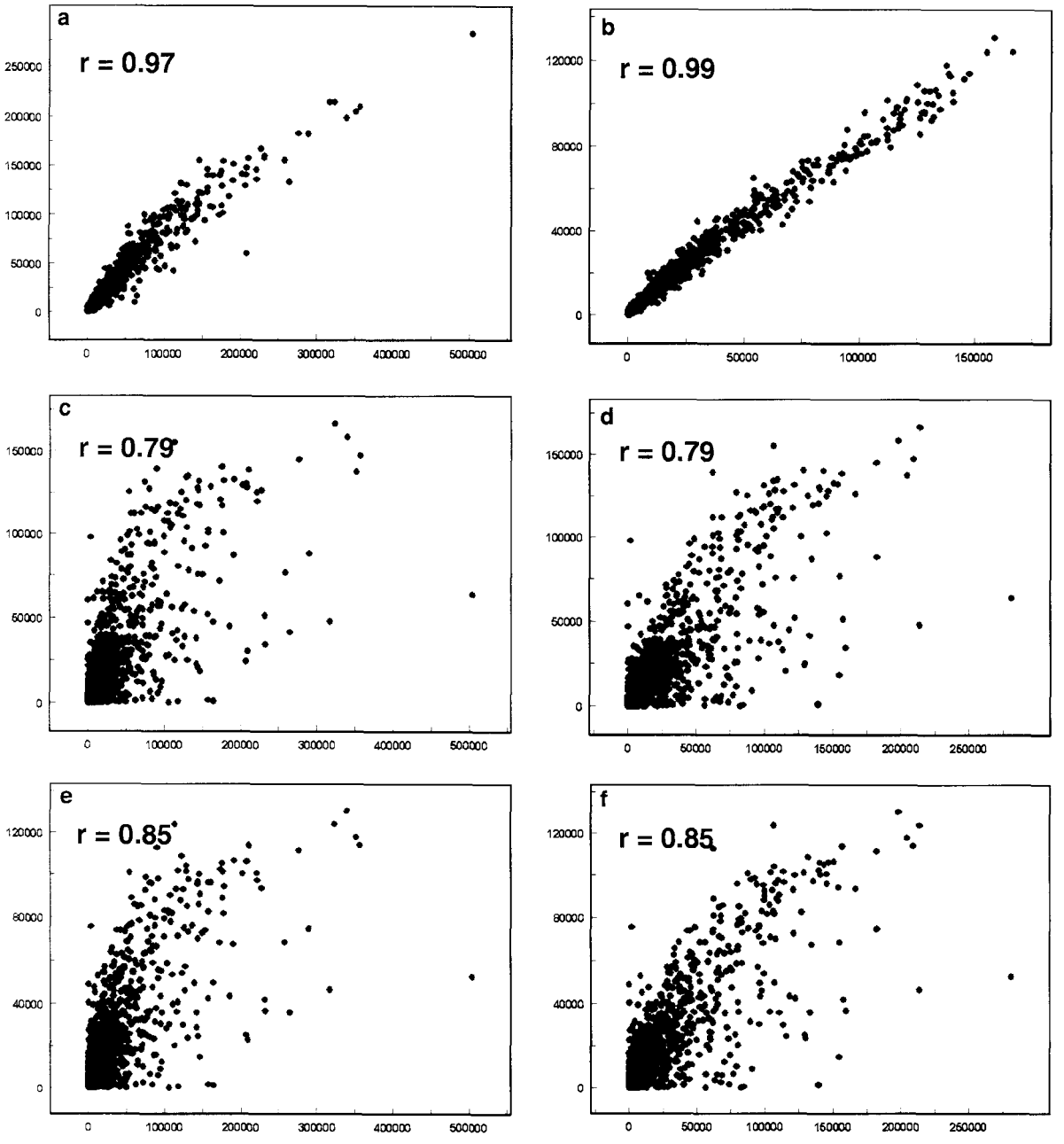

Fig. 2 a–f Scatter plots of microarray signal intensity data. **a** Replicates of NHTBE plotted against each other. **b** Replicates of H292. **c** Replicate 1 of NHTBE versus replicate 1 of H292. **d** Replicate 1 of NHTBE versus replicate 2 of H292. **e** Replicate 2 of NHTBE versus replicate 1 of H292. **f** Replicate 2 of NHTBE versus replicate 2 of H292. *r* is the correlation coefficient

successful and likely to provide reliable data for further analysis.

Differentially expressed genes and the gene expression profile

After qualification and quantification of the microarray experiment, gene expression in the two cell lines was analyzed, and differentially expressed genes were identified using dChip. Out of 12,625 genes analyzed, 418 were downregulated, and 1,265 were upregulated by at least 1.5-fold in H292 cells relative to the NHTBE cells. The downregulated genes included genes related to the cytoskeleton structure, immunoglobulins, inflammatory stress, the basement membrane, small cytokines, stress responses, and tumor suppressors. The upregulated genes were related mainly to antiapoptosis, the cell cycle, cell growth, extracellular proteins, heat shock proteins, nucleic acid-binding proteins, transcription, and translation. These differentially expressed genes provided the pool for further genomic analysis on biological pathways, biomarkers therapeutic targets (data not shown).

Elucidation of biological pathways

To elucidate the biological pathways affected in the H292 cells, we first used the 'Classify Genes' option in dChip to separate the 1,683 differentially expressed genes into ontology groups. Based on molecular functions, we obtained 1,158 gene ontology groups (approximately 1.5 unique genes per group). Disregarding the more general group categories (such as cell, receptor, kinase, inhibitor, and enzyme), we focused on identification of the groups associated with particular functions and pathways. After data mining, we found that the expression of genes in 30 ontology groups closely related to apoptosis, cell cycle, cell proliferation, and WNT responses (Table 2) were substantially altered in the H292 cell line when compared with NHTBE cells. These groups contained 594 genes representing 146 unique genes (approximately 5.1 unique genes per group), which were subsequently assigned to the four pathways. The overlapping genes were arbitrarily assigned to one or other of these pathways using published information from PubMed, EASEonline, and KEGG. In summary, 38, 56, 48, and 10 unique genes were assigned to the apoptosis, cell cycle, proliferation, and WNT pathways, respectively (data not shown). Differentially expressed genes that showed a more than three-fold change or are directly related to the WNT, cell cycle, proliferation, and apoptosis pathways are listed in Table 3.

Table 2 Gene ontology (GO) classification of differentially expressed genes related to the apoptosis, cell cycle, and proliferation pathways, identified via microarray analysis

GO group	Number of genes
Apoptosis	35
Apoptosis inhibitor	7
Apoptosis regulator	7
Cell cycle	77
Cell cycle arrest	8
Cell cycle checkpoint	8
Cell cycle control	50
Cell cycle regulator	8
Cell death	38
Cell proliferation	75
Control of mitosis	4
DNA replication and chromosome cycle	21
G1/S transition in mitotic cell cycle	8
G2/M transition in mitotic cell cycle	6
Ligand-regulated transcription regulator	11
M phase	13
M phase of mitotic cell cycle	13
Mitosis	13
Mitotic cell cycle	37
Positive control of cell proliferation	21
Negative control of cell proliferation	14
Regulation of CDK activity	6
S phase of mitotic cell cycle	16
Transcription	99
Transcription factor	20
Transcription regulator	48
Translation elongation factor	1
Translation factor	20
Translation initiation factor	5
WNT signaling	10

Validation of the differentially expressed genes

A subset of the differentially expressed genes was chosen for validation by qRT-PCR and Western analysis (Table 3). Fifteen genes, SFRP1, CDK1, MYC, AXL, GAS6, IGFBP4, AATF, AKT, API5, BCLX, CYCS, LOH11CR2A, TP53, KRT6E, and TF, were selected for qRT-PCR validation. SFRP1, which is related to the WNT pathway, was upregulated 12.8-fold in H292 cells compared to NHTBE cells. The cell cycle genes CDK1 and MYC were upregulated 8.0- and 6.2-fold, respectively; the proliferation genes AXL, GAS6, and IGFBP4 were upregulated 2.9-, 18.6-, and 2.6-fold, respectively. The antiapoptosis genes AATF, AKT, API5, and BCLX were upregulated by 43.5-, 23.0-, 38.4-, and 17.7-fold, respectively; the proapoptosis gene LOH11CR2A was downregulated by 33.9-fold, and the proapoptosis genes CYCS and TP53 were upregulated by 27.8- and 23.3-fold, respectively.

Seven genes, Beta-catenin, CDK1, CCNB1, GAS6, AKT, API5, and BCL2, were selected to validate gene expression at the translation level in the NSCLC cell lines H292, H1975, H226, H2170, H520, H1734, H1703, A549, H1536, and H2228 using Western analysis. The transcription levels of these genes in H292 cells were determined by microarray analysis or qRT-PCR. Western analysis revealed that the levels of their products were also elevated in H292 cells compared with those in NHTBE cells (Fig. 3). The expression levels of the proteins Beta-catenin, GAS6, AKT, API5, and BCL2 varied among the different lung cancer cell lines tested. Strikingly, CDK1 and CCNB1 were highly expressed in almost all of the lung cancer cell lines but not in NHTBE cells. The gene expression levels detected by qRT-PCR and Western analysis were in good agreement with those detected by microarray analysis (Table 3).

Validation by FACS analysis of changes in apoptosis, cell cycle kinetics, and cell proliferation

As the expression of genes related to the apoptosis, cell cycle, and proliferation pathways was greatly altered in H292 cells relative to the NHTBE cells, we used FACS analysis to verify that the processes they are expected to mediate or control were altered in a similar manner. Cell cycle analysis using propidium iodide staining indicated that there were significant differences in the numbers of cells in the M4 (apoptotic or necrotic cells), G1/G0, S, and G2 phases between H292 and NHTBE cells (Fig. 4a–c). A significantly lower percentage of H292 cells was found to be in the M4, G1/G0, and G2 phases compared with NHTBE cells, but a significantly higher percentage was in S phase (Fig. 4c). These findings indicate that in H292 cells both the G1/S and G2/M

Table 3 Differentially expressed genes related to WNT pathways, apoptosis, or cell proliferation-identified via microarray analysis

Gene symbol[a]	Gene (product) description	LBFC[b]	Relative change based on qRT-PCR	Western analysis
WNT pathway related				
Beta-catenin	Catenin (cadherin-associated protein), beta 1 (88 kDa)	1.9	NA	Confirmed
CBP	CREB-binding protein	2.3	NA	
CK1	Casein kinase 1	1.7	NA	
CK2	Casein kinase 2	3.8	NA	
Dvl	Human Disheveled protein	2.1	NA	
GAS6	Growth arrest-specific 6	2.4	18.6 ± 2.0	Confirmed
MYC	v-myc myelocytomatosis viral oncogene homolog	3.3	6.2 ± 2.3	
SFRP1	Secreted Frizzled-related protein 1	24.3	12.8 ± 5.4	
TCF	T-cell factor	2.1	NA	
Cell cycle related				
CCNB1	Cyclin B1	3.0	NA	Confirmed
CDK1	Cyclin-dependent kinase 1	1.4	8.0 ± 1.4	Confirmed
CITED2	Cbp/p300-interacting transactivator	5.2	NA	
E2F3	E2F transcription factor 3	3.2	NA	
FEN1	Flap structure-specific endonuclease 1	4.7	NA	
MAD2L1	MAD2 [mitotic arrest deficient-like 1 (yeast)]	3.9	NA	
PDGFA	Platelet-derived growth factor alpha polypeptide	6.6	NA	
SMC1L1	SMC1 [structural maintenance of chromosomes 1-like 1 (yeast)]	3.6	NA	
SMC4L1	SMC4 [structural maintenance of chromosomes 4-like 1 (yeast)]	3.9	NA	
TP53	Tumor protein p53 (Li-Fraumeni syndrome)	3.0	23.3 ± 11.4	
Apoptosis related				
AATF	Apoptosis-antagonizing transcription factor	2.4	43.5 ± 2.7	
AKT	v-akt murine thymoma viral oncogene	1.2	23.0 ± 2.5	Confirmed
API5	Apoptosis inhibitor 5	1.5	38.4 ± 2.3	Confirmed
BCL2	B-cell lymphoma/leukemia-2	2.3	NA	
BCLX	BCL2-like 1	1.2	17.7 ± 2.1	
CYCS	Cytochrome *c*	2.9	27.8 ± 1.7	
FANCG	Fanconi's anemia, complementation group G	−9.0	NA	
LOH11CR2A	Loss of heterozygosity, 11, chromosomal region 2, gene A	−6.2	−33.9 ± 17.5	
Cell proliferation				
AKR1C3	Aldo-keto reductase family 1, member C3	−3.6	NA	
AXL	AXL receptor tyrosine kinase	24.7	2.9 ± 1.4	
CSE1L	CSE1 [chromosome segregation 1-like (yeast)]	3.9	NA	
EGFR	Epidermal growth factor receptor (v-erb-b oncogene)	3.4	NA	
FSCN1	Singed-like (*Drosophila*) (fascin homolog, sea urchin)	5.5	NA	
GPNMB	Glycoprotein (transmembrane) Nmb	−4.5	NA	
IGFBP4	Insulin-like growth factor-binding protein 4	6.6	2.6 ± 0.7	
MATK	Megakaryocyte-associated tyrosine kinase	3.6	NA	
RARRES3	Retinoic acid receptor responder (tazarotene induced) 3	−9.6	NA	
SERPINF1	Serine (or cysteine) proteinase inhibitor	−3.5	NA	
TGFBI	Transforming growth factor beta-induced	3.5	NA	
Others				
KRT6E	Keratin 6	−5.4	−64.0 ± 29.7	
TF	Transferrin	−22.5	−18.5 ± 6.6	

transitions are altered. To confirm these findings and this interpretation, we used more specific methods to analyze apoptosis and cell proliferation in NHTBE and H292 cells (see Materials and methods). To analyze apoptosis, we used Annexin-V-FLUOS in combination with PI to distinguish apoptotic and necrotic cells from viable cells by characterizing the loss of plasma membrane asymmetry, and we performed mitochondrial membrane potential analysis with MTGreen and CMXRos to further elucidate the interaction between BCL2 and CYCS in the H292 cells. The Annexin-V-FLUOS experiment showed that 27.04% of the NHTBE cells underwent programmed cell death, but only 2.05% of the H292 cells did so (Fig. 4d). Analysis of the mitochondrial membrane potential also showed a statistically significant difference between NHTBE and H292 cells (Fig. 5). Specifically, H292 cells showed significantly less loss of membrane potential than NHTBE cells did. This may be due mainly to BCL2-dependent inhibition of the release of CYCS from the mitochondria in the H292 cells.

In addition, to measure cell proliferation, we calculated the ratio of BrdU-stained nuclei to the total number of nuclei. Immunohistochemical staining using an anti-BrdU-FITC antibody indicated that 19.75% of the H292 cells but only 5.16% of the NHTBE cells were in the S phase (Fig. 4d). Thus, the H292 cells show a significantly higher rate of cell cycle progression and cell proliferation and a lower level of apoptosis than the NHTBE cells.

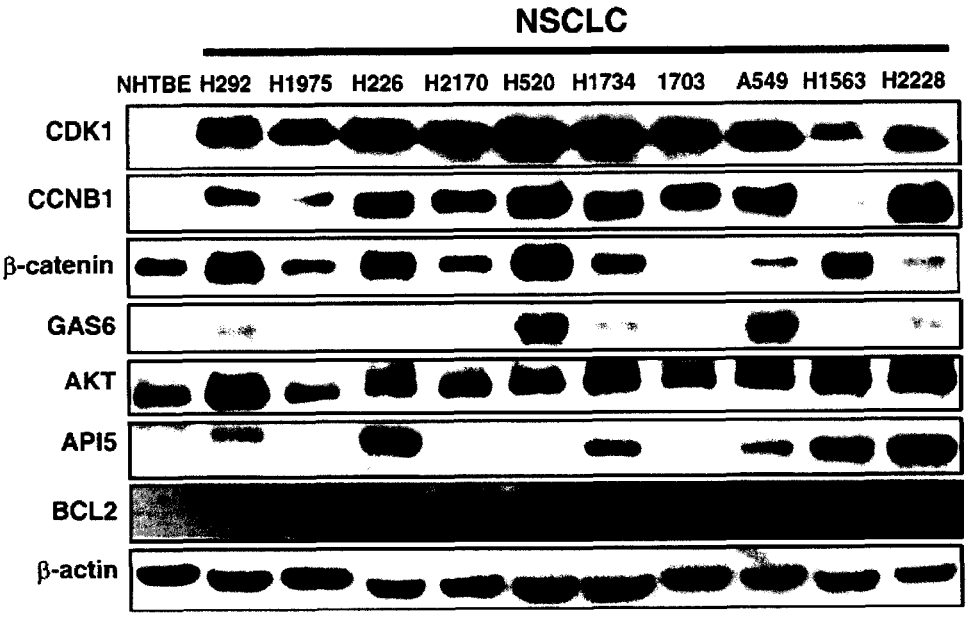

Fig. 3 Western analysis of selected gene products in various cell lines to validate that the differential expression of genes detected in H292 cells is reflected at the translation level. All of the tested proteins were evaluated in H292 cells and in NHTBE cells (β-actin was used as an internal control)

Discussion

It is generally accepted that NSCLC, adenocarcinoma and squamous cell carcinoma in the lung generally arise from airway and alveolar epithelial cells. Numerous previous microarray analyses of NSCLC tissues and cell lines focused on survival prediction, molecular characteristics, tumor classification, target identification, and tumor and cell line integration (Petty et al. 2004; Whitsett et al. 2004). However, the use of morphologically normal tissue taken from sites adjacent to tumor tissue as the normal control has provoked concern. In addition, it has been well documented that bronchial epithelia cells do not retain the normal mucociliary phenotype if they are grown and maintained submerged in culture medium on a two-dimensional plastic culture plate (Wu et al. 1990; Ostrowski and Nettesheim 1995). In this study we used organotypically cultured, fully differentiated, normal primary bronchial epithelial cells, which recapitulate the in vivo differentiation of bronchial epithelia as our normal control. The H292 NSCLC cell line was used as the tumor counterpart for microarray analysis and several NSCLC cell lines maintained under their optimal culture conditions were used to verify differential expression of selected genes.

In order to evaluate the usefulness of our model for the study of lung carcinogenesis, we compared our results with gene expression-profiling studies recently done by others using lung specimens and cell lines (Nacht et al. 2001; Amatschek et al. 2004; Kettunen et al. 2004). One should note that it is difficult to compare studies that use different array platforms or methods (cDNA array; cDNA subtraction; serial analysis of gene expression, SAGE), different types of specimens (tumor tissue vs. normal tissue; tumor tissue vs. tumor cell lines), and different analytical and statistical algorithms, as already pointed out by Kettunen et al. (2004). These differences could contribute to a certain degree of disagreement among studies. We found that our set of differentially expressed genes showed 86.7%, 68.4%, and 62.5% agreement with those presented by Kettunen et al. (2004), Amatschek et al. (2004) and Nacht et al. (2001), respectively (Table 4). Of the upregulated genes identified by Kettunen et al (2004) in a comparison of tumor tissue with normal tissue, 15 genes overlapped with our set, and 13 (86.7%) of these, including the genes for integrin beta 4 (ITGB4), retinoic acid receptor gamma (RARG), insulin-like growth factor-binding protein 5 (IGFBP5), and integrin alpha 6 (I TGA6)—those most highly upregulated in lung specimens—agreed with the expression changes detected in this study. These results indicate that the organotypically cultured primary bronchial epithelial cells could be a useful model for normal controls in the study of lung epithelial carcinogenesis.

We also assigned the differentially expressed genes to biological pathways, and found that genes related to the WNT, apoptosis and cell cycle pathways, and to cell proliferation, were concurrently deregulated in the NSCLC cells. A scheme depicting the biological network consisting of three pathways [WNT, cell cycle and apoptosis, which include the mitochondrially and tumor necrosis factor (TNF)-regulated pathways], and the proliferation phenotype, that are deregulated in H292 cells was constructed based on our findings and data mining using public database PubMed and the KEGG (Fig. 6).

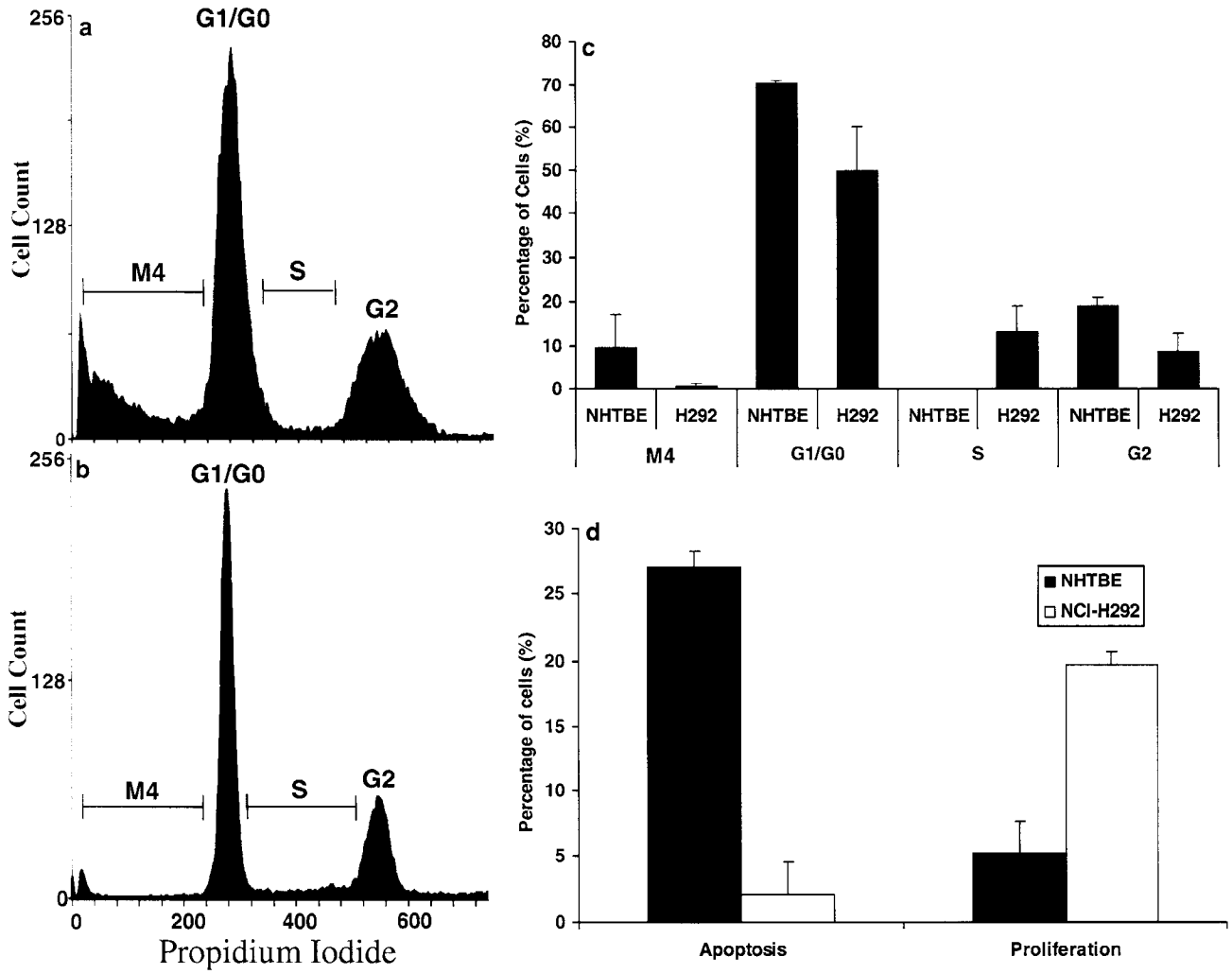

Fig. 4 a–d FACS analysis of the cell cycle, apoptosis, and proliferation in NHTBE and H292 cells. *Panels* **a** and **b** show the results of repeated experiments, which indicate that there were significant differences between the two cell lines. **a** NHTBE cells. A significantly higher percentage of the NHTBE cells is in the M4 (apoptosis or necrosis) or G2 phase. **b** H292 cells. A significantly higher percentage of H292 cells is in S phase. **c** Summary of the statistical analysis. **d** Comparisons of rates of apoptosis and cell proliferation between the NHTBE and H292 cells indicate that the H292 cells are more active in proliferation and less active in apoptosis. Thus, about 19.75% of the H292 cells progressed from the G1 checkpoint to S phase, but only about 5.16% of the NHTBE cells were in S phase. Moreover, only 2.05% of the H292 cells, compared with 27.04% of the NHTBE cells, were found to be apoptotic

The WNT pathway has been shown to be involved in approximately 90% of colorectal cancers (Giles et al. 2003), Although differential regulation of components of the the WNT pathway such as β-catenin and Disheveled (Dvl) was previously reported in lung cancer (Smythe et al. 1999), the role of the WNT pathway in lung epithelial carcinogenesis is much less clear. In the current study, we found that 10 WNT pathway-related genes (SFP, SFRP1, CK1, CK2, Dvl, GAS6, β-catenin, PP2A, CBP, and TCF) were upregulated in H292 cells. Formation of WNT-SFP complexes triggers activation of the WNT pathway by activating Dvl, which is also activated through phosphorylation by casein kinase (CK) (Willert et al. 1997). The activated Dvl inhibits formation of a complex comprising Beta-catenin, APC, Axin, and GSK. GAS6, a growth factor, inhibits GSK activity and induces upregulation of cytosolic Beta-catenin (Goruppi et al. 2001). The tumor suppressor genes coding for APC, Axin, and GSK did not show changes in expression in H292 cells, but those for CBP and TCF, which form a transcriptional regulatory complex with β-catenin, were significantly upregulated in H292 cells. Activation of the WNT pathway can account for the overexpression of MYC (which is one of the pathway's critical targets) and an oncogene that has been demonstrated to be overexpressed in NSCLC (Broers et al. 1993).

Surprisingly, SFRP1 was also overexpressed in H292 cells. SFRPs have been reported to sequester WNTs by direct binding (Uren et al. 2000), thus inactivating the WNT pathway. WNTs are secreted growth-factor-like proteins that include at least 19 different isotypes. However, not every isotype induces the release of

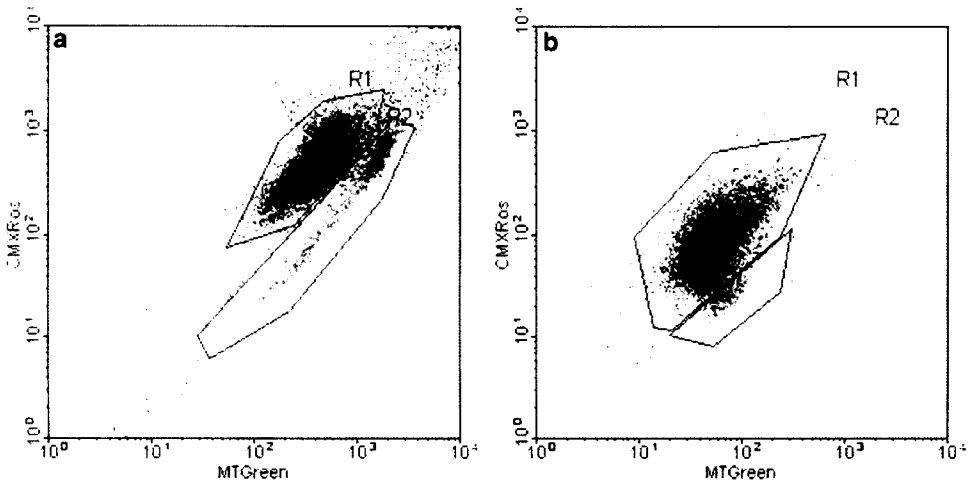

	MT Green [NS]	CM XRos [S]	LMP (R2 region) [S]
NHTBE	104.3 ±6.66	10 5.5 ±7.00	18.1 % ± 0.35%
NCI -H292	104.3 ±7.09	75.0 ±4.72	4.8 % ± 0. 78 %

Fig. 5 **a**, **b** Measurement of apoptosis based on the loss of mitochondrial membrane potential. Cells were treated with MTGreen (which stains all mitochondria) and CMXRos (which enters mitochondria that show a loss of membrane potential). *Panels* **a** and **b** show combination dot plots for total NHTBE (**a**) and H292 (**b**) cells stained with both agents. Areas marked R2 encompass the apoptotic cells, which show a loss of mitochondrial membrane potential. The Table below the graphs summarizes the data obtained from the membrane potential analysis. The values in the MTGreen and CMXRos columns represent the total events (numbers of cells) detected in the MTGreen and CMXRos channels. The MTGreen value is a measure of the number of mitochondria per cell, the CMXRos value is a measure of the induction of apoptosis, as indicated by a drop in mitochondrial membrane potential. The values in the LMP column indicate the percentages of apoptotic cells (those located in the R2 region) in the two dot plots. NS and S represent nonsignificant and significant differences between the NHTBE and H292 cells

β-catenin and enhances expression of targets of the WNT pathway. Recent discoveries have demonstrated that WNT5a inhibits B cell proliferation and suppresses hematopoietic malignancies (Liang et al. 2003), and promotes degradation of β-catenin (Topol et al. 2003). WNT7a was also reported to be absent, or present in reduced amounts, in lung cancer cells and primary tumors (Calvo et al. 2000). WNT5a and WNT7a have both been implicated as potential tumor suppressor genes (Ohiro et al. 2003; Topol et al. 2003). Thus, further studies will be needed to clarify whether SFRP1 sequesters tumor-suppressing WNTs and prevents tumor-suppressing signals from reaching the WNT pathway. Taken together, our results strongly suggest that the WNT pathways play an important role in lung epithelial cell carcinogenesis.

Genes involved in cell cycle regulation and cell proliferation were also upregulated in H292. Cell cycle genes—specifically CCNB1 and CDK1, the key regulators of the G2/M transition—were ubiquitously overexpressed in all of the NSCLC cell lines tested, but their expression levels were significantly lower in the NHTBE cells (Fig. 3). CCNB1 and CDK1 form a complex that promotes the G2/M cell cycle transition (Pines 1999; Wasner et al. 2003). It has been reported that patients whose tumors expressed CCNB1 at a high level had a significantly shorter survival time than did patients whose tumors expressed CCNB1 at a low level (Soria et al. 2000), but the roles of the CCNB1-CDK1 complex in lung carcinogenesis is unclear. Further studies of these two genes in NSCLC may contribute to the identification of biomarkers or therapeutic targets. Expression of many cell-proliferation-related genes was substantially altered (at least threefold) in H292 cells. Specifically, the antiproliferation genes RARRES3, GPNMB, AKR1C3, and SERPINF1 were downregulated, and the pro-proliferation genes EGFR, TGFBI, MATK, CSE1, FSCN1, and IGFBP4 were upregulated in H292 cells. In addition, AXL is known to be involved in the neoplastic transformation of fibroblast and leukemia cells (O'Bryan et al. 1991; Neubauer et al. 1997) and GAS6 induces expression of AXL. Both GAS6 and AXL were substantially upregulated in H292 cells. Further characterization of these genes and their functions in normal epithelial cells and lung cancer cells may be helpful in understanding cell cycle regulation and cell proliferation in NSCLC.

Apoptosis was blocked in H292 cells. Apoptosis is regulated by two pathways involving mitochondrial components and TNF, respectively (Budihardjo et al. 1999; Datta et al. 1999). In H292 cells, BCL2, BAG1, AKT, and heat shock proteins may block the mitochondrial pathway that induces apoptosis. BCL2, which has been previously reported to be abnormally expressed in NSCLC (Han et al. 2002), blocks the release of CYCS by blocking the mitochondria voltage-dependent anion channel (Shimizu et al. 1999). HSP70 and HSP90 have been reported to be antiapoptotic proteins (Beere et al.

Table 4 Comparison of differentially expressed genes identified in the present study with data from previous studies

Gene product (name)	LBFC	Compatible with previous findings
A kinase (PRKA) anchor protein (gravin) 12 (AKAP12)	26.5	No[a]
Arachidonate 5-lipoxygenase (ALOX5)	−18.3	Yes[a]
BENE	−3.1	Yes[a]
Bone morphology protein 5 (BMP5)	−2.2	Yes[a]
Caveolin 1 (CAV1)	1.8	No[a]
Cyclin B1 (CCNB1)	3.0	Yes[a, b]
Collagen 4, alpha 2 (COL4A2)	3.5	Yes[a]
Desmoplakin I (DPI)	6.4	Yes[a, b]
High-mobility group protein (HMGI)	2.2	Yes[a]
Insulin-like growth factor-binding protein 5 (IGFBP5)	2.5	Yes[a]
Integrin beta 4 (ITGB4)	1.9	Yes[a]
Integrin group	2.8	Yes[a]
Integrin, alpha 6 (ITGA6)	3.0	Yes[a]
Retinoic acid receptor, gamma (RARG)	2.3	Yes[a]
STAT induced STAT inhibitor 3 (SOCS3)	−2.1	Yes[a]
Aldo-keto reductase family 1, member C3 (AKR1C3)	−5.3	No[b]
Bullous pemphigoid antigen 1 (230/240kD) (BPAG1)	7.3	Yes[b]
Calumenin (CALU)	2.6	Yes[b]
Cytochrome P450, subfamily I (CYP1B1)	2.2	Yes[b]
Glycoprotein (transmembrane) nmb (GPNMB)	−7.9	No[b]
Glyoxalase I (GLOI)	1.9	Yes[b]
Keratin 6A (KRT6A)	−7.0	No[b]
Laminin, gamma 2 (LAMC2)	−2.8	No[b]
Ornithine decarboxylase 1 (ODC1)	4.5	Yes[b]
Parathyroid hormone-like hormone (PTHLH)	2.1	Yes[b]
Phosphoglycerate kinase 1 (PGK1)	1.9	Yes[b]
Prostaglandin-endoperoxide synthase 2 (PGES2)	5.4	Yes[b]
RAN, member RAS oncogene family (RAN)	2.8	Yes[b]
Reticulocalbin 1, EF-hand calcium-binding domain (RCN1)	2.9	Yes[b]
Transmembrane 4 super family member 1 (TM4SF1)	−2.7	No[b]
Trefoil factor 3 (intestinal) (TFF3)	−2.7	No[b]
Tripartite motif-containing 29 (TRIM29)	2.9	Yes[b]
Aldo-keto reductase family 1, member B10 (AKR1B10)	−2.4	No[c]
Keratin 14 (KRT14)	−2.3	Yes[c]
Keratin 17 (KRT17)	5.2	No[c]
Keratin 19 (KRT19)	−3.8	Yes[c]
Keratin 6A (KRT6A)	−7.0	Yes[c]
Mucin 1 (MUC1)	−6.3	No[c]
Small proline-rich protein 1B (Cornifin)	-5.5	Yes[c]
Tubulin, beta polypeptide (TubulinB)	2.5	Yes[c]

[a] Kettunen et al. (2004)
[b] Amatschek et al. (2004)
[c] Nacht et al. (2001)

2000; Pandey et al. 2000). HSP70 is localized in both the cytoplasm and the nucleus in 90% of NSCLC cells (Malusecka et al. 2001). HSP70 binds to APAF1 and prevents the recruitment of caspases to the apoptosome complex (Beere et al. 2000), while HSP90 inhibits CYCS-mediated oligomerization of APAF1 and subsequent activation of procaspase 9 (Pandey et al. 2000). The TNF pathway may contribute to the inhibition of apoptosis in H292 cells, as genes for key members of the TNF pathway (TNF, TNF receptor, nuclear factor-κB, and API) were all substantially upregulated in H292 cells.

Although we maintained primary NHTBE, H292, and other NSCLC cells under conditions that are optimal for culture of the respective lines, as shown by us and others (Rose et al. 2001; Koo et al. 2002), and performed experiments when cultures had reached a stable plateau phase in order to minimize the effect of exponential cell growth on the expression profiles, a caveat to the interpretation of our current results is that the gene expression profiles were compared between NHTBE cells and pulmonary mucoepidermoid NCI-H292 cell line, and thus some of the profiles may only represent subsets of genes unique to the in vitro culture system. Further verification of the differentially expressed genes using clinical tumor samples is required. However, it is noteworthy that the organotypic bronchial epithelial cells in culture, which mimic in vivo airway epithelium, can provide a useful model system for understanding the progression of normal bronchial epithelial cells to premalignant and malignant transformation.

In summary, by comparing the gene expression profile of H292 NSCLC cells with that of NHTBE cells cultured in a three-dimensional organotypic culture system, we were able to identify genes (CCNB1 and CDK1, etc.) which could be potential biomarkers and therapeutic targets. Our results suggest that the abnormal growth

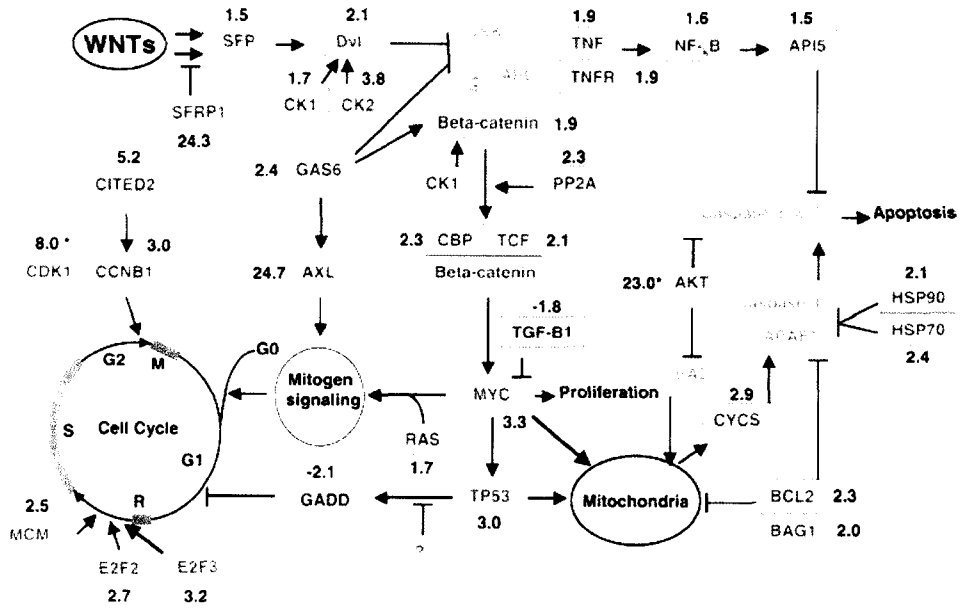

Fig. 6 Schematic representation of the genetic networks that are altered in H292 cells. The network consists of the pathways mediating WNT responses, cell cycle regulation, apoptosis (which includes mitochondrially and TNF-regulated pathways), and cell proliferation. The genes in *green* showed no change, the genes in *red* were upregulated, and the genes in *blue* were downregulated in H292 cells. The *numbers in black* indicate the LBFC (see Materials and methods), while the numbers marked with *asterisks* were obtained from qRT-PCR results. DVL, human Disheveled protein; CK1, casein kinase 1; CK2, casein kinase 2; GSK, glycogen synthase kinase 3 beta; PP2A, protein phosphatase 2A; CBP, CREB-binding protein; TCF, T-cell factor; TGF-B1, transforming growth factor-beta 1; RAS, Ras; GADD, growth arrest and DNA-damage-inducible gene; E2F2, E2F transcription factor 2; MCM, minichromosome maintenance deficient; TNFR, TNF receptor; NF-κB, nuclear factor-κB; HSP70, heat shock protein 70 kD; HSP90, heat shock protein 90 kD; APAF1, apoptotic protease activating factor 1; BAD, Bcl-XL/Bcl-2-associated death gene; BAG1, BCL2-associated athanogene 1

and survival of the NSCLC cells results from concurrent deregulation of WNT, apoptosis and cell cycle pathways. These pathways were also found to be altered in many other types of cancer cells. Our findings help to elucidate parts of the intricate networks that are altered in NSCLC cells and provide a gene pool for the identification of biomarkers or therapeutic targets.

Acknowledgements We thank Dr. Guillermina Lozano for her valuable suggestions regarding experiments and this manuscript. This work was supported by National Cancer Institute grant N01-CN-05023-39 (to L.S.), U.S. Department of Defense grant DAMD 17-02-1-0706 01 (to J.S.K.), and National Institute of Environmental Health Sciences grant 5K22-ES-000362 (to J.S.K.)

References

Amatschek S, Koenig U, Auer H, Steinlein P, Pacher M, Gruenfelder A, Dekan G, Vogl S, Kubista E, Heider KH, Stratowa C, Schreiber M, Sommergruber W (2004) Tissue-wide expression profiling using cDNA subtraction and microarrays to identify tumor-specific genes. Cancer Res 64:844–856

Beere HM, Wolf BB, Cain K, Mosser DD, Mahboubi A, Kuwana T, Tailor P, Morimoto RI, Cohen GM, Green DR (2000) Heat-shock protein 70 inhibits apoptosis by preventing recruitment of procaspase-9 to the Apaf-1 apoptosome. Nat Cell Biol 2:469–475

Braakhuis BJ, Tabor MP, Kummer JA, Leemans CR, Brakenhoff RH (2003) A genetic explanation of Slaughter's concept of field cancerization: evidence and clinical implications. Cancer Res 63:1727–1730

Braakhuis BJ, Leemans CR, Brakenhoff RH (2004) Using tissue adjacent to carcinoma as a normal control: an obvious but questionable practice. J Pathol 203:620–621

Broers JL, Viallet J, Jensen SM, Pass H, Travis WD, Minna JD, Linnoila RI. (1993) Expression of *c-myc* in progenitor cells of the bronchopulmonary epithelium and in a large number of non-small cell lung cancers. Am J Respir Cell Mol Biol 9:33–43

Budihardjo I, Oliver H, Lutter M, Luo X, Wang X (1999) Biochemical pathways of caspase activation during apoptosis. Annu Rev Cell Dev Biol 15:269–290

Calvo R, West J, Franklin W, Erickson P, Bemis L, Li E, Helfrich B, Bunn P, Roche J, Brambilla E, Rosell R, Gemmill RM, Drabkin HA (2000) Altered *HOX* and *WNT7A* expression in human lung cancer. Proc Natl Acad Sci USA 97:12776–12781

Datta SR, Brunet A, Greenberg ME (1999) Cellular survival: a play in three Akts. Genes Dev 13:2905–2927

Fry WA, Phillips JL, Menck HR (1999) Ten-year survey of lung cancer treatment and survival in hospitals in the United States: a national cancer data base report. Cancer 86:1867–1876

Giles RH, van Es JH, Clevers H (2003) Caught up in a Wnt storm: Wnt signaling in cancer. Biochim Biophys Acta 1653:1–24

Goruppi S, Chiaruttini C, Ruaro ME, Varnum B, Schneider C (2001) Gas6 induces growth, beta-catenin stabilization, and T-cell factor transcriptional activation in contact-inhibited C57 mammary cells. Mol Cell Biol 21:902–915

Gray TE, Guzman K, Davis CW, Abdullah LH, Nettesheim P (1996) Mucociliary differentiation of serially passaged normal human tracheobronchial epithelial cells. Am J Respir Cell Mol Biol 14:104–112

Han H, Landreneau RJ, Santucci TS, Tung MY, Macherey RS, Shackney SE, Sturgis CD, Raab SS, Silverman JF (2002) Prognostic value of immunohistochemical expressions of p53, HER-2/neu, and bcl-2 in stage I non-small-cell lung cancer. Hum Pathol 33:105–110

Jemal A, Murray T, Samuels A, Ghafoor A, Ward E, Thun MJ (2003) Cancer statistics, 2003. CA Cancer J Clin 53:5–26

Kettunen E, Anttila S, Seppanen JK, Karjalainen A, Edgren H, Lindstrom I, Salovaara R, Nissen AM, Salo J, Mattson K, Hollmen J, Knuutila S, Wikman H (2004) Differentially expressed genes in nonsmall cell lung cancer: expression profiling of cancer-related genes in squamous cell lung cancer. Cancer Genet Cytogenet 149:98–106

Kolodziejski PJ, Musial A, Koo JS, Eissa NT (2002) Ubiquitination of inducible nitric oxide synthase is required for its degradation. Proc Natl Acad Sci USA 99:12315–12320

Koo JS, Jetten AM, Belloni P, Yoon JH, Kim YD, Nettesheim P (1999a) Role of retinoid receptors in the regulation of mucin gene expression by retinoic acid in human tracheobronchial epithelial cells. Biochem J 338:351–357

Koo JS, Yoon JH, Gray T, Norford D, Jetten AM, Nettesheim P (1999b) Restoration of the mucous phenotype by retinoic acid in retinoid-deficient human bronchial cell cultures: changes in mucin gene expression. Am J Respir Cell Mol Biol 20:43–52

Koo JS, Kim YD, Jetten AM, Belloni P, Nettesheim P (2002) Overexpression of mucin genes induced by interleukin-1 beta, tumor necrosis factor-alpha, lipopolysaccharide, and neutrophil elastase is inhibited by a retinoic acid receptor alpha antagonist. Exp Lung Res 28:315–332

Lemjabbar H, Basbaum C (2002) Platelet-activating factor receptor and ADAM10 mediate responses to *Staphylococcus aureus* in epithelial cells. Nat Med 8:41–46

Li C, Wong WH (2001) Model-based analysis of oligonucleotide arrays: expression index computation and outlier detection. Proc Natl Acad Sci USA 98:31–36

Liang H, Chen Q, Coles AH, Anderson SJ, Pihan G, Bradley A, Gerstein R, Jurecic R, Jones SN (2003) Wnt5a inhibits B cell proliferation and functions as a tumor suppressor in hematopoietic tissue. Cancer Cell 4:349–360

Malusecka E, Zborek A, Krzyzowska-Gruca S, Krawczyk Z (2001) Expression of heat shock proteins HSP70 and HSP27 in primary non-small cell lung carcinomas. An immunohistochemical study. Anticancer Res 21:1015–1021

Nacht M et al (2001) Molecular characteristics of non-small cell lung cancer. Proc Natl Acad Sci USA 98:15203–15208

Neubauer A, Burchert A, Maiwald C, Gruss HJ, Serke S, Huhn D, Wittig B, Liu E (1997) Recent progress on the role of Axl, a receptor tyrosine kinase, in malignant transformation of myeloid leukemias. Leuk Lymphoma 25:91–96

O'Bryan JP, Frye RA, Cogswell PC, Neubauer A, Kitch B, Prokop C, Espinosa R III, Le Beau MM, Earp HS, Liu ET (1991) *axl*, a transforming gene isolated from primary human myeloid leukemia cells, encodes a novel receptor tyrosine kinase. Mol Cell Biol 11:5016–5031

Ohira T et al (2003) WNT7a induces E-cadherin in lung cancer cells. Proc Natl Acad Sci USA 100:10429–10434

Ostrowski LE, Nettesheim P (1995) Inhibition of ciliated cell differentiation by fluid submersion. Exp Lung Res 21:957–970

Pandey P, Saleh A, Nakazawa A, Kumar S, Srinivasula SM, Kumar V, Weichselbaum R, Nalin C, Alnemri ES, Kufe D, Kharbanda S (2000) Negative regulation of cytochrome *c*-mediated oligomerization of Apaf-1 and activation of procaspase-9 by heat shock protein 90. EMBO J 19:4310–4322

Petty RD, Nicolson MC, Kerr KM, Collie-Duguid E, Murray GI (2004) Gene expression profiling in non-small cell lung cancer: from molecular mechanisms to clinical application. Clin Cancer Res 10:3237–3248

Pines J (1999) Four-dimensional control of the cell cycle. Nat Cell Biol 1:E73–E79

Rose MC, Nickola TJ, Voynow JA (2001) Airway mucus obstruction: mucin glycoproteins, *MUC* gene regulation and goblet cell hyperplasia. Am J Respir Cell Mol Biol 25:533–537

Shimizu S, Narita M, Tsujimoto Y (1999) Bcl-2 family proteins regulate the release of apoptogenic cytochrome *c* by the mitochondrial channel VDAC. Nature 399:483–487

Singer M, Martin LD, Vargaftig BB, Park J, Gruber AD, Li Y, Adler KB (2004) A MARCKS-related peptide blocks mucus hypersecretion in a mouse model of asthma. Nat Med 10:193–196

Smythe WR, Williams JP, Wheelock MJ, Johnson KR, Kaiser LR, Albelda SM (1999) Cadherin and catenin expression in normal human bronchial epithelium and non-small cell lung cancer. Lung Cancer 24:157–168

Soria JC, Jang SJ, Khuri FR, Hassan K, Liu D, Hong WK, Mao L (2000) Overexpression of cyclin B1 in early-stage non-small cell lung cancer and its clinical implication. Cancer Res 60:4000–4004

Takeyama K, Dabbagh K, Lee HM, Agusti C, Lausier JA, Ueki IF, Grattan KM, Nadel JA (1999) Epidermal growth factor system regulates mucin production in airways. Proc Natl Acad Sci USA 96:3081–3086

Topol L, Jiang X, Choi H, Garrett-Beal L, Carolan PJ, Yang Y (2003) Wnt-5a inhibits the canonical Wnt pathway by promoting GSK-3-independent beta-catenin degradation. J Cell Biol 162:899–908

Uren A, Reichsman F, Anest V, Taylor WG, Muraiso K, Bottaro DP, Cumberledge S, Rubin JS (2000) Secreted Frizzled-related protein-1 binds directly to Wingless and is a biphasic modulator of Wnt signaling. J Biol Chem 275:4374–4382

Wasner M, Tschop K, Spiesbach K, Haugwitz U, Johne C, Mossner J, Mantovani R, Engeland K (2003) Cyclin B1 transcription is enhanced by the p300 coactivator and regulated during the cell cycle by a CHR-dependent repression mechanism. FEBS Lett 536:66–70

Whitsett JA et al (2004) Functional genomics of lung disease. Am J Respir Cell Mol Biol 31:S1–S81

Willert K, Brink M, Wodarz A, Varmus H, Nusse R (1997) Casein kinase 2 associates with and phosphorylates dishevelled. EMBO J 16:3089–3096

Wu R, Martin WR, Robinson CB, St George JA, Plopper CG, Kurland G, Last JA, Cross CE, McDonald RJ, Boucher R (1990) Expression of mucin synthesis and secretion in human tracheobronchial epithelial cells grown in culture. Am J Respir Cell Mol Biol 3:467–478

The Synergistic Combination of the Farnesyl Transferase Inhibitor Lonafarnib and Paclitaxel Enhances Tubulin Acetylation and Requires a Functional Tubulin Deacetylase

Adam I. Marcus,[1] Jun Zhou,[1] Aurora O'Brate,[1] Ernest Hamel,[2] Jason Wong,[3] Michael Nivens,[1] Adel El-Naggar,[4] Tso-Pang Yao,[5] Fadlo R. Khuri,[1] and Paraskevi Giannakakou[1]

[1]Winship Cancer Institute, Emory University School of Medicine, Atlanta, Georgia; [2]Screening Technologies Branch, Developmental Therapeutic Program, Division of Cancer Treatment and Diagnosis, National Cancer Institute, NIH, Frederick, Maryland; [3]Harvard University, Cambridge, Massachusetts; [4]The University of Texas M.D. Anderson Cancer Center, Houston, Texas; and [5]Department of Pharmacology and Cancer Biology, Duke University, Durham, North Carolina

Abstract

Farnesyl transferase (FT) inhibitors (FTI) are anticancer agents developed to target oncogenic Ras proteins by inhibiting Ras farnesylation. FTIs potently synergize with paclitaxel and other microtubule-stabilizing drugs; however, the mechanistic basis underlying this synergistic interaction remains elusive. Here we show that the FTI lonafarnib affects the microtubule cytoskeleton resulting in microtubule bundle formation, increased microtubule stabilization and acetylation, and suppression of microtubule dynamics. Notably, treatment with the combination of low doses of lonafarnib with paclitaxel markedly enhanced tubulin acetylation (a marker of microtubule stability) as compared with either drug alone. This synergistic effect correlated with FT inhibition and was accompanied by a synergistic increase in mitotic arrest and cell death. Mechanistically, we show that the combination of lonafarnib and paclitaxel inhibits the *in vitro* deacetylating activity of the only known tubulin deacetylase, histone deacetylase 6 (HDAC6). In addition, the lonafarnib/taxane combination is synergistic only in cells lines expressing the wild-type HDAC6, but not a catalytic-mutant HDAC6, revealing that functional HDAC6 is required for the synergy of lonafarnib with taxanes. Furthermore, tubacin, a specific HDAC6 inhibitor, synergistically enhanced tubulin acetylation in combination with paclitaxel, similar to the combination of lonafarnib and paclitaxel. Taken together, these data suggest a relationship between FT inhibition, HDAC6 function, and cell death, providing insight into the putative molecular basis of the lonafarnib/taxane synergistic antiproliferative combination. (Cancer Res 2005; 65(9): 3883-93)

Introduction

Farnesyl transferase (FT) inhibitors (FTI) are a novel class of antineoplastic agents that have high antitumor activity and are currently in clinical trials (1–3). These agents inhibit the FT enzyme, which posttranslationally modifies proteins by the addition of a 15-carbon farnesyl group. The initial driving force behind FTI development was based on the finding that oncogenic Ras, a low molecular weight GTPase, induces malignant transformation upon addition of a farnesyl group to its COOH terminus by the FTase. This in turn allows it to localize to the plasma membrane and acts as a relay switch by transducing biological information from extracellular signals to the nucleus (for review see ref. 4).

Because Ras farnesylation is required for Ras membrane localization, FTase became an attractive target for new anticancer agents (5–7). Furthermore, based on the finding that oncogenic Ras mutations are found in 30% of all human cancers (8, 9), it was hypothesized that tumor growth could be inhibited by preventing Ras farnesylation. Thus, FTIs were developed as targeted agents against Ras and were shown to inhibit Ras function (10) as well as possess potent antitumor activity in multiple cancer cell lines and animal models. Despite the initial hypothesis that FTIs inhibit tumor growth by inhibiting Ras farnesylation, it was later shown that FTIs show antitumor activity independent of Ras status (11–13), suggesting that the mechanism of FTI activity extends beyond the inhibition of Ras farnesylation (14).

To probe the molecular mechanisms of FTI action, some previous works have focused on the relationship between FTIs and microtubule-targeting agents. Microtubules are dynamic polymers composed of α- and β-tubulin subunits that elongate and shorten. In the cell, they function in a variety of processes including cell division, cell signaling, and intracellular trafficking (reviewed in ref. 15). Because microtubules are essential components of the cell division machinery, they are attractive and validated targets for anticancer therapy (16, 17) as evidenced by the clinical success of microtubule-targeting drugs such as taxanes (18–20). More recently, epothilones, a new class of microtubule-targeting drugs, are in clinical development and show very positive preliminary results (21). Notably, FTIs in combination with paclitaxel or epotholines act synergistically to inhibit cell growth in numerous human cancer cell lines and xenograft models (14, 22–24). In addition, a combination clinical study of the FTI lonafarnib (SCH66336 or sarasar) with paclitaxel yielded impressive preliminary results, with partial responses in 8 of 20 evaluable patients, including patients whose disease had previously progressed while on taxanes alone (25). Despite these promising results, the molecular mechanism of the synergistic interaction of FTIs with taxanes is unknown.

The synergy between taxanes and FTIs suggests that there may be a link between microtubules and the mechanism of FTI action. This is further supported by studies showing that FTI-2153 inhibited normal bipolar microtubule spindle formation, suggesting that spindle microtubules may have been affected by this treatment (26–28). These FTI-treated cells were arrested in early mitosis and this effect was independent of p53 and Ras status. Nevertheless, the effects of FTI treatment on interphase microtubules have not been examined.

Note: Supplementary data for this article are available at Cancer Research Online (http://cancerres.aacrjournals.org/).

Requests for reprints: Paraskevi Giannakakou Winship Cancer Institute, Emory University School of Medicine, Room D4054, 1365C Clifton Road, Atlanta, GA 30322. E-mail: pgianna@emory.edu.

Here we investigated the effects of lonafarnib (29) on interphase microtubules in lung and breast cancer cells. Our results show that exposure to lonafarnib resulted in microtubule bundle formation, stabilized interphase microtubules, and suppressed microtubule dynamics. Moreover, we show that the combination of lonafarnib and paclitaxel for 16 hours synergistically enhanced tubulin acetylation, mitotic arrest, and cell death; furthermore, this effect correlated with FT inhibition. In addition, the combination of lonafarnib and paclitaxel inhibits the deacetylating activity of histone deacetylase 6 (HDAC6) *in vitro*, whereas either drug alone does not. Importantly, we show that the lonafarnib/taxane combination is synergistic only in cells lines expressing the wild-type HDAC6, but not a catalytic-mutant HDAC6, revealing that functional HDAC6 is required for the synergy of lonafarnib with taxanes. Taken together, these data suggest a relationship between FT inhibition, HDAC6 function, enhanced tubulin acetylation, and cell death, providing a putative molecular basis for the lonafarnib/taxane antiproliferative combination.

Materials and Methods

Cell culture. The human non-small cell lung cancer cell lines A549 and H1299 were maintained in RPMI 1640 supplemented with 5% FCS, nonessential amino acids, and 0.1% penicillin/streptomycin at 37°C in 5% CO_2. Live cell microscopy was done with MCF-7 breast cancer cells stably transfected with green fluorescent protein (GFP):α-tubulin and maintained in DMEM supplemented with 5% FCS, nonessential amino acids, and 0.1% penicillin/streptomycin.. All lines were cultured at 37°C in a humidified atmosphere with 5% CO_2. NIH-3T3 cells expressing various HDAC6 constructs were previously generated (30) and were cultured in DMEM medium under the same conditions.

Immunofluorescence analysis. Immunofluorescence microscopy was done as previously described (31). Cells were fixed in PHEMO buffer (68 mmol/L PIPES, 25 mmol/L HEPES, 15 mmol/L EGTA, 3 mmol/L $MgCl_2$, 10% DMSO) with 3.7% formaldehyde, 0.05% glutaraldehyde, and 0.5% Triton X-100. Cells were washed in PBS thrice for 5 minutes then blocked in 10% goat serum for 15 minutes. The following primary antibodies were used: α-tubulin (Chemicon International, Temecula, CA; 1:500 dilution) and acetylated tubulin (Sigma, St. Louis, MO; 1:1,000 dilution) with incubation time of 1 hour. The secondary antibodies used were Alexa 563–conjugated goat anti-rat immunoglobulin G (IgG; 1:500) and Alexa 488–conjugated goat anti-mouse IgG antibody (1:500), both from Molecular Probes (Eugene, OR). Cells were imaged using a Zeiss LSM 510 Meta (Thornwood, NY) confocal microscope using a either a 63× [numerical aperture (NA) = 1.4] or 100× (NA = 1.4) Apochromat objective. To stain DNA for mitotic cell counting, we fixed cells as described above, and added Sytox Green (Molecular Probes) to the Gel Mount mounting media (Biomeda Corp., Foster City, CA). All images were acquired using Zeiss LSM 510 software and processed in Adobe Photoshop 7.0.

Cell tubulin polymerization assay. Quantitative drug-induced tubulin polymerization was done as previously described (32, 33). The percent pellet (%P) is calculated as the amount of polymerized tubulin (P) over the total amount of polymerized and soluble tubulin (P + S) times 100 {%P = [P / (P + S)] × 100} based on densitometric analysis.

Electron microscopy. A549 cells were seeded on Thermanox coverslips (Electron Microscopy Sciences, Hatfield, PA) in 24-well plates and grown overnight to 60% confluency. Cells were then treated with 10 μmol/L lonafarnib for 48 hours and fixed using a protocol described in Vanier et al. (34). Cells were then fixed in 2% glutaraldehyde for 4 hours at room temperature, rinsed in distilled water twice, postfixed in 1% OsO_4 in 0.1 mol/L sodium cacodylate buffer (pH 7.4) at 4 °C for 1 hour, and finally rinsed in distilled water as above. Samples were then dehydrated through an ethanol series (30%, 50%, 60%, 80%, 90%, 100%) followed by two changes of propylene oxide (10 minutes each). Then samples were infiltrated with Embed 812 (Electron Microscopy Science) for 3 days according to the instructions of the manufacturer. Each block was cut at 1 × 1 mm using a diamond knife and RMC MT-7000 ultramicrotome, and thin sections were made and collected onto 200 mesh copper grids. Grids were poststained with 10% uranyl acetate in distilled water and then 2% lead citrate in distilled water for 20 minutes in each treatment.

Flow cytometry analysis. To determine acetylated tubulin levels, cells were plated and on the following day treated with different concentrations of the drugs for 16 hours. After drug treatment, cells were fixed with PHEMO buffer for 10 minutes as previously described (31) and stained with an antibody against acetylated tubulin (Sigma; 1:500) followed by secondary Alexa 488–conjugated goat anti-mouse IgG antibody (1:500). Finally, cells were scraped into 1 mL of PBS, and flow cytometry analysis was done on a Becton Dickinson flow cytometer.

For cell cycle analysis, cells were scraped from plates, centrifuged at 1,000 rpm for 5 minutes, and propidium iodide buffer containing 0.1 mg/mL propidium iodide and NP40 (0.6%) in water was used to resuspend cells. Cell were incubated in this buffer for 30 minutes at room temperature in the dark, then passed through a filter to remove cell clumps, and finally read in a Becton Dickinson flow cytometer.

Microtubule dynamics assays. Experiments were done using a MCF-7 breast cancer cell line stably expressing a GFP-α-tubulin microtubule reporter protein (kind gift of Dr. Mary Ann Jordan). Cells were plated and analyzed as previously described (35). Images were taken using a Hamamatsu Orca ER camera (Middlesex, NJ) every 4 seconds for 2 minutes (250-400 seconds of exposure) on a Zeiss Axiovert epifluorescence microscope equipped with 100× Apochromat (NA = 1.4) oil lens and adjustable mercury arc lamp (set at 100% intensity). A stage heater as well as Zeiss heating chamber was used to maintain the temperature at 37 ± 0.5°C. Microtubules ends at the lamellar edge of interphase cells were imaged and subsequently tracked using the "track points" feature on Metamorph image analysis software (Universal Imaging, Downingtown, PA). The coordinates generated from this tracking feature were used to determine the distance individual microtubule ends changed from a fixed point. These values were transferred to a Microsoft Excel spreadsheet and used to generate life history plots of individual microtubules. From these graphs, the various variables shown in Table 1 were calculated. All *P* values were calculated using the Student's *t* test.

Microtubule dynamicity is defined as the total length grown and shortened during the life (measured in minutes) of an individual microtubule. A catastrophe is defined as a transition into microtubule shortening whereas a rescue is a transition from shortening to growth or pause. To calculate catastrophe frequency per unit time or per unit length, the number of catastrophes was divided by the total time in growth and pause or the total distance grown, respectively. Conversely, the rescue frequency was calculated by dividing the number of rescues by the total time spent shortening or distance shortened.

***In vitro* acetylated tubulin assay.** A549 cells were transiently transfected with Flag-tagged pBJ5-HDAC6 expression plasmids using FuGene (Roche, Basel, Switzerland) following the guidelines of the manufacturer. Untransfected cells or cells transfected with an empty vector were used as controls. In Fig. 5*A*, we used NIH-3T3 cells stably expressing FLAG-tagged HDAC6-wt and HDAC6-mt proteins and therefore cells did not have to be transfected. Cell lysates were prepared 48 hours after transfection and then immunoprecipitated with anti-Flag M2 agarose beads (Sigma). Tubulin acetylation assays were done by incubating the immunoprecipitates with preformed mitogen-activated protein–stabilized microtubules at 37°C, along with the appropriate drug, for 2 hours as described previously (30). Reactions were then placed on ice for 15 minutes and centrifuged briefly at 14,000 rpm to separate the supernatant from the agarose beads. The supernatant was analyzed by Western blotting with antibodies against acetylated α-tubulin and against α-tubulin (as described below) and the beads were analyzed with an antibody against Flag M2 (Sigma; 1:1,000).

Western blotting. Cells were plated in six-well plates at 50% confluency and treated the next day with the appropriate drug and time interval. Cells were lysed, centrifuged at 15,000 rpm for 15 minutes, and electrophoresed on a 7.5% SDS-PAGE gel (bicinchoninic acid assay was used to determine protein concentration in a spectrophotometer). Proteins were transferred to a polyvinylidene difluoride membrane (100 V for 1 hour) using a Bio-Rad

Table 1. Analysis of *in vivo* microtubule dynamics in the presence and absence of lonafarnib

Parameter	Control	Lonafarnib 10 μmol/L	Percent change
Growth			
Rate (μm/min)	11.2 ± 2.1	**7.7 ± 3.8**	−31%
Length (μm)	2.9 ± 1.6	**1.9 ± 0.9**	−34%
Time (min)	0.3 ± 0.08	0.28 ± 0.07	−7%
Shortening			
Rate (μm/min)	17.1 ± 4.0	**9.9 ± 3.3**	−41%
Length (μm)	5.3 ± 1.9	**3.1 ± 1.6**	−42%
Time (min)	0.34 ± 0.11	0.33 ± 0.1	−3%
Pause			
Time (min)	0.36 ± 0.23	0.40 ± 0.2	−11%
Percentage time spent			
Growth	30	**17**	
Shortening	17	**8.8**	
Pause	53	**74.2**	
Dynamicity (μm/min)	8.1 ± 4.0	**3.0 ± 1.9**	−63%
Rescue frequency (events/min)	4.1 ± 2.6	4.0 ± 2.5	−2%
Catastrophe frequency (events/min)	0.9 ± 0.8	0.88 ± 0.75	−2%
Rescue frequency (events/μm)	0.19 ± 0.15	**0.25 ± 0.21**	31%
Catastrophe frequency (events/μm)	0.33 ± 0.29	0.37 ± 0.31	12%
Number of cells	21	23	
Number of microtubules	81	69	

NOTE: Values in boldface differ significantly from control values at >99% confidence interval as determined by Student's *t* test. Values are mean ± SD.

transfer apparatus and blotted with antibodies against acetylated tubulin (Sigma; 1:1,000), total tubulin (Sigma DM1α; 1:1,000), HDJ-2, acetylated histone 3 (Cell Signaling, Beverly, MA; 1:1,000), actin, and HDAC6 (Cell Signaling; 1:1,000).

Cell survival and synergy assays (combination index analysis). Cells were plated in a 96-well plate at 2,000 cells/well and allowed to attach overnight. Cells were then treated with serial dilutions (1:3) of either lonafarnib alone, paclitaxel alone, or the combination of lonafarnib and paclitaxel for 72 hours. Cell were then fixed with 10% trichloroacetic acid for 30 minutes, washed thrice with water, dried, and stained with 0.4% sulfurhodamine B (protein stain) for 30 minutes. Cells were then washed with 0.1% acetic acid, air dried, and the bound sulfurhodamine B was dissolved with 10 mmol/L unbuffered Tris-base (pH 10.5). The plates were read in a microplate reader (A_{564}) and synergy was determined using CalcuSyn software, which calculates the combination index based on the percent cell survival at varying doses of the drug treatments, both alone and in combination. A combination index greater than 1 indicates antagonism, equal to 1 is additivity, and less than 1 is synergism.

Results

Lonafarnib treatment alters microtubule structure. To examine the effects of lonafarnib on interphase microtubules, we performed live cell microtubule imaging using MCF-7 breast cancer cells stably expressing GFP:α-tubulin. This cell line allows for the visualization of microtubules in living cells and eliminates the possibility of artifacts associated with fixed tissue analyses. Cells were treated for 48 hours with 5 and 10 μmol/L lonafarnib (mean 72-hour IC_{50} of lonafarnib was 8 μmol/L in seven cancer cell lines tested; data not shown) and microtubules were observed using live-cell epifluorescence microscopy (Fig. 1*A*). Nearly all untreated control cells observed had an extensive, fine, and organized microtubule network. In contrast, lonafarnib treatment led to a dose-dependent increase in microtubule bundling compared with control cells ($P < 0.05$; Fig. 1*B*). Treatment with 5 and 10 μmol/L lonafarnib led to nearly 10% and 25% of cells harboring extensive microtubule bundling, respectively. Similar microtubule bundles were observed in nearly 60% of cells treated with paclitaxel, whereas cells treated under the same condition with the non-microtubule targeting, DNA-intercalating agent Adriamycin had identical microtubule morphologies as control cells.

To examine whether these effects were cell line specific, we performed immunofluorescence microscopy with an anti α-tubulin antibody on A549 and H1299 human lung cancer cells treated with lonafarnib. Representative data from this experiment are shown in Supplementary Fig. S1-*A* depicting a dose-dependent increase in microtubule bundling following lonafarnib treatment for 48 hours.

Lonafarnib treatment increases tubulin acetylation and microtubule stability. The appearance of microtubule bundles after lonafarnib treatment in A549, H1299, and MCF-7 cells raises the possibility that lonafarnib can affect microtubule stability in a manner similar to paclitaxel. To validate this hypothesis, indirect immunofluorescence using an antibody against acetylated α-tubulin was done. Acetylation of α-tubulin at lysine 40 is an established marker of microtubule stability (36). Thus, the amount of acetylated tubulin is thought to be proportional to the stability of the microtubule. As shown in Fig. 1*C*, lonafarnib treatment for 48 hours resulted in a marked dose-dependent increase in acetylated α-tubulin, in contrast to the low basal levels of acetylated tubulin in untreated cells. This effect was similar to paclitaxel-induced tubulin acetylation, suggesting that lonafarnib may also affect microtubule stability similar to paclitaxel.

To further probe the effects of lonafarnib treatment on microtubule stabilization, a cell-based tubulin polymerization assay was done (32, 33). This quantitative tubulin polymerization assay is based on the fact that drug-stabilized microtubule polymers remain

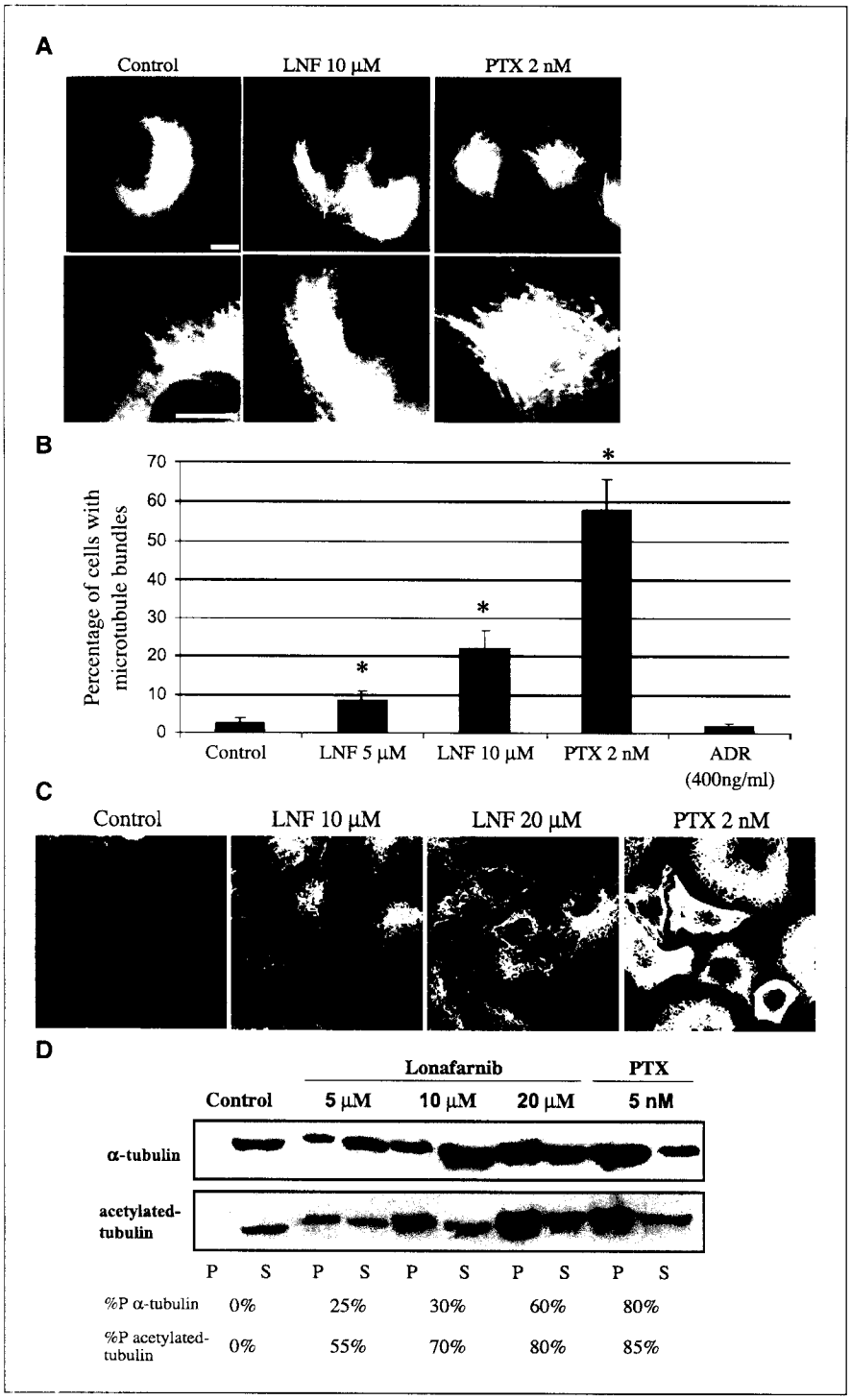

Figure 1. Lonafarnib treatment alters microtubule structure and increases tubulin acetylation. *A*, MCF-7 breast cancer cells stably expressing GFP: α-tubulin were observed using live-cell fluorescence microscopy following the indicated drug treatments for 48 hours. *Solid arrows*, microtubule bundling. Bottom row displays higher magnification of microtubules shown in the top row. Bar, 10 μm. *B*, number of cells containing microtubule bundles following drug treatments shown in *A*. Asterisks denote a significant difference in the percentage of cells having microtubule bundles compared with control ($P < 0.05$). *Bars*, ±SD. *C*, A549 cells were treated with lonafarnib (*LNF*) for 48 hours and microtubules were visualized by immunofluorescence labeling using an antibody against acetylated α-tubulin. Treatment with paclitaxel (*PTX*) is included as a positive control. Bar, 10 μm. *D*, Western blot analysis against total α-tubulin (*top*) and acetylated tubulin (*bottom*) on the polymerized (*P*) and soluble (*S*) fractions of protein lysates from A549 cells treated with the indicated drug concentrations for 48 hours. *%P*, relative percentage of polymerized tubulin for each drug treatment.

detergent insoluble when extracted in a hypotonic buffer and, therefore, remain in the pellet after centrifugation. Conversely, the pool of soluble tubulin dimers remains in the supernatant. Lonafarnib treatment resulted in a dose-dependent increase in tubulin polymerization, as shown by the increase in the percentage of tubulin found in the pellet fraction, as compared with untreated control cells (Fig. 1*D*). Specifically, untreated cells contain almost no stabilized tubulin (0% tubulin in the pellet) under our experimental conditions, whereas lonafarnib treatment (5-20 μmol/L) led to a dose-dependent increase in tubulin polymerization (25-60% of total tubulin in the pellet fraction). Similarly, treatment with 5 nmol/L paclitaxel resulted in about 80% tubulin polymerization. The same blot was reprobed with an antibody against acetylated α-tubulin. A similar dose-dependent increase in acetylated α-tubulin in the pellet was observed on lonafarnib treatment and this shift of acetylated-tubulin towards the polymerized fraction was greater than total

tubulin. Thus, the majority of tubulin polymers in the pellet fraction represent stabilized acetylated microtubules rather than random microtubules trapped in this fraction.

Transmission electron microscopy confirms microtubule bundles in lonafarnib-treated cells. To obtain high-resolution analysis of lonafarnib-induced changes of the microtubule architecture, we did transmission electron microscopy (34). In contrast to control cells, which had individual microtubules throughout the cell cytoplasm, lonafarnib treatment induced the formation of microtubule bundles, similar to the bundles observed with paclitaxel (Supplementary Fig. S2-*B*). Interestingly, lonafarnib treatment mainly led to the formation of loose microtubule clusters that were longer in length but not as tightly packed as paclitaxel-induced microtubule bundles, suggesting that lonafarnib-induced bundles may differ morphologically from paclitaxel-induced bundles (Supplementary Fig. S2-*B*, *insets*).

Lonafarnib suppresses microtubule dynamics in MCF-7 cells. Drugs that target microtubules potently suppress microtubule dynamics at relatively low concentrations (16, 34) and this function is essential for their activity. Our results show lonafarnib targets cellular microtubules; therefore, we investigated whether lonafarnib also affects microtubule dynamics, similar to other microtubule-targeting drugs. To test this hypothesis, we measured microtubule dynamics in living MCF7-GFP:tubulin breast cancer cells using live-cell fluorescence microscopy. Time-lapse sequences of microtubule movements were generated from untreated and lonafarnib-treated cells. Representative time frames show microtubule growth (*white arrows*), shortening (*black arrows*), and pause (*white dashed arrows*) in untreated control cells (Fig. 2*A*). To quantitate the effects of lonafarnib on microtubule dynamics, we tracked microtubule movements in cells treated with 10 μmol/L lonafarnib and untreated control cells. Individual microtubule life history plots, depicting changes in microtubule length over time, were generated (Fig. 2*B*).

From these life history plots various variables of microtubule dynamics were measured, comparing the dynamicity of microtubules in control cells and lonafarnib-treated cells (Table 1). These data show that there is a significant difference ($P < 0.05$) in the mean rate (μm/min) of microtubule growth and shortening with a decrease of 31% and 41%, respectively, when lonafarnib-treated cells (10 μmol/L for 48 hours) are compared with control cells. Consequently, mean growth and shortening length (μm) also decreased by 34% and 42%, respectively. When the percentage of total time that microtubules spent in growth, shortening, and pause states was determined, the growth time dropped from 30% to 17%, shortening time from 17% to 8.8%, and paused time increased from 53% to 74.2%; whereas the rescue and catastrophe frequencies per micrometer increased 31% and 12%, respectively (see Materials and Methods for definition). The overall dynamicity of microtubules, which represents the total tubulin length change per minute after lonafarnib (10 μmol/L) treatment, decreased by 63%. At 20 μmol/L lonafarnib, microtubules were almost completely stabilized and most cells had few, if any, dynamic microtubules.

Combination of lonafarnib with paclitaxel synergistically increases acetylated tubulin, mitotic arrest, and cell death. FTIs have been shown to synergize with microtubule stabilizing drugs in numerous preclinical models as well as in a phase I clinical trial (25). These observations were confirmed in our laboratory by performing combination index analysis assays of 10 different human cancer cell lines treated with paclitaxel and lonafarnib. These assays revealed a marked synergy (combination index = 0.2-0.7) between the two drugs (data not shown) and is consistent with previous findings. Our results, together with the reported literature, prompted us to hypothesize that the synergy of lonafarnib with taxanes may in part be due to their combined effects on cellular microtubule acetylation and stability.

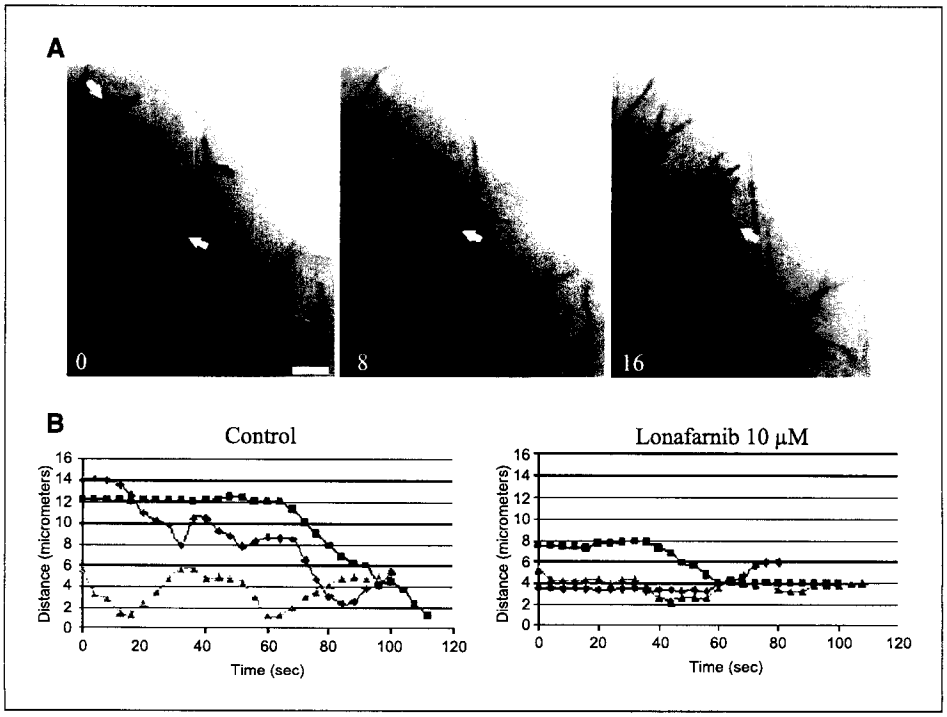

Figure 2. Lonafarnib treatment suppresses microtubule dynamics in living MCF-7 cells. *A*, time lapse sequences of microtubules in untreated living MCF-7 cells stably expressing GFP: α-tubulin. Arrows depict dynamic microtubules that change length over the course of 16 seconds: *black arrows*, microtubule shortening; *white arrows*, microtubule growth; *dashed arrows*, paused microtubules. Bar, 5 μm. *B*, individual microtubule life history plots from control untreated cells or cells treated with 10 μmol/L lonafarnib for 48 hours. Growth events are seen as an increase in distance from a fixed point (*y axis*) over time (*x axis*) and shortening events show a decrease in distance over time.

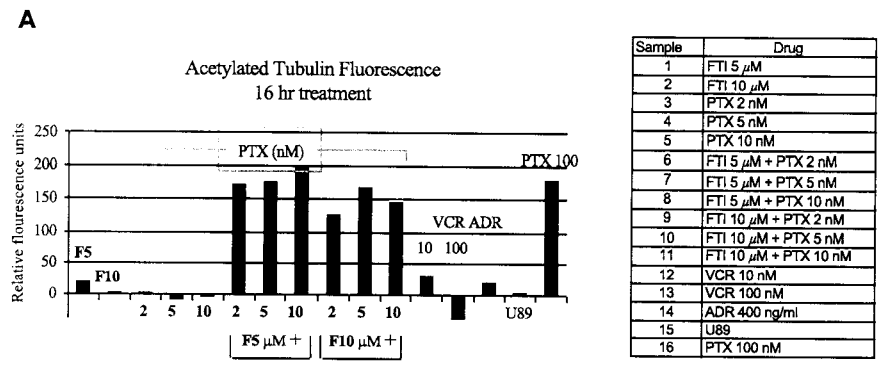

Sample	Drug
1	FTI 5 μM
2	FTI 10 μM
3	PTX 2 nM
4	PTX 5 nM
5	PTX 10 nM
6	FTI 5 μM + PTX 2 nM
7	FTI 5 μM + PTX 5 nM
8	FTI 5 μM + PTX 10 nM
9	FTI 10 μM + PTX 2 nM
10	FTI 10 μM + PTX 5 nM
11	FTI 10 μM + PTX 10 nM
12	VCR 10 nM
13	VCR 100 nM
14	ADR 400 ng/ml
15	U89
16	PTX 100 nM

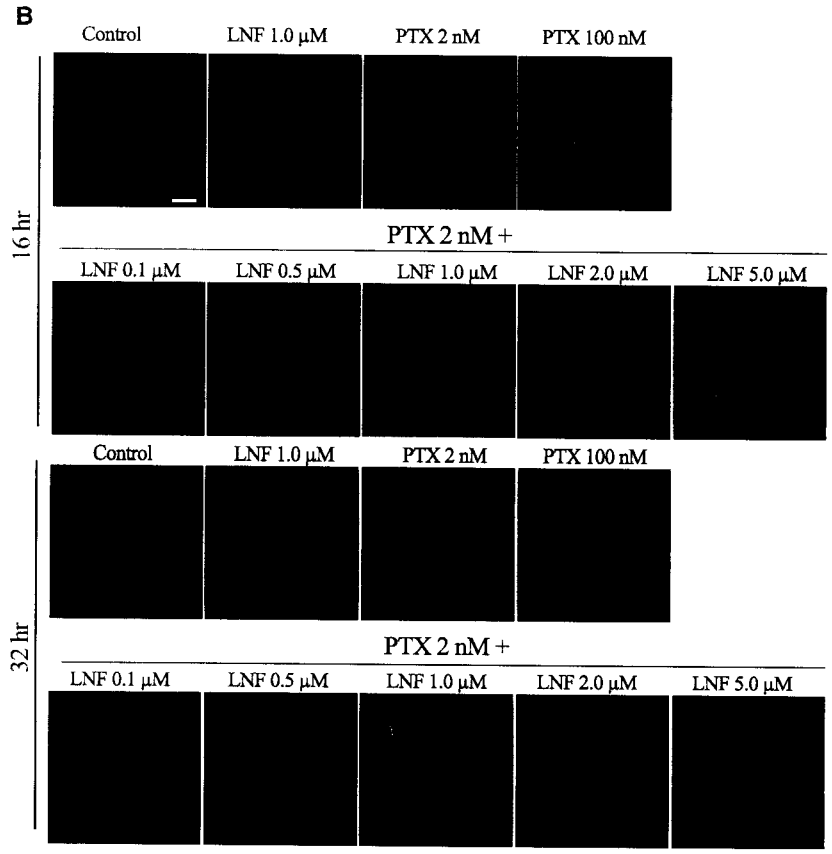

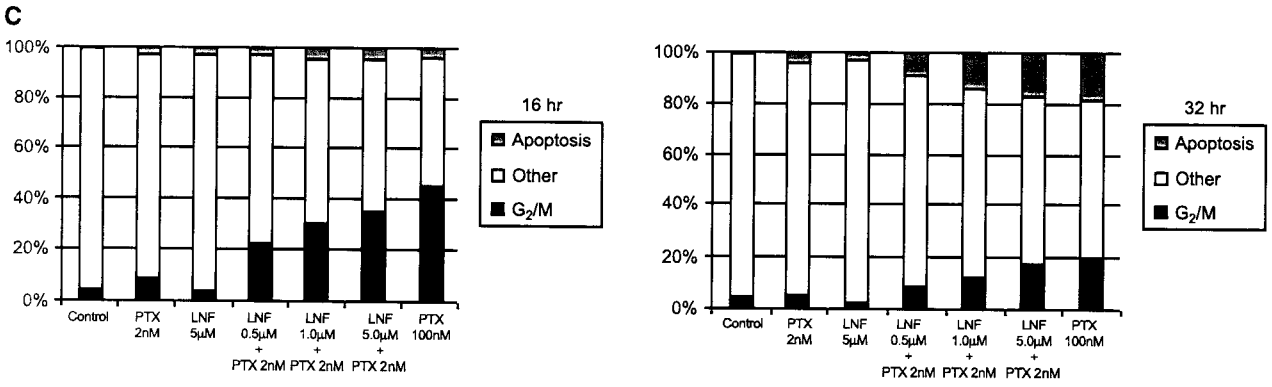

Figure 3. Lonafarnib and paclitaxel synergistically increase acetylated tubulin, mitotic arrest, and apoptosis. *A*, flow cytometry was done with an acetylated tubulin antibody in A549 cells treated with the indicated drugs. Representation of acetylated tubulin levels after 16 hours of drug treatment. *Columns*, mean fluorescence for acetylated tubulin relative to that of control untreated cells (FTI: lonafarnib). *B*, acetylated tubulin immunofluorescence of cells treated with lonafarnib and paclitaxel, both alone and in combination, for 16 and 32 hours. *C*, cell cycle analysis for 16 and 32 hours of treatment with the combination of lonafarnib and paclitaxel.

To test this hypothesis, we quantitated acetylated tubulin levels using flow cytometry in cells treated for 16 hours (unlike the 48-hour treatment in Fig. 1*B*) with lonafarnib and paclitaxel, both alone and in combination. As shown in Fig. 4*A*, there was not a significant difference in acetylated tubulin levels between control untreated cells and cells treated for only 16 hours with lonafarnib (1, 5, and 10 μmol/L) or paclitaxel (2, 5, and 10 nmol/L) alone. In contrast, the combination of 1, 5, and 10 μmol/L lonafarnib with as low as 2 nmol/L paclitaxel resulted in a marked increase of acetylated tubulin similar to that observed with 100 nmol/L of paclitaxel alone (Fig. 3*A*). Notably, non-microtubule-targeting chemotherapy drugs, such as Adriamycin (DNA-intercalating antibiotic) and U89 (antimetabolite), had no effect on acetylated tubulin levels, whereas the microtubule-destabilizing drug vincristine led to a slight decrease of acetylated tubulin levels compared with untreated cells (Fig. 3*A*).

To further explore the synergistic combination of lonafarnib with paclitaxel, immunofluorescence analysis of acetylated tubulin at two different time points was done (Fig. 3*B*). This analysis confirmed the marked increase in acetylated tubulin levels after 16 hours when low doses of lonafarnib (at 0.5, 1, and 5 μmol/L) were combined with low doses of 2 nmol/L paclitaxel. At 32 hours of treatment, similar effects on acetylated tubulin were observed, suggesting that this effect is maintained for at least 32 hours.

Because tubulin acetylation is associated with microtubule stability, we examined whether the increased levels of acetylated tubulin observed with the combination of lonafarnib and paclitaxel resulted in increased mitotic arrest and cell death. Flow cytometry analysis of DNA content revealed that the combination of lonafarnib and paclitaxel led to a synergistic increase in G_2-M arrest as compared with each drug alone (Fig. 3*C*). Specifically, 16-hour treatment with as low as 0.5 μmol/L lonafarnib + 2 nmol/L paclitaxel resulted in a dramatic increase in G_2-M arrested cells as compared with untreated cells or cells treated with each drug alone. Longer treatment (32 hours) with the same drug combinations resulted in a dose-dependent increase in apoptotic cell death that is likely due to cells previously arrested in mitosis becoming apoptotic (Fig. 3*C*). The percentage of apoptotic cells in the combination treatments was similar to that achieved with paclitaxel at 100 nmol/L, whereas either drug alone at low dose produced minimal apoptotic cells. Overall, these results show that the lonafarnib/paclitaxel-mediated increase in tubulin acetylation correlates with a synergistic increase in mitotic arrest and cell death.

The synergistic increase in tubulin acetylation correlates with farnesyl transferase inhibition. Because lonafarnib inhibits the FT enzyme, we wanted to determine if the increase in tubulin acetylation observed with the combination of lonafarnib and paclitaxel correlates with FT inhibition in cells. If so, it would suggest that the observed increase in tubulin acetylation may be a consequence of FTase inhibition. To do this, HDJ-2 was used as a readout for FT inhibition, since FTI treatment inhibits HDJ-2 farnesylation resulting in the appearance of a slower-migrating non-farnesylated HDJ-2 form. As shown in Fig. 4*A*, 1 μmol/L lonafarnib alone and in combination with paclitaxel inhibited HDJ-2 farnesylation in a time-dependent manner, as assessed by the increase of the non-farnesylated (upper band) and concomitant decrease of the farnesylated HDJ-2 band (lower band). As expected, paclitaxel alone had no effect on HDJ-2 farnesylation. When the same blots were reprobed for acetylated α-tubulin, we observed a correlation between inhibition of HDJ-2

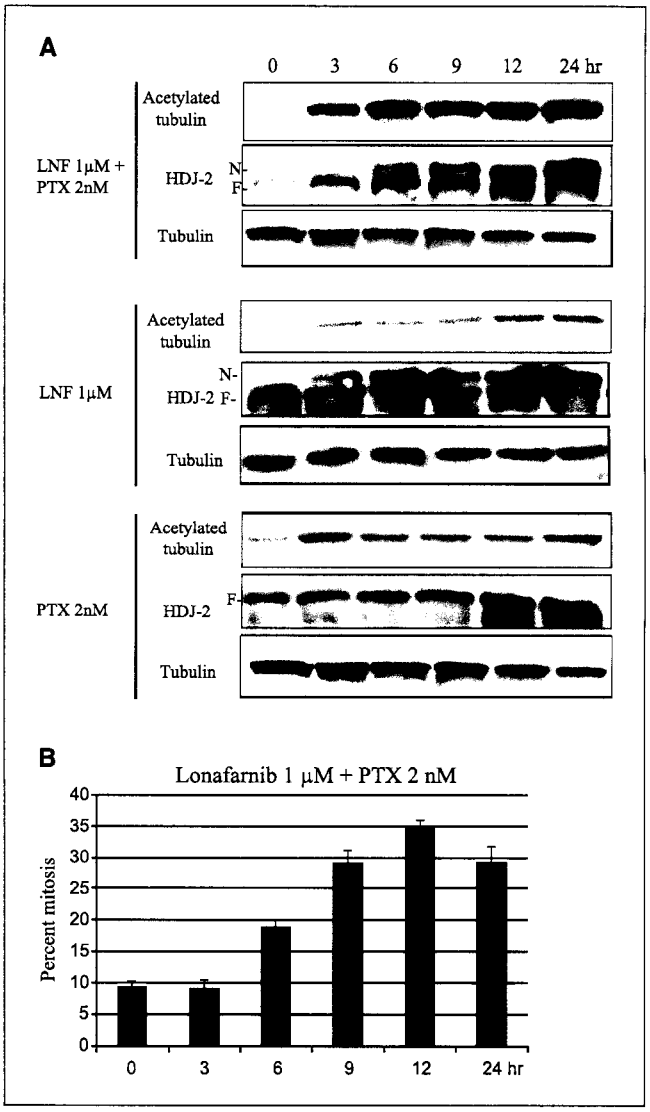

Figure 4. The synergistic increase in acetylated tubulin caused by lonafarnib and paclitaxel treatment correlates with FT inhibition and mitotic arrest. *A*, Western blot analysis for acetylated tubulin, HDJ-2 (*N*, non-farnesylated band; *F*, farnesylated band), and total tubulin following lonafarnib and/or paclitaxel treatment over time. *B*, percent mitosis assessed by DNA staining, done in parallel and with the same drug treatments over time as in *A*. *Bars*, SD.

farnesylation and tubulin acetylation beginning at 3 hours of treatment with the lonafarnib/paclitaxel combination. In contrast, minimal effect on tubulin acetylation was observed with either drug alone. Taken together, these results show a positive temporal correlation between FT inhibition and tubulin acetylation when lonafarnib and paclitaxel are combined.

Next, we wanted to determine if there is also a correlation between tubulin acetylation and mitotic arrest. Therefore, in parallel with the time course experiment described above, we quantitated the percentage of cells in mitosis after treatment with the combination of lonafarnib and paclitaxel. This result is represented in Fig. 4*B* showing that there is about a 3-hour delay between the increase in microtubule acetylation (starting at 3 hours) and the first indication of mitotic arrest (at 6 hours). Furthermore, the percentage of cells in mitosis increased with

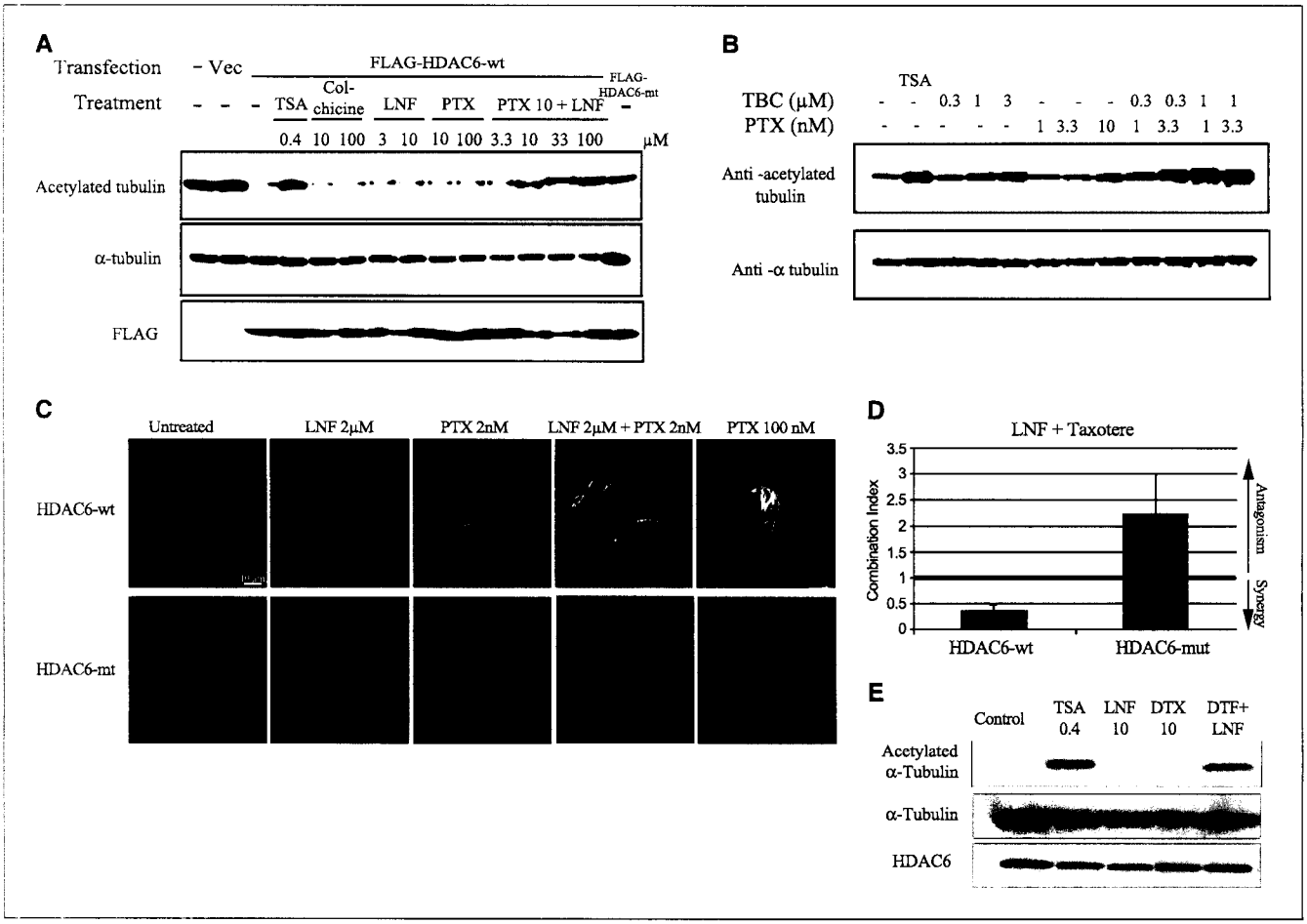

Figure 5. The synergistic combination of lonafarnib and taxane prevents HDAC6 tubulin deacetylation *in vitro* and is dependent on HDAC6 functionality. *A*, representative Western blots of acetylated α-tubulin, total tubulin, and Flag, following immunoprecipitation (IP) from A549 cells transfected with either Flag-HDAC6-WT or Flag-HDAC6-mut. Before Western blotting the Flag-IP complexes were incubated *in vitro* with preassembled purified bovine brain microtubule protein in the presence of various drugs to determine the tubulin deacetylase activity of HDAC6 (*left-hand blot*). *B*, Western blotting of acetylated tubulin after treatment with tubacin, a specific HDAC6 inhibitor, both alone and in combination with paclitaxel. Trichostatin A (*TSA*) was used as additional positive control for pan-HDAC inhibition. As a control for total tubulin levels, blots were reprobed for α-tubulin. *C*, immunofluorescence analyses of acetylated tubulin in NIH-3T3 cells stably expressing either HDAC6-wt or HDAC-mut, following 16-hour drug treatments as indicated. *D*, assessment of synergy between lonafarnib and docetaxel in HDAC6-wt and HDAC6-mut using combination index analysis. The lonafarnib/docetaxel combination is synergistic in HDAC6-wt (combination index < 1) but is antagonistic in HDAC6-mt cells (combination index > 1). *Bars*, SD. *E*, representative Western blots of acetylated α-tubulin, total tubulin, and HDAC6 following immunoprecipitation (IP) from NIH-3T3 cells stably expressing Flag-HDAC6-WT. Before Western blotting the Flag-IP complexes were incubated *in vitro* with preassembled purified bovine brain microtubule protein in the presence of various drugs to determine the tubulin deacetylase activity of HDAC6. The *in vitro* effects of trichostatin A (pan-HDAC inhibitor), lonafarnib, and docetaxel (*DTX*) on acetylated α-tubulin are shown.

longer exposures to the combination of the two drugs, peaking at 12 hours of treatment. Overall, this result shows that when lonafarnib and paclitaxel are combined, microtubule acetylation occurs before mitotic arrest and suggests that there is a correlation between tubulin acetylation/stability and mitotic arrest.

Lonafarnib in combination with paclitaxel inhibits the tubulin deacetylating activity of histone deacetylase 6. Our observation that lonafarnib and paclitaxel synergistically enhance tubulin acetylation (Fig. 3) prompted us to explore the possibility that this effect is due to the functional inhibition of the only known tubulin-specific deacetylase (30), HDAC6. To determine the effect of lonafarnib on HDAC6 function, we transfected A549 cells with FLAG-tagged HDAC6 (wild-type or catalytic subunit mutant) and these proteins were immunoprecipitated with an anti-FLAG antibody (see Materials and Methods). The tubulin deacetylase activity of HDAC6 in the presence of lonafarnib and paclitaxel was assayed *in vitro* by coincubating the immunoprecipitants with purified bovine brain microtubule protein. Western blot analyses of acetylated tubulin levels were used as a read-out for HDAC6 activity (Fig. 5*A*), such that HDAC6 functionality is evidenced by tubulin deacetylation. As a positive control, we used trichostatin A, which inhibits the function of all histone deacetylases including HDAC6. As expected, bovine brain tubulin is heavily acetylated (*lane 1*) and coincubation with wt-HDAC6 almost completely deacetylated tubulin (*lane 3*). In contrast, coincubation with the catalytically inactive mutant HDAC6 had no effect on tubulin acetylation (*last lane*). The addition of lonafarnib or paclitaxel alone to the purified wild-type HDAC6-tubulin complex had no effect on HDAC6 activity because tubulin was heavily deacetylated, indicating normal HDAC6 activity. In contrast, when lonafarnib (variable doses) and paclitaxel (kept constant at 10 μmol/L) were combined *in vitro*, there was a dose-dependent increase of tubulin acetylation, suggesting that the combination of these agents inhibits tubulin deacetylating HDAC6 activity. Paclitaxel alone

had no effect on HDAC6 activity even at 100 μmol/L. We also tested the microtubule depolymerizing agent colchicine for HDAC6 inhibitory activity, and like paclitaxel, it did not inhibit HDAC6 function.

Since our results suggest that the combination of lonafarnib and paclitaxel synergistically inhibits HDAC6 function, we wanted to determine if these drugs also affect the function of other histone deacetylases. Thus, we treated A549 cells with lonafarnib, alone and in combination with paclitaxel, for 16 hours and probed for acetylated histone 3. Trichostatin A (a pan-HDAC inhibitor) was included as a positive control. As expected, treatment with trichostatin A resulted in increased levels of acetylated histone 3. In contrast, no effect on acetylated histone 3 was observed with lonafarnib treatment either alone or in combination with paclitaxel (Supplementary Fig. S2), suggesting that lonafarnib and/or paclitaxel does not affect the function of other histone deacetylases.

To probe the importance of HDAC6 inhibition in the mechanism of synergy between lonafarnib and paclitaxel, we combined a specific HDAC6 inhibitor, tubacin, with paclitaxel. This experiment allows us to determine whether the combination of a specific HDAC6 inhibitor with paclitaxel leads to a synergistic increase in tubulin acetylation, similar to the lonafarnib/paclitaxel combination. Western blot analysis of A549 cells treated with the combination of tubacin and paclitaxel at low doses (beginning at 0.3 μmol/L tubacin and 1 nmol/L paclitaxel) led to a synergistic increase in acetylated tubulin, as compared with either drug alone (Fig. 5*B*). These findings were confirmed with acetylated tubulin immunofluorescence (data not shown). Thus, specific inhibition of HDAC6 (e.g., with tubacin) in combination with paclitaxel leads to a synergistic increase in acetylated tubulin, further suggesting that the lonafarnib/paclitaxel inhibition of HDAC6 activity provides a mechanistic basis for the enhanced tubulin acetylation. Furthermore, the addition of 3 and 10 μmol/L tubacin (IC_{50} > 1 mmol/L) to paclitaxel (IC_{50} 7.7 ± 1.7 μmol/L) decreased the IC_{50} of paclitaxel, 20.8% and 31.5%, respectively (Supplementary Table S1). Similar results were also observed when tubacin was combined with docetaxel (Supplementary Table S1), suggesting that although tubacin as a single agent is not cytotoxic, its affect on tubulin acetylation can enhance the cytotoxicity of paclitaxel.

To further explore the functional importance of HDAC6 in the synergy between lonafarnib and paclitaxel, we tested this drug combination in a pair of cell lines engineered to stably express either wild-type HDAC6 (HDAC6-wt) or a catalytic mutant HDAC6 (HDAC6-mut). These cells lines will allow us to determine if a functional HDAC6 protein is required for the observed effects on acetylated tubulin. In agreement with previously published data (30), HDAC6-wt cells had lower baseline levels of acetylated tubulin relative to HDAC6-mut cells, consistent with the presence of a functional versus a nonfunctional HDAC6 (Fig. 5*C*, untreated). Upon treatment with the lonafarnib/paclitaxel combination, there was a synergistic increase in acetylated tubulin in HDAC6-wt cells as expected; however, the lonafarnib/paclitaxel combination had no effect on tubulin acetylation in the HDAC6-mut cells. These results indicate that the synergistic increase in acetylated tubulin induced by the lonafarnib/paclitaxel combination is dependent on the presence of a functional HDAC6.

Next, we wanted to determine if functional HDAC6 is required not only for the synergistic increase in acetylated tubulin with the lonafarnib/taxane combination (Fig. 5*C*) but also for the synergistic antiproliferative activity of the drugs. Thus, we did cytotoxicity assays employing the routinely used combination index analysis to assess synergy between the two drugs against cells with HDAC6-wt and HDAC6-mut genetic background. Our results show that the combination of lonafarnib with docetaxel resulted in a robust synergistic antiproliferative effect in HDAC6-wt cells (mean combination index = 0.4, indicating strong synergy; Fig. 5*D*). In stark contrast, the combination of lonafarnib and docetaxel was antagonistic in the HDAC6-mut cells (mean combination index = 2.5), suggesting that the lack of functional HDAC6 in these cells not only precludes increased levels of acetylated tubulin with this drug combination but also abolishes their antiproliferative synergy. To confirm that the combination of docetaxel with lonafarnib inhibits the tubulin deacetylase activity of HDAC6 *in vitro*, similar to our previous results with paclitaxel (Fig. 5*A*), we used cells stably expressing wild-type HDAC6 to immunoprecipitate HDAC6, and performed an *in vitro* tubulin deacetylase assay. Our data show that the combination of 10 μmol/L lonafarnib with 10 μmol/L docetaxel resulted in a synergistic inhibition of HDAC6 function, as evidenced by the appearance of acetylated tubulin, whereas either drug alone had no effect on HDAC6 functionality (Fig. 5*E*). Collectively, these data provide a mechanistic link between HDAC6 inhibition, tubulin acetylation, and the synergistic interaction of these drugs.

Discussion

Analyzing the effects of lonafarnib as a single agent on microtubules. The FTIs were developed as targeted therapies against cancers with oncogenic Ras mutations, however, FTIs were shown to retain their activity independently of Ras status (11–13). Here we examined the effects of the FTI lonafarnib on interphase microtubules in human cancer cells. Our results show that prolonged exposure (48 hours) to lonafarnib alone leads to microtubule stabilization as evidenced by increased tubulin acetylation, suppression of microtubule dynamics, and bundle formation (Figs. 1 and 2; Table 1). Because tubulin acetylation is an established marker of microtubule stability (36), we believe that the lonafarnib-induced microtubule stabilization may contribute to its antiproliferative effects, similar to taxanes and epothilones. However, it is important to note that the microtubule-stabilizing capacity of lonafarnib is weak relative to other established microtubule stabilizing agents, which stabilize microtubules at low nanomolar concentrations. This suggests that the mechanism by which lonafarnib induces microtubule stabilization may differ from traditional microtubule-stabilizing agents (e.g., taxanes). Further supporting this hypothesis is our electron microscopy analysis (Supplementary Fig. S1-*B*), which shows that lonafarnib-induced microtubule bundles are longer and not as tightly clustered as paclitaxel-induced bundles, suggesting that their differing morphologies may stem from alternative mechanisms of bundle formation. Thus, we propose that lonafarnib is a microtubule-stabilizing agent; however, its mechanism of microtubule stabilization likely differs from that of established microtubule-stabilizing agents.

Microtubule acetylation and the mechanism of synergy between lonafarnib and taxanes. Previous reports have shown that FTIs synergize with taxanes and epothilones in a variety of human cancer cell lines *in vitro* and *in vivo* (22, 24); however, the mechanism underlying this synergy is unknown. Our results show that the combination of low doses of lonafarnib (beginning at 0.5 μmol/L) and paclitaxel (2 nmol/L) resulted in a dramatic increase in tubulin acetylation (Fig. 3*A-C*) compared with untreated cells or each drug treatment alone. Importantly, the mean Cmax of

lonafarnib achieved in patients dosed twice daily with 200 mg of lonafarnib is 4.4 μmol/L[6] and, therefore, the doses (lonafarnib beginning at 0.5 μmol/L) at which we observed synergistic enhancement of acetylated tubulin are within the Cmax. Furthermore, the effect of lonafarnib/paclitaxel on acetylated tubulin was observed in as little as 3 hours of drug treatment (Fig 4*A*) and preceded the synergistic increase in mitotic arrest (Figs. 3*C* and 4*B*), suggesting that increased microtubule acetylation/stability is associated with aberrant mitotic arrest and cell death. Nevertheless, it remains unclear if lonafarnib/paclitaxel-induced microtubule acetylation only serves as marker for cell death or instead is the catalyst, and therefore studies are under way addressing this issue.

Mechanistically, we show that the synergistic increase in microtubule acetylation is due to the effect of the combination of lonafarnib and paclitaxel on HDAC6 (Fig. 5). We propose that the enhanced tubulin acetylation we observe is due to the inhibition of HDAC6 function. We provide four lines of evidence to support this claim. First, we show that the combination of lonafarnib and paclitaxel inhibits HDAC6 tubulin deacetylating activity *in vitro*, whereas either drug alone had no effect (Fig 5*A*). Second, we can reproduce the lonafarnib/paclitaxel-induced increase in tubulin acetylation by using tubacin, a specific HDAC6 inhibitor, in combination with paclitaxel (Fig. 5*B*). This suggests that pharmacologic inhibition of HDAC6 in combination with paclitaxel synergistically increases tubulin acetylation. Third, cells expressing a catalytically inactive HDAC6 (HDAC6-mt) fail to show an increase in acetylated tubulin when lonafarnib and paclitaxel are combined (Fig. 5*C*), suggesting that this drug combination requires functional HDAC6 to retain efficacy. Fourth, the robust cytotoxic synergy of lonafarnib and docetaxel is lost in these cells expressing mutant HDAC6, whereas potent synergy remains in their wild-type HDAC6 counterparts (Fig. 5*D*). This observation provides evidence that the deacetylating activity of HDAC6 is required for the lonafarnib/taxane synergy, providing a mechanistic link between functional HDAC6, tubulin acetylation, and cell death. However, it is still unknown whether the effect of the lonafarnib/taxane combination on HDAC6 function is due to direct binding of these drugs to this enzyme or due to their effects on microtubule stability, which in turns alters the affinity of HDAC6 for the microtubule. We favor the latter scenario because either drug alone does not alter HDAC6 function, reducing the likelihood that these drugs bind HDAC6 directly.

Is there a biological link between FTase inhibition and microtubule acetylation? Because all FTIs tested to date synergize with paclitaxel, it is likely that they share a common mechanism of synergy related to FT inhibition. In Fig. 4*A*, we show that the increase in tubulin acetylation observed with the low dose lonafarnib/paclitaxel combination correlates with FT inhibition. This result suggests that inhibition of FT may be biologically linked with enhanced tubulin acetylation. Currently, there are no reports of a link between the FTase enzyme and interphase microtubules. Preliminary data from our laboratory in 50 human cancer cell lines used in the National Cancer Institute Anticancer Drug Screen (http://dtp.nci.nih.gov) have revealed that acetylated tubulin protein levels negatively correlated with FTase gene expression and protein levels (COMPARE analysis http://itbwork.nci.nih.gov/CompareServer/CompareServer;).[7] Thus, it may be possible that proteins regulating microtubule stability are farnesylated by FTase; consequently, inhibition of FTase by lonafarnib may in turn affect microtubule stability. In fact, it is already known that the mitotic microtubule-associated protein, CENP-E, is farnesylated and its association with microtubules during mitosis is altered in mitotic cells (27). Thus, further investigation of a putative link between FTase and interphase microtubules is warranted.

Overall, our data show that treatment with lonafarnib alone causes microtubule bundling, increased microtubule acetylation and stabilization, and suppression of microtubule dynamics. This result is consistent with lonafarnib being a microtubule-stabilizing agent, in addition to its role as an FTI. Importantly, our data also show that functional HDAC6 is required for the synergy between lonafarnib and taxanes and suggest that there is a link between FTase and tubulin acetylation. As there are ongoing phase II and III trials testing the efficacy of this drug combination, elucidating the molecular mechanism(s) of synergy can provide insight into the design of future combination cancer therapies.

Acknowledgments

Received 10/20/2004; revised 1/7/2005; accepted 2/16/2005.

Grant support: NIH 1R01 CA100202 and Aventis Pharmaceuticals. BESCT grant no. DAMD17-01-1-0689 (to F.R. Khuri).

The costs of publication of this article were defrayed in part by the payment of page charges. This article must therefore be hereby marked *advertisement* in accordance with 18 U.S.C. Section 1734 solely to indicate this fact.

We thank Drs. Mary Ann Jordan and Kathy Kamath (University of California Santa Barbara, Santa Barbara, CA) for providing us with the MCF-7 cells stably expressing GFP:α-tubulin and for sharing their invaluable experience on performing the live-cell microtubule dynamic assays; Dr. Stuart Schreiber (Harvard University, Boston, MA) for providing us with tubacin and FLAG-HDAC6 constructs, and for providing guidance to Jason Wong (gm38627, awarded to Stuart L. Schreiber); Dr. W. Robert Bishop for his invaluable insight and for providing us with Lonafarnib (Schering-Plough Research Institute); Dr. Robert Apkarian, director of the electron microscopy core facility at Emory University, for his help with transmission electron microscopy; Cindy Giver for her help with flow cytometry; and the Winship Cancer Institute Cancer Imaging and Microscopy Core for their support and service.

[6] R. Bishop, unpublished data.

[7] Unpublished data.

References

1. Brunner TB, Hahn SM, Gupta AK, et al. Farnesyltransferase inhibitors: an overview of the results of preclinical and clinical investigations. Cancer Res 2003;63:5656–68.
2. Adjei AA. Blocking oncogenic Ras signaling for cancer therapy. J Natl Cancer Inst 2001;93:1062–74.
3. Hahn SM, Bernhard E, McKenna WG. Farnesyltransferase inhibitors. Semin Oncol 2001;28:86–93.
4. McCormick F. Ras-related proteins in signal transduction and growth control. Mol Reprod Dev 1995;42:500–6.
5. Jackson JH, Cochrane CG, Bourne JR, et al. Farnesyl modification of Kirsten-ras exon 4B protein is essential for transformation. Proc Natl Acad Sci U S A 1990;87:3042–6.
6. Kato K, Cox AD, Hisaka MM, et al. Isoprenoid addition to Ras protein is the critical modification for its membrane association and transforming activity. Proc Natl Acad Sci U S A 1992;89:6403–7.
7. Willumsen BM, Christensen A, Hubbert NL, Papageorge AG, Lowy DR. The p21 ras C terminus is required for transformation and membrane association. Nature 1984;310:583–6.
8. Barbacid M. Ras genes. Annu Rev Biochem 1987;56:779–827.
9. Bos JL. Ras oncogenes in human cancer: a review. Cancer Res 1989;49:4682–9.
10. Li T, Sparano JA. Inhibiting Ras signaling in the therapy of breast cancer. Clin Breast Cancer 2003;3:405–16; discussion 17–20.
11. End DW, Smets G, Todd AV, et al. Characterization of the antitumor effects of the selective farnesyl protein transferase inhibitor R115777 *in vivo* and *in vitro*. Cancer Res 2001;61:131–7.
12. Nagasu T, Yoshimatsu K, Rowell C, Lewis MD, Garcia AM. Inhibition of human tumor xenograft growth by

treatment with the farnesyl transferase inhibitor B956. Cancer Res 1995;55:5310–4.

13. Sepp-Lorenzino L, Ma Z, Rands E, et al. A peptidomimetic inhibitor of farnesyl:protein transferase blocks the anchorage-dependent and -independent growth of human tumor cell lines. Cancer Res 1995; 55:5302–9.
14. Moasser MM, Rosen N. The use of molecular markers in farnesyltransferase inhibitor (FTI) therapy of breast cancer. Breast Cancer Res Treat 2002;73: 135–44.
15. Nogales E. Structural insights into microtubule function. Annu Rev Biochem 2000;69:277–302.
16. Jordan MA. Mechanism of action of antitumor drugs that interact with microtubules and tubulin. Curr Med Chem Anti-Canc Agents 2002;2:1–17.
17. Jordan MA, Wilson L. Microtubules as a target for anticancer drugs. Nat Rev Cancer 2004;4:253–65.
18. Drukman S, Kavallaris M. Microtubule alterations and resistance to tubulin-binding agents [review]. Int J Oncol 2002;21:621–8.
19. Rowinsky EK. The development and clinical utility of the taxane class of antimicrotubule chemotherapy agents. Annu Rev Med 1997;48:353–74.
20. Checchi PM, Nettles JH, Zhou J, Snyder JP, Joshi HC. Microtubule-interacting drugs for cancer treatment. Trends Pharmacol Sci 2003;24:361–5.
21. Wartmann M, Altmann KH. The biology and medicinal chemistry of epothilones. Curr Med Chem Anti-Canc Agents 2002;2:123–48.
22. Moasser MM, Sepp-Lorenzino L, Kohl NE, et al. Farnesyl transferase inhibitors cause enhanced mitotic sensitivity to taxol and epothilones. Proc Natl Acad Sci U S A 1998;95:1369–74.
23. Sun J, Blaskovich MA, Knowles D, et al. Antitumor efficacy of a novel class of non-thiol-containing peptidomimetic inhibitors of farnesyltransferase and geranylgeranyltransferase I: combination therapy with the cytotoxic agents cisplatin, Taxol, and gemcitabine. Cancer Res 1999;59:4919–26.
24. Shi B, Yaremko B, Hajian G, et al. The farnesyl protein transferase inhibitor SCH66336 synergizes with taxanes *in vitro* and enhances their antitumor activity *in vivo*. Cancer Chemother Pharmacol 2000;46:387–93.
25. Khuri FR, Glisson BS, Kim ES, et al. Phase I study of the farnesyltransferase inhibitor lonafarnib with paclitaxel in solid tumors. Clin Cancer Res 2004;10: 2968–76.
26. Crespo NC, Ohkanda J, Yen TJ, Hamilton AD, Sebti SM. The farnesyltransferase inhibitor, FTI-2153, blocks bipolar spindle formation and chromosome alignment and causes prometaphase accumulation during mitosis of human lung cancer cells. J Biol Chem 2001;276: 16161–7.
27. Crespo NC, Delarue F, Ohkanda J, et al. The farnesyltransferase inhibitor, FTI-2153, inhibits bipolar spindle formation during mitosis independently of transformation and Ras and p53 mutation status. Cell Death Differ 2002;9:702–9.
28. Ashar HR, James L, Gray K, et al. Farnesyl transferase inhibitors block the farnesylation of CENP-E and CENP-F and alter the association of CENP-E with the microtubules. J Biol Chem 2000;275: 30451–7.
29. Taveras AG, Kirschmeier P, Baum CM. Sch-66336 (sarasar) and other benzocycloheptapyridyl farnesyl protein transferase inhibitors: discovery, biology and clinical observations. Curr Top Med Chem 2003;3: 1103–14.
30. Hubbert C, Guardiola A, Shao R, et al. HDAC6 is a microtubule-associated deacetylase. Nature 2002;417: 455–8.
31. Mabjeesh NJ, Escuin D, LaVallee TM, et al. 2ME2 inhibits tumor growth and angiogenesis by disrupting microtubules and dysregulating HIF. Cancer Cell 2003;3:363–75.
32. Giannakakou P, Villalba L, Li H, Poruchynsky M, Fojo T. Combinations of paclitaxel and vinblastine and their effects on tubulin polymerization and cellular cytotoxicity: characterization of a synergistic schedule. Int J Cancer 1998;75:57–63.
33. Giannakakou P, Sackett DL, Kang YK, et al. Paclitaxel-resistant human ovarian cancer cells have mutant β-tubulins that exhibit impaired paclitaxel-driven polymerization. J Biol Chem 1997; 272:17118–25.
34. Vanier MT, Neuville P, Michalik L, Launay JF. Expression of specific tau exons in normal and tumoral pancreatic acinar cells. J Cell Sci 1998;111: 1419–32.
35. Kamath K, Jordan MA. Suppression of microtubule dynamics by epothilone B is associated with mitotic arrest. Cancer Res 2003;63:6026–31.
36. Piperno G, LeDizet M, Chang XJ. Microtubules containing acetylated α-tubulin in mammalian cells in culture. J Cell Biol 1987;104:289–302.

VOLUME 22 · NUMBER 22 · NOVEMBER 15 2004

JOURNAL OF CLINICAL ONCOLOGY

ORIGINAL REPORT

Prognostic Factors in Resected Stage I Non–Small-Cell Lung Cancer: A Multivariate Analysis of Six Molecular Markers

Charles Lu, Jean-Charles Soria, Ximing Tang, Xiao-Chun Xu, Luo Wang, Li Mao, Reuben Lotan, Bonnie Kemp, B. Nebiyou Bekele, Lei Feng, Waun K. Hong, and Fadlo R. Khuri

From the Departments of Thoracic/Head and Neck Medical Oncology, Clinical Cancer Prevention, Pathology, and Biostatistics, The University of Texas M.D. Anderson Cancer Center, Houston, TX; Institut Gustave Roussy, Villejuif, France; and Winship Cancer Institute, Emory University, Atlanta, GA.

Submitted January 13, 2004; accepted August 26, 2004.

Supported in part by National Cancer Institute grant No. K12 CA088084 and the Department of Defense, Biology, Education, Screening, Chemoprevention, and Treatment of Lung Cancer grant No. DAMD17-01-1-0689 and Translational Approaches for the Reversal, Genetic, Evaluation and Treatment of Lung Cancer grant No. DAMD17-02-1-0706.

Presented in part at the 93rd Annual Meeting of the American Association for Cancer Research, San Francisco, CA, April 6-10, 2002.

Authors' disclosures of potential conflicts of interest are found at the end of this article.

Address reprint requests to Charles Lu, M.D., SM, The University of Texas M.D. Anderson Cancer Center, 1515 Holcombe Boulevard, Box 432, Houston, TX 77030-4009; e-mail: clu@mdanderson.org.

0732-183X/04/2222-4575/$20.00

DOI: 10.1200/JCO.2004.01.091

A B S T R A C T

Purpose

To analyze the prognostic significance of six molecular biomarkers (death-associated protein kinase [*DAPK*] promoter methylation, interleukin-10 [IL-10] protein expression, cyclooxygenase-2 [COX-2] mRNA expression, human telomerase reverse transcriptase catalytic subunit [hTERT] mRNA expression, retinoic acid receptor-beta [RAR-β] mRNA expression, and K-*ras* mutational status) in stage I non–small-cell lung cancer (NSCLC) patients.

Patients and Methods

Biomarker analyses were performed on tumors from 94 patients with stage I NSCLC who underwent surgical resection at our institution. A minimum follow-up period of 5 years was required. *DAPK* methylation was assessed by methylation-specific polymerase chain reaction (PCR). RAR-β, COX-2, and hTERT mRNA levels were determined by in situ hybridization with digoxigenin-labeled antisense riboprobes. K-*ras* mutation status was determined by the PCR–primer introduced restriction with enrichment for mutant alleles method. IL-10 protein expression was analyzed by immunohistochemistry using a polyclonal antihuman IL-10 antibody. Cancer-specific survival was analyzed with a Cox proportional hazards model. To identify independent prognostic factors, a stepwise selection method was used.

Results

DAPK methylation, IL-10 lack of expression, COX-2 expression, hTERT expression, RAR-β expression, and K-*ras* mutations were observed in 46.8%, 29.8%, 59.6%, 34.0%, 23.4%, and 34.0% of patients, respectively. In the final model, *DAPK* methylation and IL-10 lack of expression were significant negative prognostic factors for cancer-specific survival, whereas COX-2 expression was of borderline significance.

Conclusion

In this cohort of resected stage I NSCLC patients, molecular markers that independently predict cancer-specific survival have been identified. The prognostic roles of *DAPK* methylation, IL-10, and other biomarkers in NSCLC merit further investigation.

J Clin Oncol 22:4575-4583. © 2004 by American Society of Clinical Oncology

Lung cancer remains a worldwide public health issue of immense proportions. In the year 2003, cancers of the lung and bronchus are expected to continue to account for the most cancer deaths in the United States (157,200 deaths or 28.2%), more than the estimated total number of deaths as a result of cancers of the breast, prostate, colon, and rectum combined.[1] Approximately 80% of lung cancers will have non–small-cell carcinoma histology.[2]

Approximately 25% of patients present with early-stage disease.[3] The standard treatment is surgical resection with appropriate lymph node sampling or dissection. Although early-stage non–small-cell lung

cancer (NSCLC) patients have a relatively favorable prognosis, the risk of disease recurrence and death remains substantial. Five-year survival rates for pathologic stages I and II disease are 57% to 67% and 38% to 55%, respectively.[4] Identification of reliable prognostic factors for disease recurrence and death could have significant clinical import. Patients in a high-risk group, for example, would be appropriate candidates for novel adjuvant or chemoprevention strategies.

Both our group[5-12] and others[13-16] have focused on identifying molecular prognostic factors in early-stage NSCLC. We have established a retrospective cohort of stage I NSCLC patients who underwent surgical resection at our institution. Over the past few years, investigators in our group have analyzed a number of tumor biomarkers within this valuable clinical research database.

Given the roles that retinoids play in the regulation of cell growth, differentiation, and apoptosis, Khuri et al[8] investigated the prognostic significance of retinoic acid receptor-beta (RAR-β) mRNA expression in 156 patients. Because RAR-β expression seems to be suppressed during carcinogenesis, these investigators hypothesized that lower RAR-β levels would predict a poor clinical outcome. Surprisingly, overall survival was significantly worse in patients with strongly positive RAR-β expression. Because one RAR-β isoform, RAR-β4, may promote hyperplasia and neoplasia,[17] the authors hypothesized that differential expression of RAR-β isoforms may be a possible explanation for their unexpected findings.

Khuri et al[9] subsequently evaluated cyclooxygenase-2 (COX-2) mRNA expression and correlated it with the expression of RAR-β in this cohort of stage I NSCLC patients. COX-2 overexpression had previously been demonstrated in lung, head and neck, and other tumors,[18-20] and cell line data indicated that retinoic acid could suppress COX-2.[21] These investigators found that COX-2 expression was associated with worse overall and disease-free survival and that COX-2 and RAR-β mRNA levels were correlated. These findings were in conflict with the prior cell line data, which would have predicted that RAR-β upregulation should downregulate COX-2.

Telomerase is a ribonucleoprotein that lengthens and maintains the ends of chromosomes that are shortened with successive cell divisions.[22] Telomerase is expressed in up to 85% of NSCLC tumors and plays a critical role in sustaining cellular immortality and carcinogenesis.[23,24] Wang et al[11] examined mRNA expression of the human telomerase reverse transcriptase catalytic subunit (hTERT) in 153 patients from our database. Positive hTERT expression was significantly associated with worse overall and disease-specific survival.

Tang et al[7] examined hypermethylation of the death-associated protein kinase (*DAPK*) promoter in 135 patients from this cohort. Epigenetic inactivation of tumor suppressor genes by promoter hypermethylation frequently occurs in NSCLC.[25,26] *DAPK* is a putative tumor-suppressor gene that encodes for a calmodulin-dependent kinase that possesses a death domain at its C terminus.[27] *DAPK* is required for interferon-gamma–induced apoptosis and seems to suppress the metastatic ability of lung cancer cells.[28] In the study by Tang et al,[7] *DAPK* hypermethylation was significantly associated with poorer overall and disease-specific survival.

Soria et al[12] examined the role of interleukin-10 (IL-10) protein expression among 135 patients. The immunomodulatory effects of IL-10 have demonstrated conflicting results in various tumor systems. Some reports support the role of IL-10 in helping tumors evade immunosurveillance because IL-10 can inhibit macrophage, T-cell, and antigen-presenting cell functions.[29,30] Others have demonstrated that IL-10 may function as a potent inhibitor of tumor growth and metastasis.[31,32] In this study, IL-10 lack of expression was significantly associated with poorer overall and disease-specific survival.

The aforementioned hypothesis-driven studies each focused on one or a few biomarkers. To simultaneously examine multiple potential molecular prognostic factors in this clinical research database, we identified 94 patients who had complete information for a panel of six biomarkers (RAR-β, COX-2, hTERT, *DAPK* promoter methylation, IL-10, and K-*ras*). Multivariate Cox regression analysis was used to identify independent predictors of cancer-specific survival in this population of resected stage I NSCLC patients.

Study Population

Five hundred ninety-five consecutive patients with stage I NSCLC underwent definitive surgical resection, defined as a lobectomy or a pneumonectomy, from 1975 to 1990 at The University of Texas M.D. Anderson Cancer Center (Houston, TX). Patients did not receive preoperative or postoperative chemotherapy or radiotherapy. We retrospectively identified 185 patients for whom both tissue samples and a median follow-up period of more than 5 years were available. All available tissue blocks were reviewed by a thoracic pathologist (B.K.), and 163 cases had adequate tumor present in the surgical specimen. The patient population was identified through a search of the Tumor Registry database maintained by the Department of Medical Informatics at The University of M.D. Anderson Cancer Center. Survival status was verified and updated from Tumor Registry records as of December 1, 2000. This study was reviewed and approved by the institutional review board and conducted in accordance with its policies.

Five published studies[7-9,11,12] had previously examined different molecular prognostic factors among the 163 patients with sufficient tumor specimens and more than 5 years of follow-up data. The sample sizes ranged from 135 to 160 patients. A total of

94 patients had complete information for a panel of six biomarkers, and these patients were included in our analysis.

Methylation-Specific Polymerase Chain Reaction (PCR)

These methods have been previously described.[7] Briefly, 8-μm sections from paraffin-embedded tissue blocks were obtained, and regions with tumor cells were dissected under a stereomicroscope. In the initial chemical modification step, 200 ng of DNA from each tumor was denatured by NaOH and treated with sodium bisulfite (Sigma Chemical Co, St Louis, MO). DNA was recovered in water and was ready to add to a PCR with the use of specific primers for either the methylated or the unmethylated *DAPK* promoter, as described previously.[33] DNA was amplified for 35 cycles, and PCR products were separated on 2% agarose gels and visualized. For each DNA sample, primer sets for methylated DNA and unmethylated DNA were used for analysis. The hypermethylation status was determined by visualizing a 98-base pair (bp) PCR product with the methylation-specific primer set. All PCRs were repeated twice, and the results were reproducible.

Immunohistochemical Staining for IL-10 Protein

Paraffin-embedded, 4-μm–thick tissue sections were stained for IL-10 protein using a primary goat polyclonal antihuman IL-10 antibody (AF-217-NA; R&D Systems, Minneapolis, MN) as previously described.[12] Routinely processed tissue sections of normal lymph nodes and tonsils were used as positive staining controls and were also stained with the primary antibody omitted to confirm staining specificity. Normal bronchial epithelial cells that constitutively produce IL-10 were also used as internal positive controls.[34]

The IL-10 labeling index was defined as the percentage of tumor cells displaying cytoplasmic immunoreactivity and was calculated by counting IL-10–stained tumor cells among at least 1,000 tumor cells for each section as previously described.[12] On the basis of previous reports, if 10% or more of the tumor cells were positive for IL-10, the case was considered to be IL-10 positive.[35] All slides were scored concomitantly by a pathologist (X.T.) and another investigator (J.-C.S.) in a blinded manner.

hTERT In Situ Hybridization (ISH)

These methods have been previously described.[11] The riboprobes were a 430-bp EcoRV-BamH1 fragment of the hTERT cDNA that has been used in other studies[36,37] as well as part of exon 1 from the heterogeneous nuclear ribonucleoprotein A1 as a control to verify sample quality. The single-strand–specific, digoxigenin-labeled riboprobes were generated by in vitro transcription. ISH was performed as previously described.[37] Slides displaying a diffuse but clear cytoplasmic signal were considered to be positive, as reported by Falchetti et al.[38] More specifically, our slides were rated as positive if a definite and clear signal was present in more than two large areas on the slide. Slides with faint signal, the absence of signal, or only focal positivity were considered to be negative. We did not grade the intensity of the hybridization signals.

COX-2 and RAR-β ISH

COX-2 and RAR-β mRNA were detected in 4-μm–thick sections from paraffin-embedded tissue using nonradioactive ISH with digoxigenin-labeled antisense riboprobes as previously described.[8,9,39] Retinoid X receptor-alpha (RXR-α), which is present in greater than 90% of NSCLCs,[40] was used as a control to detect RNA degradation. The rationale for using RXR-α as a control for intact RNA was the observation that all 70 cases of NSCLC and normal lung tissue expressed RXR-α mRNA in a previous study.[40] Stained sections were reviewed by three independent researchers, including two pathologists, in a blinded fashion. Only cytoplasmic staining was considered positive. Because normal bronchial epithelium expresses RAR-β, positive and aberrant RAR-β expression was defined as $\geq$ 10% and less than 10% intratumoral staining, respectively.[8] The RAR-β probe that was used identified all RAR-β isoforms. COX-2 expression was defined as either positive (present) or negative (absent).[9]

K-ras Mutation Analysis With PCR–Primer Introduced Restriction With Enrichment for Mutation Alleles (PCR-PIREMA)

A modified PCR-PIREMA method was used to detect K-*ras* codon 12 mutations.[41] Briefly, 8-μm sections from paraffin-embedded tissue blocks were obtained, and regions with tumor cells were dissected under a stereomicroscope. Dissected tissues were digested in 200 μL of digestion buffer containing 50 mmol/L Tris-HCl (pH 8.0), 1% sodium dodecyl sulfate, and proteinase K (0.5 mg/mL) at 42°C for 36 hours. The digested products were purified by extracting with phenol-chloroform twice. DNA was then precipitated by the ethanol precipitation method in the presence of glycogen (Roche Biochemicals, Indianapolis, IN), recovered in distilled water, and then stored at −20°C until used for PCR.

Briefly, PCR around K-*ras* codon 12 was performed using a mismatched primer (forward primer: 5′-TGAATATAAACTTGTGGTAGTTGGACCT-3′; reverse primer: 5′-CTGTATCAAAGAATGGTCC TGCACC-3′) that introduced an *Mva*I restriction site into the PCR products derived from normal alleles. *Mva*I digestion of the PCR products left only the PCR products derived from mutant alleles intact, after which further PCR selectively amplified the mutant PCR products. The first PCR reaction was performed with mixtures containing 0.5 μL of DNA recovery solution, 10 ng of each nucleotide, and the mismatched primer to introduce an *Mva* I restriction site flanking the K-*ras* exon 1, with 15 cycles at an annealing temperature of 55°C. The first PCR products were digested with *Mva*I and diluted 1:100. One microliter of the diluted product was amplified by 20 cycles of PCR with the same primers at an annealing temperature of 40°C, and the products were digested with *Mva*I a second time. The second PCR products were diluted 1:100, amplified by 35 cycles with the previous forward primer and a new reverse primer (5′-CTCTATTGTTGGATCATATTCGTCCAC-3′) at an annealing temperature of 65°C, and digested with *Mva*I a third time. The final digested products were then electrophoresed on 2.5% agarose gels and stained with ethidium bromide. A digestion-resistant 106-bp band indicated the presence of a K-*ras* codon 12 mutation. Extensive measures were taken to prevent cross-contamination of samples. A normal control sample and a known mutation sample were included in all of the experiments.

Statistical Analyses

Overall survival, disease-specific survival, and disease-free survival were analyzed in this study. Survival curves were estimated by the Kaplan-Meier method. The log-rank test was used to compare survival time between groups. Fisher's exact test was used to analyze the association between categoric variables. Using a stepwise selection method, a Cox proportional hazards model was created to identify independent predictors of survival, with adjustment for relevant clinical covariates (tumor stage, histology,

smoking status, and sex). All statistical tests were two-sided, and $P < .05$ was considered statistically significant.

All survival curves were calculated from the date of surgery. Overall survival took all deaths (cancer related or not) into account. Disease-specific survival time was calculated from the date of surgery to death from cancer-related causes. Disease-free survival time was calculated from the date of surgery to relapse or death from cancer-related causes.

Data for a panel of six molecular markers (RAR-β, COX-2, hTERT, *DAPK* promoter methylation, IL-10, and K-*ras*) were available for 94 patients in our retrospective cohort. These patients were the study population for our analysis. Patient characteristics are listed in Table 1. Median follow-up time for alive patients and those lost to follow-up was 10.9 years. Sixty-nine patients have died. Twenty-nine deaths were cancer related.

The frequency of each molecular marker, displayed as a negative prognostic factor, is listed in Table 2. Univariate analyses of each molecular marker and its association with disease-specific survival and overall survival were performed (Table 3). Similar univariate survival analyses of clinical variables (age, sex, and smoking status) were performed. A highly significant association was demonstrated between age (< 60 years *v* ≥ 60 years) and overall survival ($P = .003$). Sex and smoking status were not associated with overall or disease-specific survival. Age ≥ 60 years was associated with a significant increased risk of noncancer-related death ($P < .001$) and was not associated with disease-specific survival ($P = .577$). This phenomenon is likely explained by the relatively long follow-up of these subjects and by the fact that that the majority of deaths (40 of 69 deaths) were unrelated to cancer. In light of these findings, we reasoned that disease-specific survival would serve as a more clinically relevant end point for this cohort, although we continued to include overall survival in our analyses. Disease-specific survival stratified by each molecular marker is shown in Figure 1.

Table 1. Patient Characteristics

Characteristic	No. of Patients	%
Age, years		
Median	63.5	
Range	41-82	
Sex		
Male	72	77
Female	22	23
Race		
White	83	88
Other	11	12
Smoker		
Yes	82	87
No	5	5
Unknown	7	7
Histology		
Adenocarcinoma	39	41
Squamous cell carcinoma	39	41
Other	16	17
TNM stage		
T1N0M0	44	47
T2N0M0	50	53

Abbreviation: TNM, tumor-node-metastasis.

Table 2. Frequency of Molecular Markers in Stage I NSCLC

Molecular Marker	Frequency (%)
COX-2 expression	60
DAPK methylation	47
K-*ras* mutation	34
hTERT expression	34
IL-10 lack of expression	30
RAR-β expression	23

Abbreviations: NSCLC, non–small-cell lung cancer; COX-2, cyclooxygenase; *DAPK*, death-associated protein kinase; hTERT, human telomerase reverse transcriptase catalytic subunit; IL-10, interleukin-10; RAR-β, retinoic acid receptor-beta.

A multivariate Cox proportional hazards model was created to identify predictors of disease-specific survival (Table 4). *DAPK* promoter methylation and IL-10 lack of expression were significant negative prognostic factors for disease-specific survival, whereas COX-2 expression was of borderline significance. The same variables were selected when tumor stage, histology, smoking status, and sex were included in the model. The poorer disease-specific and overall survival of patients with both *DAPK* methylation and IL-10 lack of expression are illustrated in Figure 2. We defined these patients as a high-risk group, and the remaining patients were defined as a low-risk group. A log-rank test assessing the difference in survival between these groups was statistically significant for both disease-specific survival ($P < .0001$) and overall survival ($P < .0001$). We note that the definitions of the high- and low-risk groups are data dependent. That is, the definition of high risk was not determined a priori. A similar model for overall survival yielded three significant negative prognostic factors (age ≥ 60 years, $P = .0017$; COX-2 expression, $P = .021$; and *DAPK* methylation, $P = .044$), whereas IL-10 lack of expression was of borderline significance ($P = .069$).

Exploratory analyses of the relationships between the various molecular markers were performed. Significant associations were found between hTERT and COX-2 expression (odds ratio [OR], 6.14; 95% CI, 2.09 to 18.04; $P = .0004$) and K-*ras* mutations and *DAPK* methylation (OR, 2.64; 95% CI, 1.10 to 6.36; $P = .032$). Associations between IL-10 lack of expression and hTERT expression (OR, 2.63; 95% CI, 1.06 to 6.67; $P = .056$), IL-10 lack of

Table 3. Univariate Analysis of Molecular Markers With Disease-Specific and Overall Survival

Molecular Marker	Disease-Specific Survival			Overall Survival		
	Hazard Ratio	95% CI	*P*	Hazard Ratio	95% CI	*P*
IL-10 lack of expression	3.17	1.53 to 6.62	.002	1.98	1.21 to 3.25	.007
DAPK methylation	3.00	1.39 to 6.47	.005	1.69	1.05 to 2.72	.030
hTERT expression	2.39	1.15 to 4.97	.020	1.48	0.91 to 2.42	.116
COX-2 expression	2.44	1.08 to 5.54	.032	1.80	1.09 to 2.96	.022
RAR-β expression	1.47	0.66 to 3.25	.345	1.23	0.72 to 2.09	.446
K-*ras* mutation	1.00	0.45 to 2.20	.998	1.18	0.71 to 1.95	.517

Abbreviations: IL-10, interleukin-10; *DAPK*, death-associated protein kinase; hTERT, human telomerase reverse transcriptase catalytic subunit; COX-2, cyclooxygenase-2; RAR-β, retinoic acid receptor-beta.

expression and COX-2 expression (OR, 2.63; 95% CI, 0.99 to 7.14; $P = .066$), and COX-2 expression and RAR-β expression (OR, 2.88; 95% CI, 0.96 to 8.64; $P = .08$) were of borderline significance.

We also investigated other models by performing all two-variable, three-variable, and four-variable multivariate models. On the basis of these analyses, only *DAPK* methylation and IL-10 lack of expression were statistically significant ($P < .05$) for all models. Furthermore, the three-variable model, including *DAPK* methylation, IL-10 lack of expression, and COX-2 expression, had the lowest Akaike Information Criterion (AIC) value of 224.029 (although the two-variable model that excluded COX-2 expression had an AIC of similar value). We noted that there was some evidence of association between IL-10 lack of expression and hTERT expression (OR, 2.63; $P = .056$) and IL-10 lack of expression and COX-2 expression (OR, 2.63; $P = .066$). Moreover, hTERT and COX-2 expression were highly

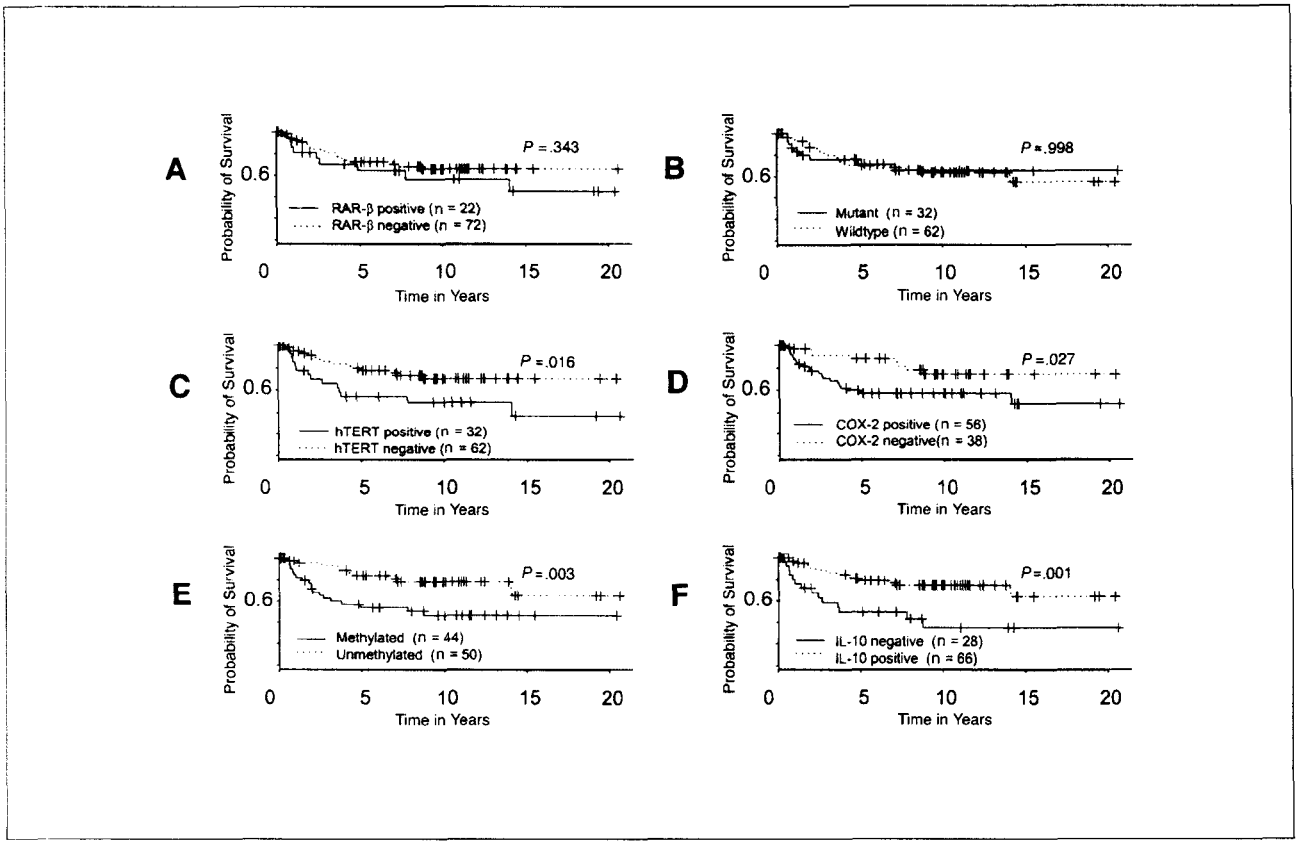

Fig 1. Disease-specific survival stratified by (A) retinoic acid receptor-beta (RAR-β) mRNA expression, (B) K-*ras* mutation status, (C) human telomerase reverse transcriptase catalytic subunit (hTERT) mRNA expression, (D) cyclooxygenase-2 (COX-2) mRNA expression, (E) death-associated protein kinase (*DAPK*) methylation, and (F) interleukin-10 (IL-10) protein expression.

Table 4. Multivariate Cox Regression Model for Disease-Specific Survival

Molecular Marker	Hazard Ratio	95% CI	*P*
DAPK methylation	3.11	1.42 to 6.79	.004
IL-10 lack of expression	2.62	1.24 to 5.56	.012
COX-2 expression	2.13	0.92 to 4.95	.077

Abbreviations: *DAPK*, death-associated protein kinase; IL-10, interleukin-10; COX-2, cyclooxygenase-2.

associated (OR, 6.14; $P = .0004$). We ensured that the effect of these variables was not masked by colinearity by modeling them separately. Specifically, we modeled COX-2 expression with *DAPK* methylation (AIC = 228.135) and hTERT expression with *DAPK* methylation (AIC = 228.654). Neither of these models provided better fit than the model chosen.

Our findings further characterize and extend our group's previous research efforts to identify novel molecular prognostic factors in patients with early-stage NSCLC. We identified 94 patients with complete information for a panel of six molecular markers. Each biomarker had been previously studied as a prognostic factor based on its role in carcinogenesis. When analyzed individually, five of these biomarkers (RAR-β, COX-2, hTERT, *DAPK* promoter methylation, and IL-10) were demonstrated in prior studies[7-9,11,12] by our group to be significant predictors of survival. One available marker (K-*ras*) was included in the current analysis based on published data demonstrating that it had prognostic significance in early-stage NSCLC,[14,42] even though it did not have prognostic significance in univariate analysis in our patients. Our multivariable analysis indicates that two biomarkers (*DAPK* promoter methylation and IL-10) function as independent predictors of disease-specific survival, and a third biomarker (COX-2) is of borderline significance in this cohort. These findings should be confirmed in other NSCLC patient populations.

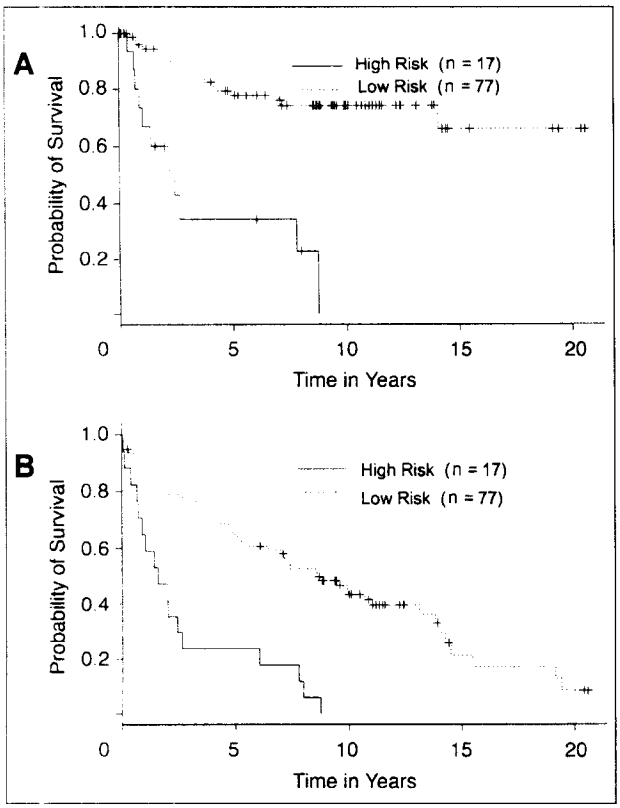

Fig 2. Disease-specific survival (A) and overall survival (B) of patients with both death-associated protein kinase methylation and interleukin-10 lack of expression (high risk) versus other patients (low risk).

Our results further support the importance of epigenetic gene regulation in lung carcinogenesis. Others have demonstrated that aberrant promoter methylation of *DAPK* and other genes frequently occurs in NSCLC tumors,[25,26] suggesting that methylation may be a common mechanism of inactivation of cancer-related genes. *DAPK* promoter methylation was the most statistically significant predictor of survival in our study. Kim et al[43] investigated the role of *DAPK* methylation in 185 NSCLC patients who underwent surgical resection, including 102 patients with stage I disease. *DAPK* methylation was significantly correlated with advanced stage, suggesting that *DAPK* may be important in the progression of NSCLC. Stage I patients with *DAPK* methylation had worse overall survival, although this association was not statistically significant. The authors noted that patient follow-up data was limited, and this factor may have contributed to their findings. Harden et al[44] examined promoter methylation of a panel of five genes in tumors and lymph nodes of 90 stage I NSCLC patients. Interestingly, patients with both *DAPK* and *adenomatous polyposis coli* gene methylation had poorer overall survival that did not reach statistical significance, although the methylation of either gene alone was not a predictor of survival. Possible explanations for these results include the relatively low frequency of *DAPK* methylation (17%) compared with our findings (47%). The smaller number of patients with *DAPK* methylation (n = 15) would result in the study having less power to detect significant associations with survival.

The role of IL-10 in carcinogenesis remains controversial. Our findings indicate that loss of IL-10 expression predicts poor disease-specific survival in early-stage NSCLC. Human bronchial epithelial cells constitutively produce IL-10, which may regulate the local immune response in normal lungs.[34] IL-10 also seems to have

significant inhibitory effects on tumor growth and metastasis in multiple animal models and tumor types, including melanoma, breast cancer, prostate cancer, and Burkitt's lymphoma.[31,32,45-47] Evidence suggests that IL-10 exerts its antitumor and antimetastatic activity by inhibiting angiogenesis, and this activity is, in part, mediated by the downregulation of angiogenic molecules, such as vascular endothelial growth factor, IL-1β, tumor necrosis factor-α, IL-6, and matrix metalloproteinase-9 (MMP-9), in tumor-associated macrophages.[31] In addition, IL-10 may also directly affect the secretion of angiogenic molecules from the tumor. Stearns et al[46] demonstrated that IL-10 induces tissue inhibitor of metalloproteinase-1 production and inhibits MMP-2 and MMP-9 secretion by human prostate cancer cell lines orthotopically implanted into mice, resulting in decreased tumor microvessel formation and increased mice survival. In a murine mammary tumor model, the antitumor and antimetastatic effects of IL-10 gene transfection were associated with elevated nitric oxide levels in tumors.[48] Others have shown that IL-10 can directly inhibit the proliferation of endothelial cells stimulated with vascular endothelial growth factor or fibroblast growth factor-2 in vitro.[47] An intriguing molecular epidemiologic case-control study demonstrated that IL-10 promoter polymorphisms that resulted in lower IL-10 expression were associated with an increased risk of developing melanoma.[49] Furthermore, some authors have suggested that lung cancer cells can modulate IL-10 expression by stromal components. In the present study, only nine of 94 samples displayed tumor-infiltrating lymphocytes or tumor-associated macrophages, therefore hindering any relevant analysis of IL-10 production by infiltrating immune cells.

The data supporting the antitumor and antimetastatic activity of IL-10 are compelling, but most preclinical models using IL-10 to mediate such effects do so at concentrations that far exceed the levels demonstrated in lung cancer patients. Other authors have demonstrated that IL-10 is a potent immunosuppressive molecule that may promote lung cancer growth by suppressing T-cell and macrophage function and enabling tumors to escape immune detection.[50-52] Elevated baseline serum IL-10 levels were found to be independent predictors of poorer survival in 60 advanced-stage NSCLC patients receiving platinum-based chemotherapy.[53] Hatanaka et al[54] measured IL-10 mRNA levels by reverse transcriptase PCR in the tumors of 82 NSCLC patients who underwent surgical resection. Their assay demonstrated IL-10 expression in 83% of the surgical specimens. In contrast to our results, IL-10 expression was significantly associated with worse survival. The reasons for these discrepant findings remain unclear. These investigators included patients with stages I to IIIb disease in their study and used a different IL-10 assay (mRNA *v* protein) than the assay we used in our study. These factors may have contributed to these divergent results.

Our exploratory analyses demonstrate a highly significant association between hTERT expression and COX-2 expression ($P = .0004$). A precise explanation for this correlation is lacking, although various COX-2 inhibitors have been reported to inhibit both tumor growth and telomerase activity in mice.[55,56] We also observed a significant association between K-*ras* mutations and *DAPK* methylation ($P = .032$). Reports suggesting that DNA methylation may be regulated by the ras signaling pathway[57,58] are consistent with these findings. However, others have not found correlations between ras mutations and promoter hypermethylation in NSCLC tumors.[43,59] Clearly, a better understanding of the significance of these associations will require future studies. Our analyses also demonstrate a borderline significant association between IL-10 lack of expression and COX-2 expression ($P = .066$).[60,61] This finding is consistent with data suggesting that IL-10 has the capacity to potently downregulate COX-2. Therefore, in the absence of IL-10, COX-2 and its derived products would be more abundant and could further promote tumor progression.

This study is limited by its retrospective nature and the inclusion only of patients with complete information for all six biomarkers. It is difficult to speculate on potential biases affecting our results. It is possible, for example, that small tumors with limited tissue availability were underrepresented in this cohort. These results should be validated in a separate population of NSCLC patients.

In conclusion, our analysis of six molecular markers in patients with resected stage I NSCLC yielded two independent predictors of poorer disease-specific survival: *DAPK* methylation and IL-10 lack of expression. Future studies are warranted to further define their roles in tumor proliferation and metastasis. However, these and other potential molecular prognostic factors have yet to be validated, and thus, the integration of molecular marker assessments into the routine clinical management of NSCLC has remained an elusive goal. As the number of potential molecular markers increases, it has become more difficult to assess which prognostic factors are likely to be clinically relevant. A comprehensive multivariable analysis is not feasible because the majority of studies analyze only a single or a few biomarkers at a time. In this regard, the development of high-throughput technologies to determine gene-expression profiles and proteomic patterns of tissue specimens represents a significant methodologic advance. Several recent reports have demonstrated that mRNA and protein patterns of NSCLC tumors may be predictive of survival.[62,63] Hopefully, these technologies will eventually provide the clinician with a reliable, validated molecular staging system that will improve therapeutic strategies for NSCLC.

Authors' Disclosures of Potential Conflicts of Interest

The authors indicated no potential conflicts of interest.

1. Jemal A, Murray T, Samuels A, et al: Cancer statistics, 2003. CA Cancer J Clin 53:5-26, 2003

2. Travis W, Travis LB, Devesa SS: Lung cancer incidence and survival by histologic type. Cancer 75:191-202, 1995 (suppl 1)

3. Fry W, Phillips JL, Menck HR: Ten-year survey of lung cancer treatment and survival in hospitals in the United States. Cancer 86:1867-1876, 1999

4. Mountain CF: Revisions in the International System for Staging Lung Cancer. Chest 111:1710-1717, 1997

5. Tseng JE, Kemp BL, Khuri FR, et al: Loss of Fhit is frequent in stage I non-small cell lung cancer and in the lungs of chronic smokers. Cancer Res 59:4798-4803, 1999

6. Herbst RS, Yano S, Kuniyasu H, et al: Differential expression of E-cadherin and type IV collagenase genes predicts outcome in patients with stage I non-small cell lung carcinoma. Clin Cancer Res 6:790-797, 2000

7. Tang X, Khuri FR, Lee JJ, et al: Hypermethylation of the death-associated protein (DAP) kinase promoter and aggressiveness in stage I non-small-cell lung cancer. J Natl Cancer Inst 92:1511-1516, 2000

8. Khuri FR, Lotan R, Kemp BL, et al: Retinoic acid receptor-beta as a prognostic indicator in stage I non-small-cell lung cancer. J Clin Oncol 18:2798-2804, 2000

9. Khuri FR, Wu H, Lee JJ, et al: Cyclooxygenase-2 overexpression is a marker of poor prognosis in stage I non-small cell lung cancer. Clin Cancer Res 7:861-867, 2001

10. Zhou X, Kemp BL, Khuri FR, et al: Prognostic implication of microsatellite alteration profiles in early-stage non-small cell lung cancer. Clin Cancer Res 6:559-565, 2000

11. Wang L, Soria JC, Kemp BL, et al: HTERT expression is a prognostic factor of survival in patients with stage I non-small cell lung cancer. Clin Cancer Res 8:2883-2889, 2002

12. Soria JC, Moon C, Kemp BL, et al: Lack of interleukin-10 expression could predict poor outcome in patients with stage I non-small cell lung cancer. Clin Cancer Res 9:1785-1791, 2003

13. Pastorino U, Andreola S, Tagliabue E, et al: Immunocytochemical markers in stage I lung cancer: Relevance to prognosis. J Clin Oncol 15:2858-2865, 1997

14. Kwiatkowski DJ, Harpole DH Jr, Godleski J, et al: Molecular pathologic substaging in 244 stage I non-small-cell lung cancer patients: Clinical implications. J Clin Oncol 16:2468-2477, 1998

15. D'Amico TA, Massey M, Herndon JE II, et al: A biologic risk model for stage I lung cancer: Immunohistochemical analysis of 408 patients with the use of ten molecular markers. J Thorac Cardiovasc Surg 117:736-743, 1999

16. Ahrendt SA, Hu Y, Buta M, et al: p53 mutations and survival in stage I non-small-cell lung cancer: Results of a prospective study. J Natl Cancer Inst 95:961-970, 2003

17. Berard J, Gaboury L, Landers M, et al: Hyperplasia and tumours in lung, breast and other tissues in mice carrying a RAR beta 4-like transgene. EMBO J 13:5570-5580, 1994

18. Taketo MM: Cyclooxygenase-2 inhibitors in tumorigenesis (Part II). J Natl Cancer Inst 90:1609-1620, 1998

19. Hida T, Yatabe Y, Achiwa H, et al: Increased expression of cyclooxygenase 2 occurs frequently in human lung cancers, specifically in adenocarcinomas. Cancer Res 58:3761-3764, 1998

20. Wolff H, Saukkonen K, Anttila S, et al: Expression of cyclooxygenase-2 in human lung carcinoma. Cancer Res 58:4997-5001, 1998

21. Li M, Song S, Lippman SM, et al: Induction of retinoic acid receptor-beta suppresses cyclooxygenase-2 expression in esophageal cancer cells. Oncogene 21:411-418, 2002

22. Hahn WC: Role of telomeres and telomerase in the pathogenesis of human cancer. J Clin Oncol 21:2034-2043, 2003

23. Hiyama K, Hiyama E, Ishioka S, et al: Telomerase activity in small-cell and non-small-cell lung cancers. J Natl Cancer Inst 87:895-902, 1995

24. Kim NW, Piatyszek MA, Prowse KR, et al: Specific association of human telomerase activity with immortal cells and cancer. Science 266: 2011-2015, 1994

25. Zochbauer-Muller S, Fong KM, Maitra A, et al: 5' CpG island methylation of the FHIT gene is correlated with loss of gene expression in lung and breast cancer. Cancer Res 61:3581-3585, 2001

26. Esteller M, Corn PG, Baylin SB, et al: A gene hypermethylation profile of human cancer. Cancer Res 61:3225-3229, 2001

27. Deiss LP, Feinstein E, Berissi H, et al: Identification of a novel serine/threonine kinase and a novel 15-kD protein as potential mediators of the gamma interferon-induced cell death. Genes Dev 9:15-30, 1995

28. Inbal B, Cohen O, Polak-Charcon S, et al: DAP kinase links the control of apoptosis to metastasis. Nature 390:180-184, 1997

29. Beissert S, Hosoi J, Grabbe S, et al: IL-10 inhibits tumor antigen presentation by epidermal antigen-presenting cells. J Immunol 154:1280-1286, 1995

30. Rohrer JW, Coggin JH Jr: CD8 T cell clones inhibit antitumor T cell function by secreting IL-10. J Immunol 155:5719-5727, 1995

31. Huang S, Ullrich SE, Bar-Eli M: Regulation of tumor growth and metastasis by interleukin-10: the melanoma experience. J Interferon Cytokine Res 19:697-703, 1999

32. Kundu N, Beaty TL, Jackson MJ, et al: Antimetastatic and antitumor activities of interleukin 10 in a murine model of breast cancer. J Natl Cancer Inst 88:536-541, 1996

33. Esteller M, Sanchez-Cespedes M, Rosell R, et al: Detection of aberrant promoter hypermethylation of tumor suppressor genes in serum DNA from non-small cell lung cancer patients. Cancer Res 59:67-70, 1999

34. Bonfield TL, Konstan MW, Burfeind P, et al: Normal bronchial epithelial cells constitutively produce the anti-inflammatory cytokine interleukin-10, which is downregulated in cystic fibrosis. Am J Respir Cell Mol Biol 13:257-261, 1995

35. Fujieda S, Lee K, Sunaga H, et al: Staining of interleukin-10 predicts clinical outcome in patients with nasopharyngeal carcinoma. Cancer 85:1439-1445, 1999

36. Kolquist KA, Ellisen LW, Counter CM, et al: Expression of TERT in early premalignant lesions and a subset of cells in normal tissues. Nat Genet 19:182-186, 1998

37. Soria JC, Moon C, Wang L, et al: Effects of N-(4-hydroxyphenyl)retinamide on hTERT expression in the bronchial epithelium of cigarette smokers. J Natl Cancer Inst 93:1257-1263, 2001

38. Falchetti ML, Pallini R, D'Ambrosio E, et al: In situ detection of telomerase catalytic subunit mRNA in glioblastoma multiforme. Int J Cancer 88:895-901, 2000

39. Xu XC, Ro JY, Lee JS, et al: Differential expression of nuclear retinoid receptors in normal, premalignant, and malignant head and neck tissues. Cancer Res 54:3580-3587, 1994

40. Xu XC, Sozzi G, Lee JS, et al: Suppression of retinoic acid receptor beta in non-small-cell lung cancer in vivo: Implications for lung cancer development. J Natl Cancer Inst 89:624-629, 1997

41. Jacobson DR, Mills NE: A highly sensitive assay for mutant ras genes and its application to the study of presentation and relapse genotypes in acute leukemia. Oncogene 9:553-563, 1994

42. Slebos RJ, Kibbelaar RE, Dalesio O, et al: K-ras oncogene activation as a prognostic marker in adenocarcinoma of the lung. N Engl J Med 323:561-565, 1990

43. Kim DH, Nelson HH, Wiencke JK, et al: Promoter methylation of DAP-kinase: Association with advanced stage in non-small cell lung cancer. Oncogene 20:1765-1770, 2001

44. Harden SV, Tokumaru Y, Westra WH, et al: Gene promoter hypermethylation in tumors and lymph nodes of stage I lung cancer patients. Clin Cancer Res 9:1370-1375, 2003

45. Gerard CM, Bruyns C, Delvaux A, et al: Loss of tumorigenicity and increased immunogenicity induced by interleukin-10 gene transfer in B16 melanoma cells. Hum Gene Ther 7:23-31, 1996

46. Stearns ME, Garcia FU, Fudge K, et al: Role of interleukin 10 and transforming growth factor beta1 in the angiogenesis and metastasis of human prostate primary tumor lines from orthotopic implants in severe combined immunodeficiency mice. Clin Cancer Res 5:711-720, 1999

47. Cervenak L, Morbidelli L, Donati D, et al: Abolished angiogenicity and tumorigenicity of Burkitt lymphoma by interleukin-10. Blood 96: 2568-2573, 2000

48. Kundu N, Dorsey R, Jackson MJ, et al: Interleukin-10 gene transfer inhibits murine mammary tumors and elevates nitric oxide. Int J Cancer 76:713-719, 1998

49. Howell WM, Turner SJ, Bateman AC, et al: IL-10 promoter polymorphisms influence tumour development in cutaneous malignant melanoma. Genes Immun 2:25-31, 2001

50. Sharma S, Stolina M, Lin Y, et al: T cell-derived IL-10 promotes lung cancer growth by suppressing both T cell and APC function. J Immunol 163:5020-5028, 1999

51. Spagnoli GC, Juretic A, Schultz-Thater E, et al: On the relative roles of interleukin-2 and interleukin-10 in the generation of lymphokine-

activated killer cell activity. Cell Immunol 146: 391-405, 1993

52. Huang M, Sharma S, Mao JT, et al: Non-small cell lung cancer-derived soluble mediators and prostaglandin E2 enhance peripheral blood lymphocyte IL-10 transcription and protein production. J Immunol 157:5512-5520, 1996

53. De Vita F, Orditura M, Galizia G, et al: Serum interleukin-10 levels as a prognostic factor in advanced non-small cell lung cancer patients. Chest 117:365-373, 2000

54. Hatanaka H, Abe Y, Kamiya T, et al: Clinical implications of interleukin (IL)-10 induced by non-small-cell lung cancer. Ann Oncol 11:815-819, 2000

55. Nishimura G, Yanoma S, Mizuno H, et al: A selective cyclooxygenase-2 inhibitor suppresses tumor growth in nude mouse xenografted with human head and neck squamous carcinoma cells. Jpn J Cancer Res 90:1152-1162, 1999

56. Lonnroth C, Andersson M, Lundholm K: Indomethacin and telomerase activity in tumor growth retardation. Int J Oncol 18:929-937, 2001

57. Rouleau J, MacLeod AR, Szyf M: Regulation of the DNA methyltransferase by the Ras-AP-1 signaling pathway. J Biol Chem 270: 1595-1601, 1995

58. Bigey P, Ramchandani S, Theberge J, et al: Transcriptional regulation of the human DNA methyltransferase (dnmt1) gene. Gene 242:407-418, 2000

59. Pulling LC, Divine KK, Klinge DM, et al: Promoter hypermethylation of the O6-methylguanine-DNA methyltransferase gene: More common in lung adenocarcinomas from never-smokers than smokers and associated with tumor progression. Cancer Res 63:4842-4848, 2003

60. Moore KW, de Waal Malefyt R, Coffman RL, et al: Interleukin-10 and the interleukin-10 receptor. Annu Rev Immunol 19:683-765, 2001

61. Molina-Holgado E, Arevalo-Martin A, Ortiz S, et al: Theiler's virus infection induces the expression of cyclooxygenase-2 in murine astrocytes: Inhibition by the anti-inflammatory cytokines interleukin-4 and interleukin-10. Neurosci Lett 324:237-241, 2002

62. Beer DG, Kardia SL, Huang CC, et al: Gene-expression profiles predict survival of patients with lung adenocarcinoma. Nat Med 8:816-824, 2002

63. Yanagisawa K, Shyr Y, Xu BJ, et al: Proteomic patterns of tumour subsets in non-small-cell lung cancer. Lancet 362:433-439, 2003

American Association for Cancer Research

4051 Building a comprehensive quantitative risk assessment model for lung cancer

Carol J. ■Etzel■, Qing Zhang, Matthew Schabath, Qiong Dong, Xifeng Wu, Qingyi Wei, Margaret Spitz, Christopher I. Amos. *UT M. D. Anderson Cancer Ctr., Houston, TX.*

Introduction: Lung cancer (LC) is still the leading cause of cancer death and the ability to distinguish individuals (smokers and non-smokers) at high risk for LC has significant preventive implications. High-risk smoking subgroups could be targeted for intensive cessation interventions and recruited into chemoprevention and specialized screening trials. The goal of this project was to develop a comprehensive LC risk assessment model that included epidemiologic and nutritional data from 24 hour food frequency questionnaires to identify such high-risk groups. Methods: We constructed our models from data derived from 2768 Caucasian LC cases (recruited through UT MD Anderson Cancer Center) and controls (recruited from a multispecialty physician practice and matched on age, sex and smoking status). Models were constructed for never, former and current smokers using multiple logistic regression. We also completed model diagnostics including identification of multi-collinearities and model goodness-of-fit. Many of the nutritional variants were highly correlated and resulted in model multi-collinearities. When such a situation occurred, we constructed separate models for the correlated variants and compared their ROC values.Results and Conclusions: For never smokers, the epidemiologic model included second-hand smoke (ETS) which was associated with a two-fold risk for LC (ROC=.581). We also obtained three nutritional models with similar yet slightly higher ROC scores as compared to the epidemiologic model: ETS and daily servings of vegetables (ROC=.635), ETS and proVitamin A carotenoids (ROC=.662) and ETS and beta-Carotene (ROC=.661). For former smokers, a physician's diagnosis of emphysema, asbestos exposure, family history of LC and years since smoking cessation were all independently associated with increased risk of LC while hay fever was protective (ROC=.671). With the inclusion of nutritional variants, we obtained two subsequent models, one including number of different sources of weekly fat intake and daily servings of vegetables (ROC=.688) and the other including amount of saturated fat and total carotenoid intake (ROC=.689). For current smokers, the epidemiologic model included risk factors of emphysema, family history of LC, years smoked and number of cigarettes smoked per day while hay fever was protective (ROC=.711). The nutritional model for current smokers also included number of different sources of weekly fat intake and daily servings of vegetables (ROC=.714). These results show that LC is a complex disease with varying etiology based on smoking history; hence, the development of risk models must account for smoking history. The amount of increase in model prediction afforded by the inclusion of nutritional variants did not justify the time and expense of collecting such data. This project was supported by NCI grants CA55769 and CA093592 (K07) and DAMD17-02-1-07-06.

Citation format: Proc Amer Assoc Cancer Res 2005;46:4051.

5021 Inactivation of c-Abl and c-Kit activities and inhibition of SCLC cell growth by a combination treatment with FUS1-nanoparticle and Gleevec in vitro and in vivo

Guanglin Wu, Futoshi Uno, Ralph Arlinghuas, Vikas Kundra, John D. Minna, Jack A. Roth, Lin Ji. *U.T.M.D.Anderson Cancer Center, Houston, TX and U.T. Southwestern Medical Center, Dallas, TX.*

FUS1 is a novel tumor suppressor gene identified in a critical human chromosome 3p21.3 region that has either LOH in more than 95% of SCLC cells or is homozygously deleted in some SCLCs. Expression of FUS1 protein is lost in all SCLC cells tested and reactivation of wt-FUS1 in FUS1-deficient lung cancer cells inhibits their growth by induction of apoptosis. On the other hand, protein tyrosine kinases (PTKs) such as BCR-Abl, c-Kit and PDGFR are frequently altered and amplified in SCLC and are important therapeutic targets. The small molecular drug gleevec has been shown to inhibit SCLC cell growth by targeting c-Kit/SCF pathway *in vitro* but exhibits no significant therapeutic efficacy either in animal models or in human clinic trials. We hypothesized that a combination treatment strategy with DOTAP:Chol-complexed *FUS1*-nanoparticle and gleevec might promote a synergistic inhibition on SCLC growth by simultaneously inactivating the oncogenic PTK signaling and activating the pro-apoptotic pathways. A significant growth inhibition and apoptosis were observed in SCLC H69, H128, H146, and N417 cells treated by either the *FUS1*-nanoparticle or the wt-FUS1-derived peptide (wt-FP) for 72 h but not by dysfunctional mutants of FUS1 protein or peptide, compared to these treated by the *GFP*-nanoparticle or peptide controls. An enhanced growth inhibition was detected in gleevec-resistant H69R and N417 cells treated by a combination of *FUS1*-nanoparticle or wt-FP with gleevec compared to those treated by either agent alone. Activities of the phosphorylated c-Abl and c-Kit proteins were also significantly inhibited in H69 and N417 cells treated by *FUS1*-nanoparticle or wt-FP alone or in combination with gleevec, as shown by both the immuno-blot analysis and the activity assay using the immuno-precipiated phosho-c-Abl or phospho-c-Kit proteins. We developed an intrathoracic SCLC N417 tumor xenograft model in nude mouse and evaluated the therapeutic efficacy of systemic treatment with *FUS1*-nanoparticles and oral administration with Gleevec by a non-invasive and quantitative MR imaging analysis. We found that the growth of N417 tumor xenograft was significantly inhibited ($P<0.001$) in mice treated by *FUS1*-nanoparticles alone or in combination with gleevec in less than 2 weeks of treatment but no significant efficacy was detected in mice treated by gleevec alone, as demonstrated by MR imaging and volume analysis. Our results clearly demonstrate the therapeutic efficacy of *FUS1*-nanoparticle on SCLC in vitro and *in vivo* and implicate the translational applications of using the systemic administration of *FUS1*-nanoparticle alone or in combination with other chemotherapeutic agents and the MRI for SCLC therapy. This abstract is supported by grants of NIH NCI (SPORE P50CA70907) and DOD (TARGET, DAMD17002-1-0706).

Citation format: Proc Amer Assoc Cancer Res 2005;46:5021.

American Association for Cancer Research

3358 A novel synthetic hTERT-Mini-CMV chimera promoter-driven tumor-selective and high-efficiency expression of transgene for systemic cancer gene therapy

Guanglin Wu, Wuguo Deng, Vikas Kundra, Bingliang Fang, Jack A. Roth, Lin Ji. *UT M.D. Anderson Cancer Center, Houston, TX.*

One of the major obstacles to a successful cancer gene therapy is the lack of an effective systemic delivery system that can be specifically targeted to primary and metastatic tumors. The hTERT promoter has been cloned and showed to be capable of targeting transgene expression in tumors but not in the normal cells. However, the weak transcription-promoting strength of hTERT promoter, like most other intrinsic mammalian promoters, has hampered its direct use for cancer gene therapy. To circumvent these problems, we have developed a novel chimera hTERT-mini-CMV (hTMC) promoter that was engineered by optimally fusing essential hTERT regulatory sequence with minimal CMV promoter elements. We transfected various human cancers and normal cells with various *EGFP*-constructs, in which EGFP expression is driven by either the original CMV and hTERT promoters or by the hTMC promoter in vitro. Expression of *EGFP* in the transfectants was visualized by a fluorescence imaging (FI) under a fluorescence microscope and the population of EGFP-positive cells and fluorescence intensity were quantified by FACS analysis. A high level of EGFP expression driven by the hTMC promoter was detected in all tumor cells but not in normal cells. While a similar tumor-selectivity of EGFP expression driven by hTERT promoter could be seen but the level of expression was several hundred-fold lower than that driven by hTMC promoter under the same transfection efficiency. We also evaluated the effectiveness of hTMC promoter in vivo by systemic injection of DOTAP:cholesterol-complexed hTMC-*EGFP*-nanoparticles into nude mice that bear intrathoracic human N417 lung tumor xenografts. Consistently, a high level of EGFP expression could be detected only in the tumor cells in animals treated with hTMC-*EGFP* but not in any other normal tissues. Furthermore, we used the above N417 tumor mouse model to evaluate the therapeutic efficacy of systemic treatment with a novel hTMC-*FUS1*-nanoparticle by a non-invasive and quantitative MR imaging analysis. A significant inhibition ($P<0.001$) of tumor growth was detected in animals treated by hTMC-*FUS1*-nanoparticles in less than 2 weeks of treatment compared to those untreated or treated by hTMC-*EGFP*-nanoparticles, as demonstrated by MR imaging and volume analysis. Induction of apoptosis was also detected in tumor cells but not in surrounding normal lung or other normal tissues in mice treated by hTMC-*FUS1*-nanoparticles, as shown by an in situ cell apoptosis analysis with TUNEL staining in frozen tissue samples. Our results clearly demonstrate the capability of using the hTMC promoter to achieve both the high tumor-specificity and high-efficiency therapeutic gene expression *in vitro* and *in vivo* and indicate the translational applications of using the systemic administration of therapeutic hTMC-nanoparticle for tumor-targeted molecular cancer therapy.

Citation format: Proc Amer Assoc Cancer Res 2005;46:3358.

Meeting: 2005 ASCO Annual Meeting
Category: Lung Cancer
SubCategory: Non-Small Cell Lung Cancer

Bookmark

Synergistic inhibition of EGFR tyrosine kinase and tumor cell growth in non-small cell lung cancer (NSCLC) by combination treatment with FUS1-nanoparticles and Gefitinib

Abstract No: 7081

Author(s): L. Ji, H. Kawashima, C. Lu, J. Kurie, S. Chada, J. D. Minna, J. A. Roth

Abstract: **Background:** FUS1 is a novel tumor suppressor gene (TSG) identified in the human chromosome 3p21.3 region that functions in the Apaf1-associated apoptotic pathway, and is a potent tumor suppressor. We explored the use of FUS1 for enhancing chemotherapeutic potency of Gefitnib and overcoming Gefitnib-resistance in both Gefitnib-sensitive and resistant NSCLC cells. **Methods and Results:** We found that expression of wt-FUS1 by FUS1-nanoparticle-mediated gene transfer in FUS1-deficient and Gefitinib-resistant NSCLC H1299, H358, and H460 cells significantly sensitized the response to Gefitinib treatment, as demonstrated by a more than additive inhibitory effect on tumor cell growth and a synergistic induction of apoptosis. Enhanced growth inhibition was also observed in the Gefitnib-sensitive HCC827 (EGFR mutant) and H1819 (EGFR amplification) cells co-treated with FUS1-nanoparticles and a low dose of Gefitnib (IC_{10}). A marked inhibition of phosphorylated EGFR protein was also detected in cells treated with FUS1-nanoparticles alone or in combination with Gefitnib, as shown by Western-blot analysis with phospho-EGFR-specific antibodies. A significant inhibition ($P<0.001$) of tumor growth was detected in animals treated by FUS1-nanoparticles in less than 2 weeks of treatment compared to those untreated or treated by GFP-nanoparticles, as shown by MR imaging and volume analysis. Induction of apoptosis was also detected in tumor cells in mice treated by FUS1-nanoparticles by an in situ apoptosis assay with TUNEL staining in frozen tissue samples. We have an ongoing phase I study of single agent FUS1-nanoparticles given intravenously in stage IV NSCLC patients who have progressed on chemotherapy. The treatment is well-tolerated in seven patients entered to date with a median survival of 17+ months. **Conclusions:** Our results suggest that wt-FUS1 may play a critical role in modulating the sensitivity of tumor cells to protein tyrosine kinase inhibitors. Supported by grants from NIH NCI (SPORE P50CA70907), DOD (TARGET, DAMD17002-1-0706) and Introgen Therapeutics, Inc.

Associated Presentation(s):

1. **Synergistic inhibition of EGFR tyrosine kinase and tumor cell growth in non-small cell lung cancer (NSCLC) by combination treatment with FUS1-nanoparticles and gefitinib**
   Event: 2005 ASCO Annual Meeting
   Presenter: Lin Ji, PhD
   Session: Lung Cancer
   (No presentation available)

Other Abstracts in this Sub-Category:

1. **Vaccination with EGF active immunotherapy improves survival in advanced non small cell lung cancer (NSCLC) patients: interim analysis of a randomized Phase II trial.**
   Meeting: 2005 ASCO Annual Meeting Abstract No: 7210 First Author: E. Neninger

2. **14-3-3 s (s) methylation (M) in pre-treatment serum DNA of cisplatin (cis)/gemcitabine (gem)-treated non-small-cell lung cancer (NSCLC)**
   Meeting: 2005 ASCO Annual Meeting Abstract No: 7042 First Author: J. L. Ramirez

American Association for Cancer Research

2707 Synergistic inhibition of EGFR tyrosine kinase activity and NSCLC cell growth by combination treatment with FUS1-nanoparticle and gefitinib

Hiroyuki Kawashima, Futoshi Uno, Jonathan Kurie, John D. Minna, Jack A. Roth, Lin Ji. *The UT M.D. Anderson Cancer Center, Houston, TX and The UT Southwestern Medical Center, Dallas, TX.*

New cancer treatments designed to restore functions of defect genes and gene products in tumor suppressing and apoptotic pathways by gene transfer and to target at the specific and frequently occurring molecular alterations in key signaling pathways by "smart drugs" such as protein tyrosine kinase inhibitors (PTKIs) are fundamentally changing cancer therapy and holding a promise for lung cancer treatment. *FUS1* is a novel tumor suppressor gene (TSG) identified in the human chromosome 3p21.3 region that is frequently altered or deleted in many human cancers and has been shown to function as a key mediator in Apaf1-associated apoptotic pathway and as a potent tumor suppressor *in vitro* and *in vivo*. In light of our recent observations on the FUS1-mediated PTK inhibition and the direct interactions of FUS1 with PTK and Apaf1 proteins together with the current findings of activating mutations of EGFR gene in gefitinib-responders in NSCL patients and the role of these mutations in selectively activating cell survival signaling and blocking pro-apoptotic pathway by other researchers, in this study we explored the capability of using the multifunctional FUS1 as a modulator for enhancing chemotherapeutic potency of gefitinib and overcoming gefitinib-resistance by simultaneously inactivating cell survival and proliferation signaling and activating proapoptotic pathways in both gefitinib-sensitive and resistant NSCLC cells. We found that reactivation of wt-FUS1 by *FUS1*-nanoparticle-mediated gene transfer or treatment with a wt-FUS1-derived peptide (wt-FP) in 3p-deficeint and Gefitinib-resistant NSCLC H1299, H358, and H460 cells significantly sensitized these cells' response to Gefitinib treatment, as demonstrated by a more than additive inhibitory effect on tumor cell growth and a synergistic induction of apoptosis. An enhance growth inhibition was also observed in gefitinib-sensitive HCC827(with an activating mutation of EGFR) and H1819 (with amplification of EGFR) cells co-treated with FUS1-nanoparticles and a very low dose of gefitinib (at a level of IC_{10}). A marked inhibition on activities of phosphorylated EGFR and Erk proteins was also detected in cells treated by FUS1-nanoparticle or wt-FP alone or in combination with gefitinib, as demonstrated by Western-blot analysis with phosphor-EGFR or Erk-specific antibodies. Our results suggest that the wt-Fus1 may play a critical role in modulating the sensitivity of tumor cells to the chemotherapeutic agents such as PTKIs and that a combination treatment of the FUS1-nanoparticle-mediated molecular therapy with these small molecule chemotherapeutics may be an efficient treatment strategy for lung cancer. This abstract is supported by grants of NIH NCI (SPORE P50CA70907) and DOD (TARGET, DAMD17002-1-0706).

Citation format: Proc Amer Assoc Cancer Res 2005;46:2707.

96th Annual Meeting, Anaheim, CA - April 16-20, 2005

Detection of clonal and subclonal outgrowths in the upper aerodigestive tract of current and former smokers with lung cancer

Tao Lu, Ignacio I. Wistuba, and Walter N. Hittelman
The University of Texas MD Anderson Cancer Center, Houston, Texas

Our prior results using chromosome in situ hybridization suggested the existence of genetic instability and clonal/subclonal mosaicism in the bronchial epithelium of current and former smokers without cancer. To verify these results by an independent methodology and to develop an assay system to quantitatively detect clonal/subclonal variations with high sensitivity and dynamic range, we adapted and modified the technique of fluorescence simple-sequence repeat PCR (FISSR-PCR) so that as little as 500 cell groups could be analyzed. We microdissected groups of cells from the stroma (from 1 to 8 regions per case), adjacent bronchial epithelium (from 1 to 10 regions per case), and tumor (from 1 to 12 regions per case) from frozen tissue sections of resected lung cancer specimens from 11 patients with a history of tobacco exposure. Genomic DNA was extracted from the microdissected cells and subjected to FISSR-PCR analysis using a Fam-$(CA)_8$RG primer. Lung tumor regions exhibited a relatively high degree of clonal/subclonal alterations (median, 7.2; range, 2 to 25 DNA band changes) and heterogeneity when compared to normal stromal regions. Bronchial epithelial cells in the field of lung tumors also showed evidence of clonal/subclonal outgrowths, albeit fewer than that observed in the lung tumor regions (median, 2.5; range, 0 to 7 DNA band changes). Of interest, there was a correlation between the number of band changes in the tumor and bronchial epithelium within individual lung tumor specimens (linear regression analysis, $R^2 = 0.56$). In some cases, a common subset of band changes was observed in the bronchial epithelium and associated lung tumor, suggesting a precursor-tumor relationship. In other cases, distinct band changes were observed in the adjacent epithelium that were not present in the associated tumor regions, suggesting multifocality of initiated clones. Significantly, we also detected clonal/subclonal populations in the lung stroma, albeit at a lower frequency than that observed in the bronchial epithelium (median, 1.8; range, from 0 to 4 DNA band changes). These results provide further support to the prior finding of clonal and subclonal outgrowths in tobacco-exposed lung. These results also suggest the extent of the multifocal changes can be quantified by FISSR-PCR analysis and might be exploited in the future for assessing lung cancer risk in current and former smokers. Supported in part by DAMD17-02-1-0706, NIH/NCI CA-91844, and EDRN NCI CA-86390.

Print this Page for Your Records Close Window

American Association for Cancer Research

Control/Tracking Number : 04-AB-6227-AACR
Activity : Abstract Submission
Current Date/Time : 11/7/2003 4:54:08 PM

Biology and therapy of human small cell lung cancer (SCLC) in novel orthotopic nude mouse models.

Takeshi Isobe, Amir Onn, Wenjuan Wu, Tomoaki Shintani, Satoshi Itasaka, Keiko Shibuya, Waun K. Hong, Michael S. O'Reilly, Roy S. Herbst. UT M. D. Anderson Cancer Center, Houston, TX

SCLC is one of the most aggressive phenotypes of human lung cancer and conveys a poor prognosis due to the limited efficacy of existing treatment strategies. To provide clinically relevant strategies for studying new therapeutics and tumor biology, we developed three orthotopic models of human SCLC in nude mice. Three different human SCLC cell lines (H69A, a variant of the NCI-H69 cell line selected for invasiveness in vitro on semisolid agarose; NCI-H187; and NCI-N417) were studied. Tumor cells (1.5×10^6 cells in growth factor reduced Matrigel) were injected into the left lung of anesthetized nude mice. Tumors developed within 8 to 12 weeks and new cell lines were established from the lung tumors (H69ALu, H187Lu, and N417Lu) to select for a reproducible growth pattern for the orthotopic tumors and to minimize variation of tumor size. For each model, tumors started as a solitary mass in the left lung tumor that then spread to mediastinal and axillary lymph nodes, and to the right lung in a pattern similar to that observed in the clinic. N417Lu and H187Lu formed a 100 mm^3 left lung mass within 30-40 days of injection, and mice were moribund within 50 to 60 days of injection. H69ALu tumors reached a volume of 100 mm^3 within 60 days of injection and mice became moribund within 4 to 6 months. All tumors larger than 100mm^3 expressed the proangiogenic factors bFGF and IL-8 (at the tumor periphery), and VEGF/VPF (tumor center and periphery).To compare the efficacy of different chemotherapeutic agents in each of our models, groups of mice (n = 5) were randomized to weekly i.p. treatment with saline (control), 6 mg/kg/mouse of cisplatin (CDDP), 50 mg/kg/mouse of paclitaxel, 125 mg/kg/mouse of irinotecan (CPT-11), or 40 mg/kg/mouse of etoposide. Therapy was initiated on day 10 (H187Lu and N417Lu) or day 20 (H69ALu) after tumor injection coincident with the formation of microscopic lesions. Therapy was well tolerated and mice were killed after five (H187Lu and N417Lu) or seven (H69ALu) weeks of therapy. Tumor burden was assessed by lung and tumor weight (g) and primary tumor volume (mm^3). CPT-11 significantly inhibited the growth and progression of N417Lu tumors as compared to control (lung and tumor weight 0.23 ± 0.01 vs. 0.62 ± 0.15, $p = 0.02$; tumor volume 0.3 ± 0.1 vs. 364 ± 156, $p = 0.03$) and CDDP significantly inhibited the growth and progression of H69ALu tumors as compared to control (tumor volume 0.3 ± 0.1 vs. 100 ± 0.01, $p = 0.04$). The development of our orthotopic models of SCLC provides a better understanding the biology of this disease and will enable evaluation of novel therapeutic strategies (supported by a grant from the Department of Defense (DAMD 17-02-1-0706 to W.K.H.).
Author Disclosure Block: T. Isobe, None; **A. Onn**, None; **W. Wu**, None; **T. Shintani**, None; **S. Itasaka**, None; **K. Shibuya**, None; **W.K. Hong**, None; **M.S. O'Reilly**, None; **R.S. Herbst**, None.

Category and Subclass (Complete): CB11-01 Mouse models of human cancer

Keyword (Complete): Orthotopic model ; Lung cancer ; Chemotherapy
Sponsor (Complete):
2004 Travel Awards (Complete):
Payment (Complete): Your credit card order has been processed on Friday 7 November 2003 at 4:35 PM.
Status: Complete

If you have any questions or experience any problems, please contact Customer Support at aacr@dbpub.com or call (617) 621-1398 or (800) 375-2586.

1494 Inactivation of the potential 3p21.3 tumor suppressor NPRL2 significantly correlates with the cisplatin-induced resistance in human NSCLC Cells

Kentaro Ueda, Hiroyuki Kawashima, Wuguo Deng, John D. Minna, Jack A. Roth, Lin Ji. *UT M.D. Anderson Cancer Center, Houston, TX and UT Southwestern Medical Center, Dallas, TX.*

NPRL2 is one of the candidate tumor suppressor genes residing on a 120-kb homozygous deletion region in human chromosome 3p21.3. NPRL2 protein shares a high degree of amino acid sequence homology to the yeast nitrogen permease regulator 2 and the disruption of *NPRL2* gene in yeast cells has been shown to attribute to the cellular resistance to cisplatin (CDDP)- and doxorubicin-mediated cell killing. NPRL2 has been speculated to be involved in DNA mismatch repair, cell cycle checkpoint signaling, and regulation of apoptotic pathway. In this study, first we analyzed expression of NPRL2 protein by Western-blot, determined IC50 values of CDDP by a XTT assay in NSCLC cell lines, and evaluated the potential correlation between NPRL2 protein expression and CDDP sensitivity. In 21-NSCLC cell lines tested, 10 (83%) out of 12 NPRL2-positive cell lines showed high sensitivity to CDDP (IC50 < 5 μM), and 6 (67%) out of 9 NPRL2-negative cell lines were CDDP- resistant (IC50 >5 μM). A high level of expression of NPRL2 protein was detected in a clinic-originated CDDP-sensitive NSCL cell line H1437 (IC50 = 1.2 μM) but no expression of NPRL2 protein was detected in a CDDP-resistant H1437 subline (IC50 = 16 μM), which was experimentally established by selecting against CDDP from the parental H1437 cells. In addition, we measured the density of NPRL2 protein band on the Western-blot from each cell line and examined the relationship between the level of NPRL2 expression and the IC50 value of CDDP in these NSCLC cells and found that expression of NPRL2 was significantly and reciprocally correlated to CDDP sensitivity, with a Pearson's correlation coefficient of - 0.57($P = 0.006$). Next, we constructed a NPRL2 protein expressing plasmid to studied the effect of exogenous expression of NPRL2 on tumor cell growth and apoptosis by DOTAP:cholesterol nanoparticle-mediated gene transfer in both CDDP-sensitive and resistant NSCLC cells. We found that re-expression of NPRL2 in NPRL2-negative and CDDP-resistant cells significantly re-sensitize these cells' response to CDDP treatment with a reduced relative cell viability from 70% in the absence of NPRL2 expression to 20% in re-expression of NPRL2 at a sub-optimal dose of CDDP (at a IC20 level) in each cell line. Furthermore, an approximately 2.3-fold higher induction of apoptosis was also detected in those cells transfected by *NPRL2*-nanoparticles compared to those untransfected cells at the same level of CDDP treatment. Our results implicate the potential of using NPRL2 as a biomaker for the prediction of CDDP responsiveness and prognosis in lung cancer patients and as a molecular therapeutic agent for enhancing and re-sensitizing response of CDDP-non-responders to CDDP treatment. This abstract is supported by grants of NIH NCI (SPORE P50CA70907).

Citation format: Proc Amer Assoc Cancer Res 2005;46:1494.

4551

ZD6474, a small molecule targeting VEGF and EGF receptor signaling, inhibits lung angiogenesis and metastasis and improves survival in an orthotopic model of non-small cell lung cancer

W Wu, T Isobe, S Itasaka, T Shintani, RR Langley, A Onn, JC Hansen, MS O'Reilly, and RS Herbst

University of Texas MD Anderson Cancer Center, Houston, Texas, USA

Introduction

- Angiogenesis plays an essential role in tumor growth and metastasis, and inhibition of angiogenesis provides a novel approach for treating a wide range of human malignancies.[1,2]
- Vascular endothelial growth factor (VEGF) is an important growth factor for angiogenesis that regulates cell proliferation, invasion and vascular permeability by binding to VEGFR-1, VEGFR-2 and other receptors. VEGF overexpression, and resultant increased neovascularization, is observed in many human cancers. Epidermal growth factor receptor (EGFR) regulates cell proliferation and tumor progression and is overexpressed in non-small cell lung and other cancers.
- ZD6474 is a selective small molecule inhibitor of VEGFR-2 tyrosine kinase with additional activity against EGFR tyrosine kinase. This agent has been shown to inhibit the growth of a wide range of human tumor xenografts.[3]
- In this study, we examined the antiangiogenic, antivascular, antimetastatic and antitumor effects of ZD6474 *in vitro* and *in vivo* to better understand the role of VEGFR and EGFR signaling in human lung cancer progression.

Methods

In vitro assessments

Assessment of cell proliferation, colony formation, migration and invasion

- NCI-H441 lung adenocarcinoma cells (ATCC) or mouse lung endothelial cells (MLEC; courtesy of Dr R Langley, University of Texas) were plated in triplicate in 96-well plates at a density of 5 x 10^3/well and incubated overnight. Cells were then washed and cultured in medium containing increasing concentrations of ZD6474.
- Cell proliferation was measured by MTT after 72 hours. For the colony assay, 1 x 10^4 cells were seeded into 6-well plates; after 72 hours' treatment with ZD6474, the medium was replaced with normal culture medium and cells were cultured for another 92 hours.
- Colony number was counted using a dissecting microscope.
- Assessment of cell migration and invasion was performed as previously described.[4]

Apoptosis assay

- Cells treated with ZD6474 for 48 hours in serum-free medium were incubated with 50 mg/ml propidium iodide and 100 units/ml RNAase. Apoptosis was analyzed by flow cytometry.

In vivo assessments

Gelfoam angiogenesis assay

- Blood vessel development was assessed using subcutaneously implanted gelfoam-agarose sponges, as previously described.[5]

Orthotopic lung cancer model

- A suspension of 5 x 10^5 NCI-H441 cells mixed with 20% Matrigel was injected into the left lung of nude mice (5–10 per group).[6] Treatment with ZD6474 (25 or 50 mg/kg p.o. daily) was initiated 5, 10 or 15 days after tumor injection. Mice were sacrificed 4 weeks after tumor cell inoculation, and lung weight, pleural effusion and pleural invasion were measured.

Immunohistochemistry

- CD31 expression was determined in frozen tissue sections using rat anti-mouse CD31 MAb (Pharmingen).
- PCNA expression was determined in paraffin-embedded tissue sections using monoclonal mouse anti-PCNA (DAKO).
- TUNEL was performed on frozen tissue sections using the DeadEnd Fluorometric TUNEL system (Promega).

Statistical analysis

- The data were analyzed by Student's *t* test (two-tailed).

Results

In vitro assessments

- ZD6474 inhibited proliferation and colony formation of NCI-H441 and MLEC (Figure 1). Inhibition was greater than that seen with inhibitors of PI3K (LY294002), MEK (U0126), or a combination of these two agents.
- ZD6474 treatment induced apoptosis of both NCI-H441 and MLEC (Figure 2).
- ZD6474 prevented migration and invasion of NCI-H441 and MLEC.

Figure 1. Effect of ZD6474 on proliferation and colony formation of NCI-H441 and MLEC. a. MTT assay b. Colony assay

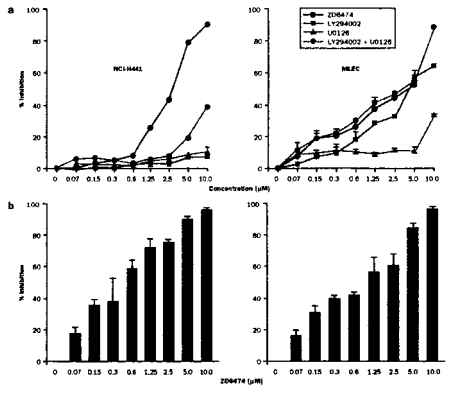

Figure 2. Effect of ZD6474 on apoptosis of NCI-H441 and MLEC

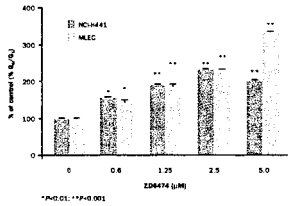

In vivo assessments

- ZD6474 inhibited *in vivo* angiogenesis. Systemic therapy with ZD6474 resulted in decreased microvessel density of subcutaneously implanted gelfoam-agarose sponges (Figure 3).

Figure 3. Effect of ZD6474 on angiogenesis formation in subcutaneous gelfoam-agarose sponges

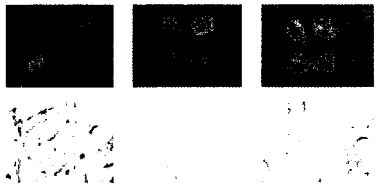

Microvessel density (MVD)	30.27 ± 6.9 Control	8.07 ± 2.25 ZD6474 25 mg/kg	2.42 ± 1.94 ZD6474 50 mg/kg

- ZD6474 blocked the formation of pleural effusion and pleural invasion of established lung adenocarcinomas (NCI-H441) growing orthotopically in the lung (Table 1; Figure 4).

Table 1. Effect of ZD6474 on orthotopic lung adenocarcinoma growth at different stages

Group	Lung weight (mg)		Pleural effusion (μl)		Pleural tumor	
	Incidence	Median (range)	Incidence	Median (range)	Incidence	Median (range)
Day 5						
Control	10/10	520 (309–1124)	10/10	65 (20–1090)	10/10	7 (1–21)
ZD6474 25 mg/kg	9/10	172 (149–199)**	0/10	0 (0–0)**	1/10	0 (0–1)
ZD6474 50 mg/kg	6/10	182 (167–206)**	0/10	0 (0–0)**	0/10	0 (0–0)**
Day 10						
Control	10/10	845 (410–1260)	7/10	75 (0–230)	10/10	19 (3–30)
ZD6474 25 mg/kg	9/10	269 (233–374)**	0/10	0 (0–0)**	8/10	1 (0–4)**
ZD6474 50 mg/kg	9/10	214 (151–259)**	0/10	0 (0–0)**	9/10	3 (0–6)**
Day 15						
Control	5/5	970 (467–1500)	5/5	100 (50–300)	5/5	18 (9–19)
ZD6474 25 mg/kg	5/5	412 (313–878)	1/5	0 (0–30)	4/5	4 (0–21)
ZD6474 50 mg/kg	5/5	411 (319–609)*	0/5	0 (0–0)*	5/5	8 (2–15)

**P<0.05; **P<0.01*

Figure 4. Effect of ZD6474 on orthotopic lung growth

Control | ZD6474 25 mg/kg | ZD6474 50 mg/kg

Treatment began at day 5 following tumor injection

- ZD6474 was effective against both early and locally advanced lung cancer (therapy initiated on day 5 or day 15 after tumor injection, respectively) and significantly prolonged survival, by 300%, relative to control (Figure 5).

Figure 5. Effect of ZD6474 on survival of mice with orthotopic lung adenocarcinomas (NCI-H441). Therapy was initiated on day 15 following tumor injection (n=9 per group). Mice were monitored daily and sacrificed when signs of onset of morbidity were evident

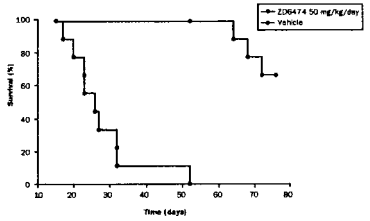

- Treatment with ZD6474 impaired lung cancer angiogenesis and tumor vascularization (CD31) with a corresponding reduction in tumor cell proliferation (PCNA) (Figure 6) and enhancement of endothelial cell apoptosis (Figure 7).

Figure 6. Effect of ZD6474 on proliferation (PCNA) and angiogenesis (MVD) for lung adenocarcinomas (NCI-H441)

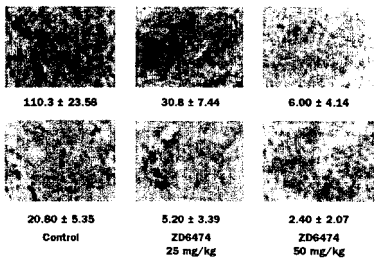

PCNA	110.3 ± 23.56	30.8 ± 7.44	6.00 ± 4.14
MVD	20.80 ± 5.35	5.20 ± 3.39	2.40 ± 2.07
	Control	ZD6474 25 mg/kg	ZD6474 50 mg/kg

Figure 7. Effect of ZD6474 on tumor and endothelial cell apoptosis for lung adenocarcinomas (NCI-H441)

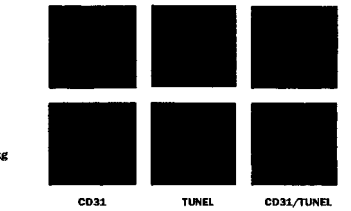

Control			
ZD6474 50 mg/kg			
	CD31	TUNEL	CD31/TUNEL

Conclusions

- ZD6474 targets multiple pathways that are critical for tumor progression, metastasis and angiogenesis, including proliferation, migration and invasion of tumor and endothelial cells.
- ZD6474 significantly inhibits angiogenesis *in vivo* and suppresses tumor growth, pleural effusion and metastasis in these early and locally advanced orthotopic lung tumor models.
- ZD6474 has direct effects on the existing tumor vasculature and induces apoptosis of tumor and tumor-associated endothelial cells with an associated decrease in tumor cell proliferation.
- The substantial antiangiogenic, antivascular and antitumor effects of ZD6474 *in vivo* provide a basis for the design of clinical trials.

References

1. Folkman J & Shing Y. *J Biol Chem* 1992;267:10931–10934
2. Hanahan D & Folkman J. *Cell* 1996;86:353–364.
3. Wedge SR, *et al. Cancer Res* 2002;62:4645–4655
4. Wu WJ, *et al. Clin Exp Metastasis* 2000;18:1–10.
5. McCarty MF, *et al. Int J Oncol* 2002;21:5–10.
6. Onn A, *et al. Clin Cancer Res* 2003;9:5532–5539

AstraZeneca ONCOLOGY

AACR March 2004

3516 Synergistic tumor suppression by coexpression of *FUS1* and *p53* concurrences with FUS1-mediated down regulation of MDM2, accumulation of p53, and activation of Apaf1-dependent apoptotic pathway in human NSCLC cells

Wuguo Deng, Futoshi Uno, John D Minna, Jack A. Roth, Lin Ji. *UT-MD Anderson Cancer Center, Houston, TX and UT Southwestern Medical Center, Dallas, TX.*

FUS1 is a novel tumor suppressor gene (TSG) identified in human chromosome 3p21.3 region where allele loss and genomic alterations are frequently found in a wide spectrum of human cancers and occur at the earliest stage of cancer development. Loss of expression and deficiency of posttranslational modification of FUS1 protein have been found in a majority of NSCLCs and in almost all SCLCs. Restoration of wt-FUS1 function in 3p21.3-deficient human lung cancer cells by adenoviral vector- or DOTAP:cholesterol nanoparticle-mediated gene transfer inhibits the growth of these tumor cells by induction of apoptosis and alteration of cell kinetics *in vitro* and *in vivo*. We previously also noticed that the tumor suppression function of *FUS1* as well as several other potential 3p21.3 TSGs were directly or indirectly dependent of p53 activity. In this study, we evaluated the combined effects of FUS1 and p53 on tumor cell growth and apoptosis induction in NSCLC cells co-transfected with *FUS1*- and *p53*-nanoparticles and explored molecular mechanisms of their mutual actions *in vitro*. We found that co-expression of wt-p53 with the wt-FUS1, but not the dysfunctional myristoylation-deficient mutant (mt-FUS1), synergistically inhibited cell proliferation and induced apoptosis in various human NSCLC cells. We also found that co-expression of FUS1 and p53 enhanced the sensitivities of NSCLC cells to treatments with the DNA-damaging agents γ-radiation and cisplatin. Furthermore, we found that the observed synergistic tumor suppression by FUS1 and p53 concurred with the FUS1-mediated down-regulation of MDM2 expression and the resultant accumulation and stabilization of p53 protein as well as up-regulation of Apaf-1 expression and activation of caspase cascade in Apaf-1-associated apoptotic pathway in human NSCLC cells. Our results therefore revealed a novel molecular mechanism involving FUS1-mediated tumor suppression function and its interaction with other cellular components in the pathways regulating p53 and Apaf-1 activities. Our findings imply that a treatment targeting multiple pathways by combining functionally synergistic tumor suppressors such as *FUS1* and *p53* with chemotherapy or radiotherapy may be an effective therapeutic strategy for NSCLC and other cancers. This abstract is supported by grants of NIH NCI (SPORE P50CA70907) and DOD (TARGET, DAMD17002-1-0706).

Citation format: Proc Amer Assoc Cancer Res 2005;46:3516.

96th Annual Meeting, Anaheim, CA - April 16-20, 2005